Measurement of the Transverse Single-Spin Asymmetry for Mid-rapidity Production of Neutral Pions in Polarized p+p Collisions at 200 GeV Center-of-Mass Energy

Christine Angela Aidala

Submitted in partial fulfillment of the
requirements for the degree
of Doctor of Philosophy
in the Graduate School of Arts and Sciences

COLUMBIA UNIVERSITY
2006

ABSTRACT

Measurement of the Transverse Single-Spin Asymmetry for Mid-rapidity Production of Neutral Pions in Polarized p+p Collisions at 200 GeV Center-of-Mass Energy

Christine Angela Aidala

The spin structure of the proton has revealed itself to be extremely complex and is an area of ongoing research. The Relativistic Heavy Ion Collider (RHIC) at Brookhaven National Laboratory (BNL) inaugurated its operation as the first polarized-proton collider during the 2001-2002 run, marking the beginning of a new era in the study of proton spin structure.

From the data collected in this run, the PHENIX experiment measured the transverse single-spin asymmetry (A_N) for neutral pion production at $x_F \approx 0.0$ over a transverse momentum range of 1 to 5 GeV/c from polarized proton-proton interactions at a center-of-mass energy ($\sqrt{s}$) of 200 GeV and found it to be zero within a few percent. Interest in these measurements arises from the observation of large ($\sim$30%) transverse single-spin asymmetries in $p+p^{\uparrow}\rightarrow\pi+X$ at forward angles by the E704 collaboration at Fermilab ($\sqrt{s} = 19.4$ GeV), found by the STAR and BRAHMS experiments to persist at RHIC energies, as well as single-spin, azimuthal asymmetries observed recently in semi-inclusive deep-inelastic scattering experiments. Such large asymmetries were initially surprising because at leading order, perturbative quantum chromodynamics (pQCD) predicted only small effects.

Several possible origins of these large asymmetries have been proposed. Despite great theoretical progress in recent years, no single, clear formalism has emerged in which to interpret the available data. Further theoretical work and a variety of additional experimental measurements will be necessary to understand current results and elucidate the transverse spin structure of the proton.

Contents

1 Introduction **1**

1.1 Proton structure 1

1.2 The "proton spin crisis" 1

1.3 Studying proton spin structure at the Relativistic Heavy Ion Collider 2

1.4 Aims and outline of this thesis 3

2 Nucleon structure **5**

2.1 Unpolarized nucleon structure 5

2.1.1 Elastic structure 5

2.1.2 Inelastic structure: QCD and the quark-parton model 6

2.1.3 pQCD, factorization, and universality 11

2.1.4 Current status of the unpolarized structure of the proton . . . 13

2.2 Polarized proton structure 14

2.2.1 Historical overview 14

2.2.2 Polarized structure functions 15

2.2.3 Polarized parton distribution functions 17

2.2.4 Current status of the longitudinally polarized structure of the proton 17

2.2.5 Understanding the transverse spin structure of the proton . . 21

2.2.6 Recent experimental results in transverse spin physics 30

3 QCD at RHIC **35**

3.1 Cross section measurements and NLO pQCD 36

3.2 Spin asymmetries in factorized QCD 38

4 Experimental setup **41**

4.1 The Relativistic Heavy Ion Collider 41

4.2 RHIC as a polarized $p + p$ collider 42

4.2.1 RHIC-AGS complex 42

4.2.2 Polarized source 43

4.2.3 Siberian snakes 44

4.2.4 Polarimeters 46

4.2.5 Spin rotators 48

4.2.6 Spin flippers 49

4.3 The PHENIX experiment and detector 50

4.3.1 Interaction and vertex detectors 50

4.3.2 PHENIX central arms 51

4.3.3 Local polarimeter 54

4.3.4 Muon arms 54

4.3.5 Detectors and triggers used in the analysis for this thesis . . . 55

5 Data and analysis **59**

5.1 Overview 59

5.2 Data selection and quality 59

5.2.1 Fill and run selection 60

5.2.2 Event and crossing selection 61

5.3 EMCal-RICH trigger 62

5.4 Reduction of background 64

5.5 Asymmetry calculation 67

5.5.1 Overview 67

5.5.2 Determination of relative luminosity 68

5.5.3 Fill-by-fill polarization correction 70

5.5.4 Acceptance correction 71

5.5.5 Subtraction of background asymmetry . . . 73
5.5.6 Calculation of statistical uncertainties . . . 76
5.5.7 Asymmetry scale uncertainty . . . 77
5.6 Studies and checks . . . 78
5.6.1 Alternative asymmetry calculation . . . 78
5.6.2 Left and right detector arms . . . 81
5.6.3 Two independent beams . . . 83
5.6.4 Triggered and minimum-bias data . . . 85
5.6.5 Different background regions in invariant mass . . . 85
5.6.6 Different π^0 invariant-mass integration regions . . . 86
5.6.7 Bunch shuffling . . . 87
5.7 Results . . . 95
5.8 Comparison to charged hadron asymmetry results . . . 97

6 Future prospects for transverse spin physics 99
6.1 BRAHMS . . . 99
6.2 STAR . . . 100
6.3 PHENIX . . . 101

7 Conclusions 105

A Relative luminosity considerations 127

List of Figures

2.1 World DIS data on the unpolarized structure function of the proton, F_2. 9
2.2 World DIS data on the polarized structure function of the proton, g_1. 16
2.3 Global fits to world data for the polarized pdf's of valence quarks. . . 19
2.4 Global fits to world data for the polarized pdf's of gluons and sea quarks. 20
2.5 A_{LL} for neutral pions 21
2.6 Predicted A_{LL} of positive pions for various Δg assumptions 22
2.7 Predicted A_{LL} of negative pions for various Δg assumptions 22
2.8 A_N of high-x_F neutral and charged pions at $\sqrt{s} = 19.4$ GeV. 25
2.9 Collinear and k_T-dependent leading-twist pdf's. 27
2.10 A_N of high-x_F neutral pions at $\sqrt{s} = 200$ GeV. 31
2.11 A_N of moderate-x_F charged pions at $\sqrt{s} = 200$ GeV. 32
2.12 Measured analyzing power of the Collins FF for pions. 33

3.1 Mid-rapidity π^0 cross section compared to NLO pQCD 37
3.2 Mid-rapidity charged hadron cross section compared to NLO pQCD . 38
3.3 Forward π^0 cross section compared to NLO pQCD 39

4.1 RHIC-AGS complex. 43
4.2 PHENIX central arms 52
4.3 PHENIX local polarimeter measurement. 55
4.4 PHENIX muon arms 56

5.1 Schematic illustration of the spin pattern in RHIC. 62
5.2 Trigger efficiency for neutral pions. 63
5.3 Fitted photon-pair invariant-mass spectrum. 65
5.4 Transverse momentum spectrum for photon pairs falling under the π^0 mass peak. 66
5.5 Fill-by-fill asymmetries. 68
5.6 Combined asymmetry results for the two beams and particle production to the left and right. 70
5.7 Asymmetry results before and after correction for background. 75
5.8 π^0 multiplicity per MB event, $1 < p_T < 2$ GeV/c 76
5.9 π^0 multiplicity per MB event, $2 < p_T < 3$ GeV/c 77
5.10 Comparison of two methods of asymmetry calculation. 80
5.11 Comparison of results for particle production to the left and the right, blue beam polarized. 82
5.12 Comparison of results for particle production to the left and the right, yellow beam polarized. 83
5.13 Comparison of results obtained for the two polarized beams. 84
5.14 Comparison of results for minimum-bias and triggered events. 86
5.15 Comparison of asymmetries obtained after subtracting two different background regions. 87
5.16 Comparison of results for different π^0 peak integration regions. 88
5.17 Bunch-shuffled asymmetry distributions. 90
5.18 Bunch-shuffled χ^2 distributions. 91
5.19 Final π^0 asymmetry results. 96
5.20 Comparison of asymmetry results for mid-rapidity neutral pions and charged hadrons. 98

7.1 Relative contributions of partonic processes to π^0 production. 106

List of Tables

5.1 Trigger effects on mean p_T of photon pairs. 63
5.2 π^0 yields and peak widths. 64
5.3 Reduction of background contribution. 66
5.4 Asymmetry results. 69
5.5 Combined asymmetry results for the two beams and particle production on the two sides of the beam. 69
5.6 Fill-by-fill beam polarization values. 71
5.7 Azimuthal acceptance correction factors. 72
5.8 Background asymmetries. 74
5.9 Background-subtracted π^0 asymmetries. 74
5.10 Mean p_T values of the background and of neutral pions after correction for background. 75
5.11 Deviation of particle production from a Poisson distribution. 77
5.12 Asymmetry results, alternative calculation. 79
5.13 Agreement of asymmetry results from the two methods of calculation, blue beam. 80
5.14 Agreement of asymmetry results from the two methods of calculation, yellow beam. 81
5.15 Systematic uncertainty on the asymmetry. 81
5.16 Agreement of results for particle production to the left and right of the beam. 82
5.17 Agreement of results for individual beams. 84
5.18 Comparison of background asymmetries. 85

5.19 Shuffled asymmetry distribution means. 90
5.20 Comparison of statistical uncertainties on the physics asymmetry and widths of shuffled asymmetry distributions. 92
5.21 Bunch shuffling results for two different statistical sample sizes and three different simulated asymmetry values. 94
5.22 Comparison of simulated shuffling results for 10 and 48 bunches per beam. 95
5.23 Modified bunch shuffling simulation with correlations removed. 95
5.24 Asymmetry results. 96
5.25 Charged hadron asymmetry results. 97

Acknowledgements

First and foremost, I have to express my gratitude to my husband, Gabriele Carcassi, for all the sacrifices he has made in order to make it possible for me to pursue a Ph.D. in physics here in the U.S., my home country. Without his dedicated support and infinite patience, in particular through rough times in the past, I would not be where I am today. He inspires me to achieve more, to think big, to dream what I never otherwise would have imagined for myself. I only hope that his own immense talents and creativity can find a worthy outlet, his own great ambitions fulfilled, through his life with me. I could hardly acknowledge Gabriele without recognizing how rewarding it has been to share the experience of watching our son, Matteo, grow and develop since he came into our world in November 2004. Becoming parents has rounded out our lives, bringing new adventures and experiences, leading us to grow in turn as adults. I look forward to many more years drawing energy and strength from my family.

I would like to thank my own parents, Paul and Susan Aidala, who instilled in me an appreciation of nature, science, and mathematics. Through them I learned integrity, the value of hard work, and the importance of attention to detail. They taught me to be active in the pursuit of knowledge. Countless questions of mine were answered by trips to our shelves of reference books; thus were my humble beginnings as an elementary-school researcher. The influence of my parents is made even more evident by the fact that my sister, Kathy, shares a similar interest in science. She is currently a Ph.D. candidate in the Applied Physics Department at Harvard, and it is a pleasure to be able to continue to share so much with her intellectually.

I am grateful to Brian Cole as my thesis sponsor. He has always been ready with a wealth of ideas and suggestions whenever I have discussed my work with him. During the course of my three years at Columbia, he has provided detailed input and feedback on my efforts involving PHENIX software triggers, data analysis, and this dissertation. He has been extremely flexible regarding the details of where, how, and when I have worked. He has listened to understand my needs and goals

and helped me to further my own interests. Such an accommodating and supportive supervisor is not something a graduate student can take for granted.

Being a part of the PHENIX group at Columbia has been a rewarding experience overall. Brian, along with Bill Zajc, graciously allowed me to pursue a physics topic outside the group's area of focus; I feel that the intellectual independence granted to me has served me well. My professional development has also been enriched by extensive travel. I have been able to take advantage of numerous conferences, workshops, and summer schools, thanks largely to financial support provided by the group. Moreover, Brian and Bill have both provided invaluable career advice and have consistently encouraged me to pursue my professional interests. The other junior members of the group with whom I have overlapped, especially Justin Frantz, Sotiria Batsouli, Mickey Chiu, and David d'Enterria, have been a friendly support network and resource for me to draw upon. Furthermore, I was surprised and touched by the overwhelming support I received from the group when I informed them of my decision to have Matteo during the last year of my Ph.D. The success I have had in balancing my studies with my family life is due in part to their unhesitating confidence in me.

Bill Zajc, as spokesperson of PHENIX, has provided a role model of great responsibility, amazing time management, and politics without pettiness. His ability to keep a handle on the experiment and collaboration on a multitude of focus levels, from the place of PHENIX in the context of the broader field of nuclear physics to the details of many individual careers, is impressive. He has made me feel that even in a large collaboration, individuals matter.

I would like to thank Matthias Grosse Perdekamp for the role he has played as my "spin advisor" on PHENIX. His in-depth knowledge and understanding of a wide spectrum of physics has set a standard for me to aspire towards as a young experimentalist. He has been extremely supportive of my career and has provided a number of useful career discussions.

I would like to express my sincere appreciation to Werner Vogelsang for a wealth

of ready physics information and advice over the past several years. My quests for knowledge, big and small, were always received with respect and interest, and frequently with enthusiasm. He has been a valuable asset throughout my time as a student, and I expect to continue to learn from him in the years to come.

I would like to acknowledge Sam Aronson for the role he played in bringing me back to physics in 2001 after I spent nearly two years out of the field. I found myself with limited options at that time, and if he had not hired me to do research at BNL, I feel that life, for better or worse, would have most likely taken me down a completely different path. He opened the door to all the positive experiences I have had as a part of PHENIX for the past four years. I appreciate the gamble he took, hiring me based on such little information, and I have done my best to prove myself a worthwhile investment.

Recalling my early days in PHENIX, warm memories of all the support I received from Saskia Mioduszewski come immediately to mind. I was indeed lucky to find myself sharing an office with her when I came to BNL. She made me feel welcome when I first arrived, and over time she became a friend and mentor, offering ready and reliable advice on technical problems, analysis issues, career paths, or life in general.

After Saskia was promoted and moved down the hallway, my good fortune in officemates at BNL continued. Henner Büsching has become a valued friend and colleague. He has provided an example of dedication to his work and of caring about doing it well. Through him, I have witnessed the contribution a single young scientist can make toward the successful functioning of a large collaboration. I greatly appreciate the technical and moral support he has offered for nearly three years now, as well as the positive and pleasant work environment he has created.

Also at BNL, I would like to thank Craig Woody and Gabor David for all that I learned through them during my first year on PHENIX. They helped lay the foundation for my ability to work relatively independently in subsequent years.

Other PHENIXians who supported my efforts, in particular on my thesis anal-

ysis, were Frank Bauer and Hisayuki Torii. Frank provided numerous helpful conversations regarding transverse spin physics and analysis as well as moral support. I was pleased to bring his own work to eventual publication after he moved on to pursue a career outside of physics. Hisa furnished lots of help and technical support in the early stages of my thesis analysis.

Turning back to Columbia, I would like to thank Lalla Grimes, the Administrative Coordinator in the Physics Department, for being so warm, welcoming, competent, efficient, and simply a delight to deal with. She has done a great deal to make me feel at home in the Department right from the beginning.

I am also grateful to many of my fellow classmates for making my experience at Columbia such a positive one, especially Mike Cheng, Oleg Loktik, Sasha Lyulko, Alexis Aguilar, Chad Johnson, Azfar Adil, Bahar Moezzi, and Christina Tosti. They created a friendly and cooperative atmosphere during the time we shared in classes and, of course, working on problem sets. It was great to know there were so many people I could reliably turn to when I wanted to discuss course work or physics in general. I would specifically like to thank Sasha for hosting me periodically in the city and Alexis for inspiring me to study so hard for the quals.

During the three semesters in which I was taking classes, I was fortunate to have the local hospitality of Angela and Genevieve Aidala and Jean Schmidt available. Their kindness in opening their Upper West Side home to me gave some respite from the challenge of commuting into campus several days a week from eastern Long Island.

Last but not least, I would like to express my deep appreciation to Stefan Bathe for his staunch encouragement and support over the past several years we have spent together on PHENIX. The close friendship we have developed has uplifted my spirits time and again. I am grateful for the countless, valuable conversations we have had regarding careers and life paths in general. I am also indebted to him for his careful reading of and extensive feedback on earlier drafts of this dissertation; the present version is greatly improved thanks to his thorough comments.

To Yale University Prof. Emer. Frank W. K. Firk, who, ten years ago, inspired the beginnings of a career.

Chapter 1

Introduction

1.1 Proton structure

The proton, together with the neutron and electron, is one of the basic building blocks of everyday atomic matter. Far from the point particle it was once believed to be, it has proven to be an extremely complex entity, and more than 80 years after it was discovered in the first decades of the twentieth century, the composition of the proton is still not completely understood. A very rich structure has gradually been uncovered over the past 40 years of research, with the appropriate description depending on the energy scale at which the proton is probed. The composition of the proton is now described by *partons*, including *quarks* and the particles carrying the force that binds them, *gluons*. More specifically, quarks can be categorized as either *valence* or *sea*. In the simplest composite model of the proton, it can be viewed as three valence quarks, each carrying 1/3 of the proton's linear momentum. In reality, measurements have demonstrated that there is a multitude of gluons and sea quark-antiquark pairs present as well, each carrying generally a small fraction of the proton's momentum but with a large summed momentum contribution overall.

1.2 The "proton spin crisis"

In the naive model of the proton as simply three valence quarks of spin $\frac{1}{2}\hbar$ each, one might expect the proton's spin to be the straightforward sum of two parallel quark

spins and one antiparallel. However, in the late 1980's it was discovered that in fact only a small fraction of the proton's spin, less than 30%, was carried by quarks. This revelation, surprising at the time, came to be known as the "proton spin crisis." In retrospect, considering the complex linear-momentum structure of the proton, it is reasonable to expect a complex angular-momentum structure as well. Not only the spin of the partons is involved, but also their orbital angular momentum.

Due to the fact that spatial rotations and Lorentz boosts do not commute, polarized proton structure must be considered separately for a proton with spin vector parallel to or perpendicular to its (linear) momentum. This difference between the longitudinal and transverse spin structure adds further complexity to the problem. As will be discussed, significant progress has been made in understanding the longitudinal spin structure of the proton, while transverse structure remains a largely open field. Despite impressive advances in just the past few years, numerous additional experimental measurements will need to go hand-in-hand with further theoretical investigation in order to elucidate the transverse spin structure of the proton.

1.3 Studying proton spin structure at the Relativistic Heavy Ion Collider

Resolution of the proton spin crisis, in particular determination of contributions from sea quarks and gluons, remains the goal of extensive ongoing study. The PHENIX experiment at the Relativistic Heavy Ion Collider (RHIC) at Brookhaven National Laboratory is in a unique position to make significant contributions to improve our understanding of the origin of the proton's spin.

RHIC is the most versatile hadron collider in the world. It is capable of colliding heavy ions with energies as high as $\sqrt{s} = 200$ GeV per colliding nucleon pair and polarized protons anywhere from 50 to 500 GeV, as well as different species in the two beams. In the first five years of running, RHIC has provided gold collisions at four different energies, copper collisions at three energies, deuteron-gold collisions,

and polarized-proton collisions. The flexibility of RHIC allows for a very diverse physics program. The heavy ion physics program investigates strongly-interacting matter at extreme temperatures and energy densities, seeking to create and study the properties of a state of matter known as the quark-gluon plasma (QGP).

The polarized proton program seeks a better understanding of the proton's spin structure, in particular contributions to its longitudinal spin structure from the gluons and sea quarks. By studying the proton using hadronic collisions rather than electromagnetic probes, which do not couple to the electromagnetically neutral gluon, RHIC experiments may directly observe gluon-scattering processes. As a collider, RHIC can provide collisions at much higher energy than can be achieved in fixed-target measurements. As a result hard processes, describable by perturbative quantum chromodynamics (pQCD), can be studied, and new probes such as W bosons will eventually become available.

1.4 Aims and outline of this thesis

This thesis aims to motivate the study of the structure of the proton, in particular the polarized structure, as a fundamental question in QCD. It also seeks to describe how spin-dependent observables can be and have already been measured at RHIC, with focus on a transverse single-spin asymmetry (SSA) measurement, providing information on the transverse spin structure of the proton.

This thesis will present a review of proton structure, both unpolarized and polarized, in terms of history and the current status. An overview of pQCD as applicable to proton-proton collisions at RHIC will be given. The RHIC polarized-proton accelerator complex and the PHENIX experiment and detector will be described. A measurement of the transverse single-spin asymmetry of neutral pions will be presented and discussed. Finally, the prospects for future measurements to shed further light on the transverse spin structure of the proton will be explored.

Chapter 2

Nucleon structure

2.1 Unpolarized nucleon structure

2.1.1 Elastic structure

2.1.1.1 Magnetic moments

The first evidence of proton substructure came from a measurement of its magnetic moment in 1933 by Esterman, Frisch, and Stern. It was found to be anomalously large and is now known to be approximately 2.79 times the Dirac magnetic moment, given by $\overrightarrow{\mu}_p = \frac{e}{Mc}\overrightarrow{S}$, for a point-like spin-$\frac{1}{2}$ particle of the same mass. The anomalous magnetic moment of the proton is now understood in terms of its valence quark structure (see Section 2.1.2 below) and can be given by $\mu_p = \frac{1}{3}(4\mu_u - \mu_d)$, where μ_u and μ_d are the magnetic moments of the up and down valence quarks, respectively.

Similarly, the magnetic moment of the neutron was also found to be anomalous by Esterman and Stern in 1934 and is now understood in terms of its own valence quark structure.

2.1.1.2 Form factors

Charge and current distributions within the nucleon can be described by electromagnetic form factors, measurable via elastic electron-proton scattering. Viewed in a particular frame known as the Breit frame ($\overrightarrow{p}_{\text{final}} = -\overrightarrow{p}_{\text{initial}}$ for the proton), the form factors G_E and G_M are proportional to the Fourier transforms of the charge

and magnetization distributions, respectively.

The cross section for elastic electron-proton scattering can be expressed in terms of the form factors, as given in Eq. 2.1,

$$\frac{d\sigma}{d\Omega}|_{lab} = \frac{\alpha^2}{4E^2 \sin^4 \frac{\theta}{2}} \frac{E'}{E} \left(\frac{G_E^2 + \tau G_M^2}{1+\tau} \cos^2 \frac{\theta}{2} + 2\tau G_M^2 \sin^2 \frac{\theta}{2} \right) \tag{2.1}$$

where $\tau \equiv -q^2/4M^2$, q is the four-momentum transfer in the scattering, M is the proton mass, α is the fine structure constant, θ is the electron scattering angle in the laboratory frame, and E and E' are the incident and scattered electron energies. The electric and magnetic form factors can be determined either via differential cross section measurements of unpolarized $e + p$ scattering or via measurement of the recoil proton polarization in the reaction $\overrightarrow{e} + p \rightarrow e + \overrightarrow{p}$, where the arrows indicate polarization. For a relatively recent summary of proton electromagnetic form factor measurements performed at Jefferson Lab, see [129].

2.1.2 Inelastic structure: QCD and the quark-parton model

In the 1960's deep-inelastic lepton-nucleon scattering (DIS) experiments at SLAC, analogous to the famous Rutherford scattering experiment that led to the discovery of the atom's hard core, found that protons also had "hard" subcomponents [62, 73]. These hard subcomponents came to be known as partons. It took some time before the experimentally observed partons inside the proton were identified as the so-called "quarks," which had been theoretically hypothesized based on hadron spectroscopy data as part of the "Eightfold Way" by Gell-Mann and Ne'eman independently in the early 1960's [99]. But eventually the quark-parton model of the proton came into being. As experimental work progressed and higher-energy lepton beams were used as probes, the proton came to reveal a much more intricate structure than that of the three so-called "valence" quarks. These other subcomponents are now known to be sea quarks and gluons.

The experimental and theoretical work in the 1960's and 1970's regarding hadronic interactions and structure led to the development of the theory of quantum chromodynamics (QCD), describing the behavior of the strong force. A central concept

of QCD is that of *asymptotic freedom*. While quarks are strongly bound at distance scales larger than a typical hadron radius ($r \approx 10^{-15}$ m), at shorter distances they behave as nearly free.

2.1.2.1 Structure functions

The nucleon structure functions describe the inelastic structure of the proton and neutron, probed principally via DIS. The double differential cross section for inelastic cross section for electron-proton scattering can be expressed as in Eq. 2.2,

$$\frac{d^2\sigma}{dE'd\Omega}|_{\text{lab}} = \frac{4\alpha^2 E'^2}{q^4}\left[W_2(\nu, q^2)\cos^2\frac{\theta}{2} + 2W_1(\nu, q^2)\sin^2\frac{\theta}{2}\right] \tag{2.2}$$

in which q, α, θ, and E' are as in Eq. 2.1, $\nu = (p \cdot q)/M$ with p being the initial nucleon four-momentum, and W_1 and W_2 are the proton structure functions. Note the similarity of Eq. 2.2 to Eq. 2.1, the cross section for elastic electron-proton scattering, with the structure functions playing the role of the form factors.

It is common to express the proton structure functions slightly differently, as given in Eq. 2.3.

$$\begin{aligned} F_1 &= MW_1 \\ F_2 &= \nu W_2 \end{aligned} \tag{2.3}$$

F_1 and F_2 can be written as functions of $Q^2 = -q^2 > 0$ and the dimensionless variable $x = Q^2/2p \cdot q$. They can be related to the cross sections for scattering of transversely and longitudinally polarized virtual photons off of the proton, σ_T and σ_L, as given in Eq. 2.4.

$$\begin{aligned} \sigma_T &\propto F_1 \\ \sigma_L &\propto \left(\frac{F_2}{2x} - F_1\right) \end{aligned} \tag{2.4}$$

The total virtual photon-proton cross section is the sum of these components and is proportional only to F_2.

In 1969 Bjorken predicted that at large Q^2, scattering off of "point-like" subcomponents that were approximately free in the proton would lead to proton structure

functions with no Q^2 dependence for a given value of x, i.e. that scale with just this single, dimensionless variable [61]. That is, assuming point-like constituents of the proton, at large Q^2, *inelastic* electron-*proton* scattering could be viewed as *elastic* scattering of an electron off of a hard, point-like particle *within* the proton.

The experiments performed at SLAC mentioned above [62, 73] discovered the scaling behavior predicted by Bjorken. The structure functions they measured had very little explicit dependence on Q^2 and could in fact be written simply as functions of x.

In Figure 2.1 showing world DIS data for F_2 of the proton, one sees that for $x \gtrsim 0.02$, F_2 is nearly flat in Q^2. This indicates that the hard subcomponents being probed are approximately free. The early measurements included here provided evidence leading to development of the concept of asymptotic freedom in QCD. Note, however, the scaling violations observed at low x and low Q^2. These are now understood in terms of gluon radiation emitted by the parton prior to the hard scattering. See Section 2.1.2.2 for discussion of the relation of scaling violations to the gluon distribution function.

In 1969 Callan and Gross predicted that for spin-$\frac{1}{2}$ charged components within the nucleon, the scaling structure functions would be related as given in Eq. 2.5, known as the Callan-Gross relation [77].

$$F_2(x) = 2xF_1(x) \tag{2.5}$$

Experimental confirmation of the Callan-Gross relation came from SLAC in the late 1970's [64] and thus provided strong evidence for the spin-$\frac{1}{2}$ nature of what are now known to be quarks.

2.1.2.2 Parton distribution functions

Feynman's introduction of the quark-parton model (QPM) in 1969 [98] offered a relatively intuitive explanation of Bjorken scaling. The virtual photon in DIS could be viewed as scattering elastically off of a collection of hard partons within the proton; the DIS cross section is the incoherent sum of the individual cross sections.

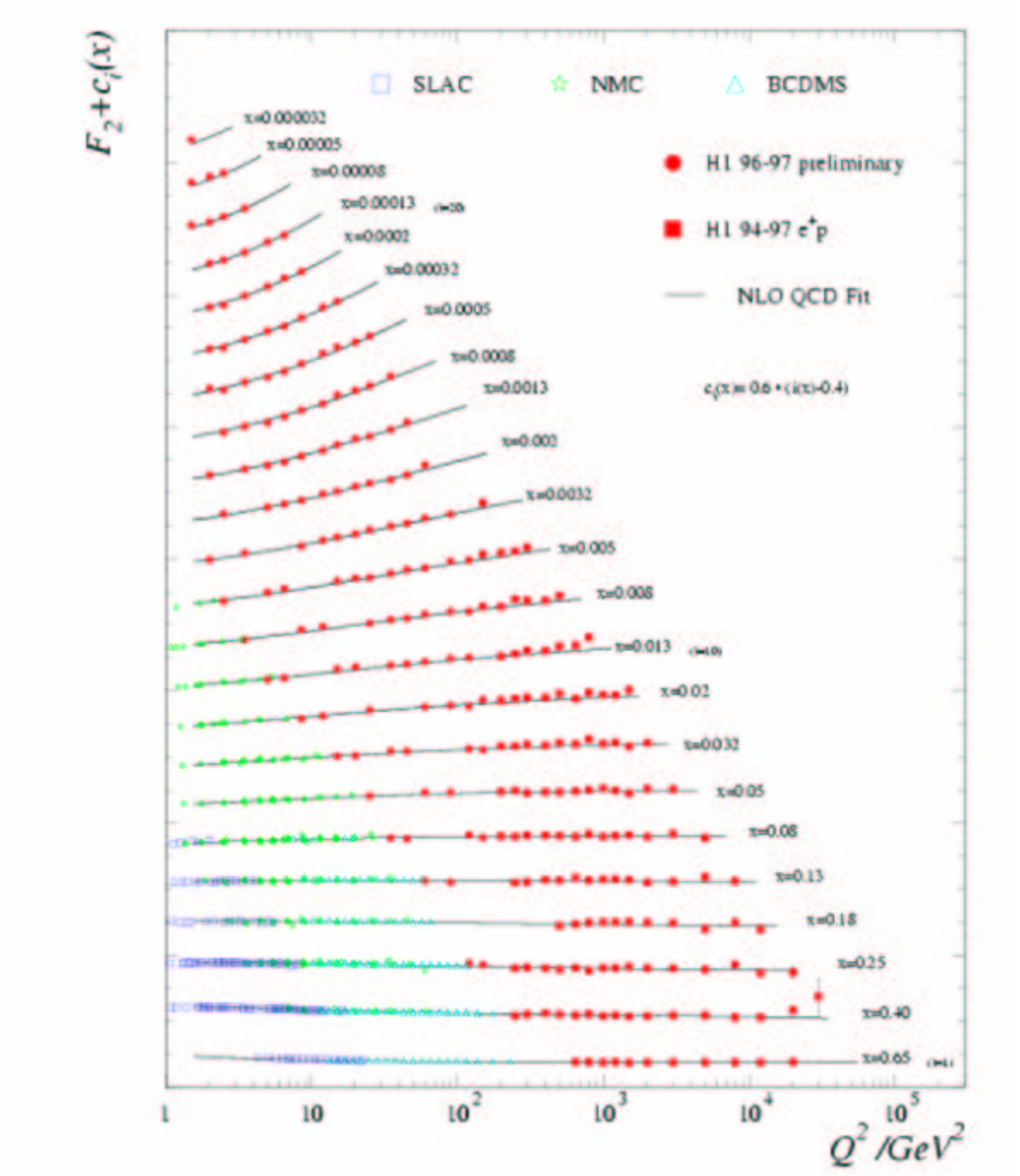

Figure 2.1: World DIS data on the unpolarized structure function of the proton, shown compared to next-to-leading order (NLO) pQCD fits.

As the proton momentum approaches infinity, x can be seen as the fraction of the proton's linear momentum carried by the parton. The size of the cross section for scattering off of a particular parton is proportional to the probability, $q(x)$, of hitting a quark of flavor q carrying momentum fraction x of the proton. $q(x)$ is known as a parton distribution function (pdf). The scaling structure functions, $F_1(x)$ and $F_2(x)$, can then be viewed as representing the probability of scattering off of a parton within the proton carrying momentum fraction x. They can be expressed in terms of the pdf's for different quark flavors as follows, where e_i indicates the electromagnetic charge of the quark of flavor i.

$$\begin{aligned} F_1(x) &= \frac{1}{2}\sum_i e_i^2 q_i(x) \\ F_2(x) &= \sum_i e_i^2 x q_i(x) \end{aligned} \tag{2.6}$$

Including all partons in the proton and not only the charged particles, which couple electromagnetically and can be probed directly by DIS, a momentum sum rule is obtained (Eq. 2.7).

$$\sum_i \int dx x f_i(x) = 1 \tag{2.7}$$

It has been found experimentally that approximately half of the proton's total momentum is carried by (electromagnetically neutral) gluons, which are present as mediators of the strong interactions among the quarks in the nucleon and dominate at low x values. In the Bjorken-scaling regime, at large x, the interactions among the quarks, i.e. the gluons, do not play a significant role. While DIS experiments cannot directly probe the gluon distribution function, g, the scaling *violations* and the evolution of the structure functions in Q^2 provide information on the gluon. The gluon distribution can be obtained from the logarithmic scaling violations of the structure function F_2, as given in Eq. 2.8.

$$g \propto dF_2/d(\ln Q^2) \tag{2.8}$$

See Section 2.1.4 for a discussion of the current status of pdf measurements.

2.1.3 pQCD, factorization, and universality

Performing calculations in QCD presents a number of challenges that quantum *electro*dynamic (QED) calculations do not. In QCD the force carriers themselves are charged; gluons carry color charge, whereas photons, the force transmitters in QED, are electrically neutral. Contributions from higher-order Feynman scattering diagrams in QED, i.e. higher powers in the electromagnetic coupling constant, $\alpha \approx 1/137$, representing additional lepton-photon vertices, quickly become negligibly small, due to the fact that α is much less than one. An analogous expansion in QCD is only possible in the regime where the coupling, $\alpha_s(Q^2)$, is small, which is generally the case for processes involving a large momentum transfer. Perturbative QCD (pQCD) is the calculation technique used in this kinematic regime.

A hadron can be viewed as a collection of free, massless partons with parallel momenta. The collinear factorization theorem in pQCD starts from this assumption of *collinearity* of the partons and hadrons, i.e. no transverse momentum of the partons in the proton with respect to the initial proton momentum, and no transverse momentum of the final-state hadron with respect to the scattered parton momentum. The collinear factorization theorem separates cross sections for hard-scattering processes into parts that are soft, or non-perturbative, and hard, or perturbative, in a self-consistent way. The soft components, pdf's and fragmentation functions (FF's), must be obtained from experimental measurements. The hard components, partonic hard-scattering cross sections, are directly calculable in pQCD. Parton distribution functions, discussed above in Section 2.1.2.2, correspond to the probability of striking a particular parton carrying momentum fraction x of the proton; FF's represent the probability of the scattered parton fragmenting into a particular final-state hadron, as a function of the fraction z of the scattered parton's momentum passed along to the final-state hadron.

The factorization theorem was developed and proven over the course of the late

1970's to the mid-1980's. Early work can be found in [118, 95, 96, 31, 32, 90]; complete proofs are available in [86, 88, 124, 65]. The factorized cross section for hard scattering in hadron-hadron collisions ($A + B \rightarrow C$) is given by Eq. 2.9,

$$d\sigma = \sum_{abc} f_a(x_a, \mu_f) \otimes f_b(x_b, \mu_f) \otimes d\hat{\sigma}_{ab}(x_a, x_b, z_c, \mu_f, \mu_{f'}) \otimes D_c^C(z_c, \mu_{f'}) \qquad (2.9)$$

in which f_a (f_b) is the density of parton a (b) in hadron A (B), D_c^C is the fragmentation function of parton c into hadron C, and μ_f and $\mu_{f'}$ are arbitrary scales known as factorization scales, which can be thought of as the amount of parton radiation incorporated into the pdf's and FF, or as the separation scale chosen to distinguish between the hard and soft components of the cross section. While the scales chosen are arbitrary, they must be chosen consistently between the soft components and the partonic hard-scattering cross section, $d\hat{\sigma}_{ab}$. The partonic cross section depends on an additional arbitrary scale, the renormalization scale, which controls the running of the strong coupling, α_s. It is common practice to set the factorization and renormalization scales to be equal; a typical value chosen is one close to the momentum transfer of the process.

The principle of *universality* in conjunction with the factorization theorem makes the formalism of pQCD extremely powerful. The principle of universality states that pdf's and FF's are the same regardless of the scattering processes involved. Universality implies the dominance at high momentum transfer of leading-twist (twist-two) contributions, with interactions only between the two hard-scattering partons. A higher-twist calculation takes into account the exchange of additional gluons between the hard-scattering partons and the nucleon remnants. The twist expansion is in successive powers of $1/Q^2$; therefore, higher-twist contributions are suppressed for processes with large momentum transfer. Because of universality, pdf's and FF's can be measured in the environment which allows the most accurate determination and then utilized as input for pQCD calculations in other processes. For example quark distribution functions can be measured in DIS experiments, in which the kinematics and thus the probed x values are straightforward to understand, then utilized

in calculations for the more complicated environment of hadron-hadron collisions. FF's are most easily measured in $e^+ + e^-$ collisions because the four-momenta of the outgoing quarks are well known. Decades of comparison between experimental cross section measurements and pQCD have provided a testing ground for the assumption of universality, and by now it is a well established and accepted principle.

While pdf's are not calculable in pQCD and are typically obtained from experiment, they are in principle calculable using other theoretical techniques such as lattice QCD. For recent calculations of structure and distribution functions on the lattice, see [128] and references therein.

Over the course of the 1970's, a formalism emerged in which it was possible to take a measurement of a pdf at a particular value of x and Q^2 and predict the pdf at the same x but different Q^2. This formalism is known as DGLAP, acknowledging important contributions from Dokshitzer, Gribov, Lipatov, Altarelli, and Parisi [101, 119, 93, 30]. DGLAP has been essential to the relevant application of factorized pQCD, which requires as input experimentally measured pdf's, which necessarily are available at only a finite set of x and Q^2 values. Using DGLAP, calculations can be done for any Q^2 value desired.

There is additionally a prescription for evolution of measured pdf's to different values of x for fixed Q^2, formulated by Balitsky, Fadin, Kuraev, and Lipatov, also in the 1970's [56, 116, 117]. The BFKL technique has demonstrated itself to be similarly useful in performing calculations at desired values of x and Q^2.

Factorized pQCD has proven to be a valuable and successful theoretical technique for many years now. Its applicability to measurements in $p + p$ collisions at RHIC will be discussed in Chapter 3.

2.1.4 Current status of the unpolarized structure of the proton

A long history of experiments, in particular DIS experiments at SLAC, CERN, and DESY, has measured the unpolarized structure of the proton well. Gluons have

been found to play an important role, carrying approximately 50% of the proton's momentum. A comprehensive review of the contributions to unpolarized proton structure made by the experiments at the HERA electron-proton collider at DESY is given in [2]. A thorough review of nucleon structure functions and pdf's is available in [89].

The wealth of accumulated data regarding the unpolarized structure of the proton is evident in Figure 2.1. Measured x values range from deep into the sea at $x = 3.2 \times 10^{-5}$ to well into the valence region at $x = 0.65$, with Q^2 values as high as 10^4 GeV^2. Periodic efforts have been made to examine all data available and perform a global analysis in order to obtain the best-fit pdf's; see for example [131].

In the 1990's it was discovered by the NMC experiment at CERN that there is a flavor asymmetry in the unpolarized sea of light quarks in the proton [33, 43]. There is a significant excess of $\bar{d}$ with respect to $\bar{u}$. Although no known symmetry requires $\bar{d}/\bar{u} = 1$, the experimental result was unexpected. It has since been confirmed by other experiments at CERN [55], Fermilab [102, 145], and DESY [4] but is still not well understood.

2.2 Polarized proton structure

2.2.1 Historical overview

For many years it was assumed that the proton's spin of $\frac{1}{2}\hbar$ was due to the spins of the three spin-$\frac{1}{2}$ valence quarks, with two oriented in one direction and one in the other. In the late 1980's, however, the EMC experiment at CERN [46, 47] discovered that only approximately $13 \pm 16\%$ of the proton's spin was due to the spin of the quarks. This surprising result became known as the "proton spin crisis." With so little of the proton's spin coming from the total quark spin ($\Delta\Sigma$), the remainder is expected to come from gluon spin contributions (Δg) and the orbital angular momentum (OAM) of both quarks and gluons (L_{g+q}), as indicated in the spin sum

rule given in Eq. 2.10, which is valid in the infinite momentum frame.

$$\frac{1}{2} = \frac{1}{2}\Delta\Sigma + \Delta g + L_{g+q} \tag{2.10}$$

Experimental work following the EMC discovery, mostly exploiting DIS, has continued to explore this problem for more than 15 years, yet there remains much to be understood. In particular, the magnitude and even sign of the gluon spin contribution to the spin of the proton remains to be determined, the flavor breakdown of the sea quark spin contributions is largely unknown, and no definitive experimental technique with which to access OAM directly has yet been proposed.

2.2.2 Polarized structure functions

Similar to the unpolarized structure functions discussed in Section 2.1.2.1, spin-dependent structure functions can also be defined. The difference in cross sections for deep-inelastic scattering of leptons polarized antiparallel and parallel to the spin of the target proton can be written as in Eq. 2.11,

$$\frac{d^2\sigma^{+-}}{dQ^2 d\nu} - \frac{d^2\sigma^{++}}{dQ^2 d\nu} = \frac{4\pi\alpha^2}{E^2 Q^2}[M(E + E'\cos\theta)G_1(\nu, Q^2) - Q^2 G_2(\nu, Q^2)] \tag{2.11}$$

in which the kinematic variables are defined as in Equations 2.1 and 2.2 and G_1 and G_2 represent polarized structure functions of the proton. In the Bjorken scaling limit of large Q^2 and ν, these structure functions depend only on x and can be given as in Eq. 2.12.

$$\begin{aligned} g_1(x) &= M^2\nu G_1(\nu, Q^2) \\ g_2(x) &= M\nu^2 G_2(\nu, Q^2) \end{aligned} \tag{2.12}$$

$g_1(x)$ can be viewed as the difference in probability of scattering off of a parton carrying momentum fraction x of the proton with parton helicity antiparallel versus parallel to the proton spin. Figure 2.2 shows the world DIS data for g_1 as a function

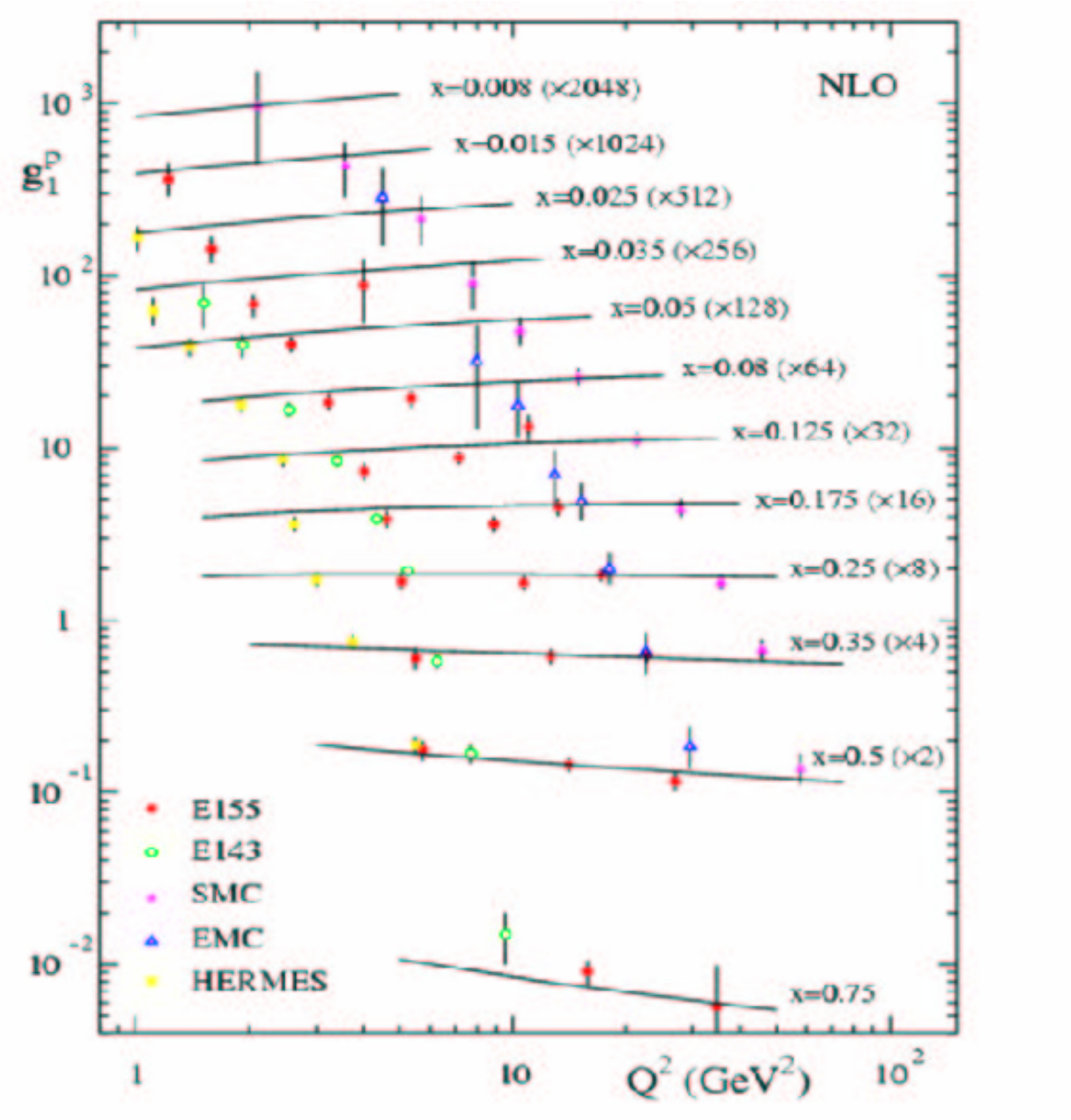

Figure 2.2: World DIS data on the polarized structure function of the proton.

of Q^2; the scaling behavior can be seen over most of the kinematic range that has been measured, which is limited compared to the kinematic range over which F_2 has been measured (refer back to Figure 2.1).

2.2.3 Polarized parton distribution functions

Polarized pdf's, or helicity distribution functions, denoted Δf, represent the *difference* in probability of scattering off of a parton f with its spin vector parallel versus antiparallel to the proton's spin, in the case of longitudinal polarization, i.e. polarization along the direction of proton motion. The transverse spin structure of the proton is discussed separately in Section 2.2.5. Helicity distributions can be obtained for example from global fits to DIS measurements of $g_1(x)$ for the proton and neutron. It is well accepted that polarized pdf's can be used as input to calculations in pQCD in a similar fashion to unpolarized pdf's. Arguments for collinear factorization involving *spin-dependent* processes are given in [79].

2.2.4 Current status of the longitudinally polarized structure of the proton

There are multiple ongoing experiments making measurements to study the polarized structure of the nucleon. The HERMES experiment at DESY makes use of the longitudinally polarized electron (or positron) beam at the HERA collider and performs DIS measurements on nucleon targets which can be longitudinally or transversely polarized. The COMPASS experiment at CERN also performs spin measurements through DIS, using a polarized muon beam from pion decays on a polarized fixed target. The PHENIX and STAR experiments at RHIC study polarized proton-proton collisions and have the ability to choose either longitudinal or transverse beam polarization, while the BRAHMS experiment at RHIC can only study transverse spin physics (see Section 4.2).

In 2004 HERMES published its final longitudinal results, the first five-flavor fit for quark polarizations measured in DIS [21]. Their results yield $\Delta u/u > 0$ and increasing with x, $\Delta d/d < 0$, and polarizations consistent with zero for $\bar{u}$, $\bar{d}$, and s quarks. In contrast to the unpolarized case, the polarized light-quark sea does not appear to have a significant flavor asymmetry.

Various different groups have performed global fits to the world data available

from DIS experiments on the helicity structure of the proton [63, 100, 104]. Figure 2.3 depicts the results of several such fits for valence quarks; Figure 2.4 for gluons and sea quarks. Both figures are taken from [104]; see the reference for details regarding the different curves. The best constraints are naturally available for valence quarks. As can be seen, the polarization for valence up quarks is significant and positive, while for valence down quarks it is significant and negative, consistent with the HERMES results mentioned above, which were not entirely available at the time of these fits. A global analysis of the sea quarks yields a negative polarization of smaller magnitude than for valence down quarks and with a larger relative uncertainty.

As mentioned above for the unpolarized case, DIS experiments cannot access the gluon directly because it does not couple electromagnetically. Consequently, Δg can only be inferred through scaling violations of the g_1 polarized structure function, as given in Eq. 2.13,

$$\Delta g \propto dg_1/d(\ln Q^2) \tag{2.13}$$

or via di-hadron or heavy flavor production, both of which provide some sensitivity to the gluon. The magnitude of Δg remains almost completely unknown, and its sign is not yet clear, as can be seen in Figure 2.4. A recent comprehensive review of the longitudinal spin structure of the proton can be found in [59].

2.2.4.1 Recent results from RHIC

From the 2003 polarized proton run at RHIC, a measurement of the longitudinal double-spin asymmetry (A_{LL}) of neutral pions at mid-rapidity has been made by PHENIX [17] for a transverse-momentum (p_T) range of 1 to 5 GeV/c. Pion production in this kinematic region is due mainly to gluon-gluon and gluon-quark scattering; thus, this measurement is sensitive to the polarized gluon distribution. (See Figure 7.1 in Chapter 7 indicating the relative contributions of different partonic scattering processes to π^0 production as a function of p_T.) The asymmetry is shown

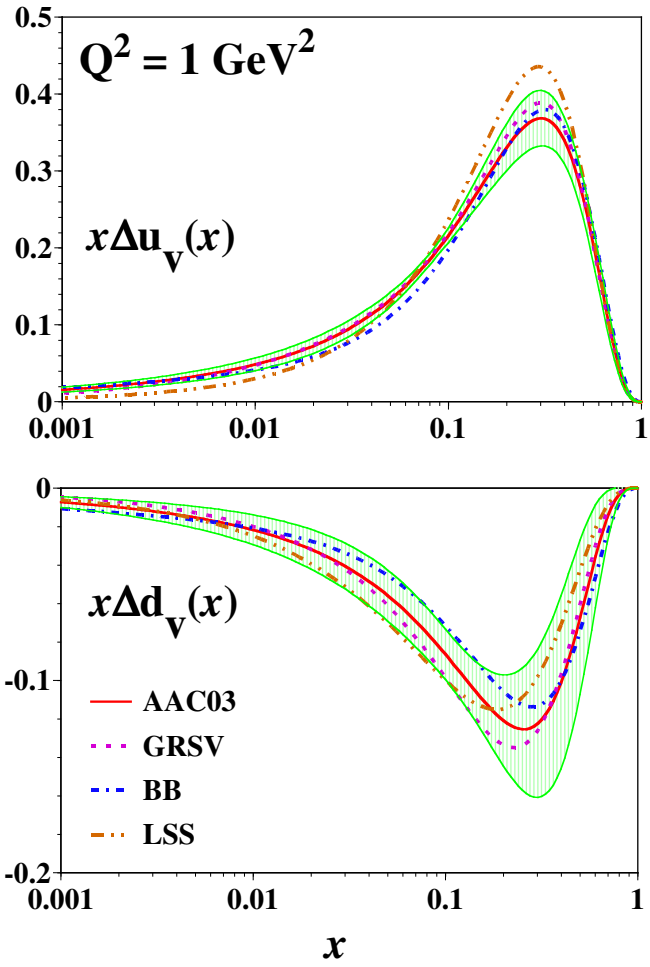

Figure 2.3: Global fits to world data for the polarized pdf's of valence quarks, taken from [104].

in Figure 2.5. The theoretical curves in the figure represent next-to-leading-order (NLO) pQCD calculations using two different assumptions for Δg [100, 107]. GRSV-std takes Δg as the value that best fits the world DIS data, and GRSV-max takes Δg to be equal to the unpolarized gluon distribution at a scale of $Q^2 = 0.6$ GeV^2.

Due to the significant contribution of gluon-gluon scattering and the isospin symmetry of the neutral pion, its double-spin asymmetry is largely insensitive to the sign of the polarized gluon distribution. Future results for A_{LL} of positive and negative pions for $p_T \gtrsim 5$ GeV/c will provide independent measurements of Δg and allow determination of its sign. See Figures 2.6 and 2.7 for expected charged

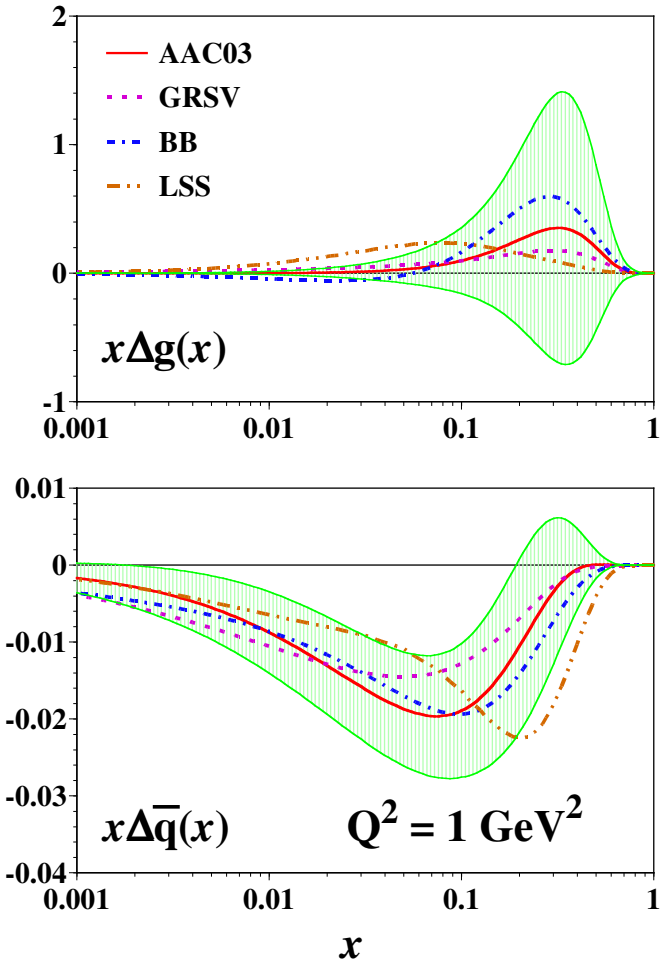

Figure 2.4: Global fits to world data for the polarized pdf's of gluons and sea quarks, taken from [104].

pion asymmetries as a function of p_T for different-sign polarized gluon distributions, calculated by M. Stratmann. PHENIX expects to be able to make a significant measurement of charged pions in the next long polarized proton run at RHIC, expected to occur in 2006 or 2007. A_{LL} of direct photon production, measurable on a slightly longer time scale, will provide a clean measurement of both the magnitude and sign of Δg, as discussed in Section 3.2.

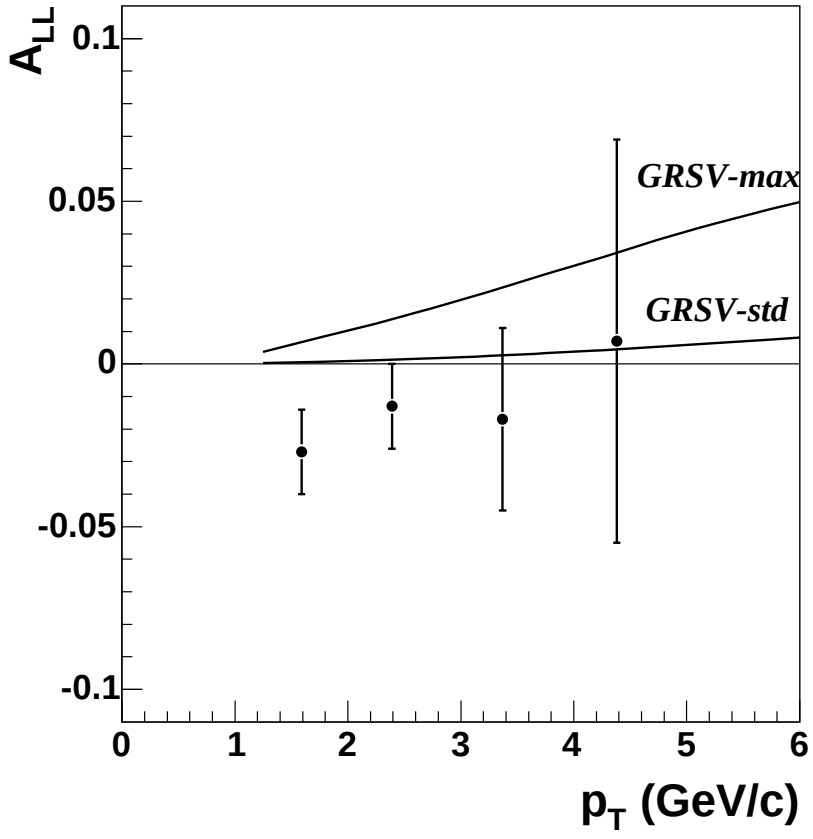

Figure 2.5: Longitudinal double-spin asymmetry for neutral pion production at PHENIX, compared to predicted asymmetries assuming various values of Δg (see text), taken from [17].

2.2.5 Understanding the transverse spin structure of the proton

2.2.5.1 Longitudinal versus transverse spin structure of the proton

The transverse spin structure of the proton cannot be determined from its longitudinal spin structure. A simple explanation for this fact is the non-commutation of Lorentz boosts and spatial rotations. Differences between the transverse and longitudinal polarization structure of the nucleon provide insight into the relativistic nature of partons bound within the nucleon. A concise description of transverse spin

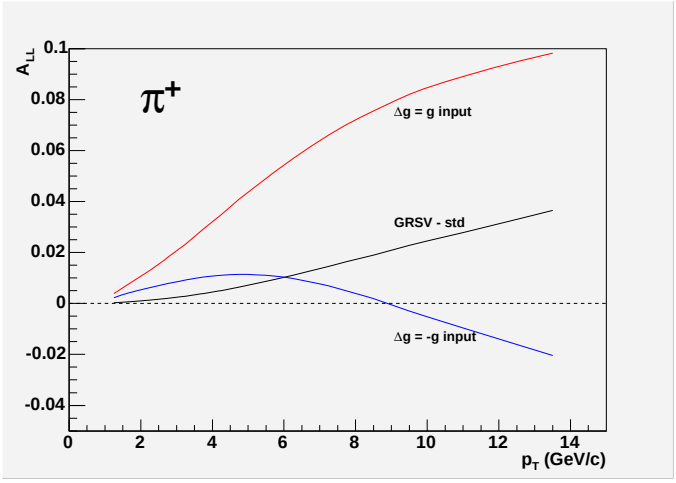

Figure 2.6: Predicted A_{LL} of positive pions for various Δg assumptions, from M. Stratmann.

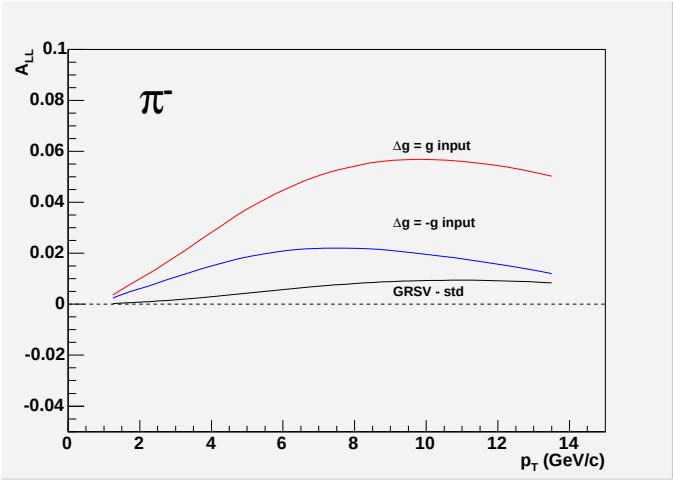

Figure 2.7: Predicted A_{LL} of positive pions for various Δg assumptions, from M. Stratmann.

structure functions and their relation to the longitudinal structure of the proton can be found in [106].

Inelastic and elastic scattering can be related by the optical theorem. Thus inelastic proton-proton or quark-proton scattering can be considered in terms of elastic quark-proton scattering. In the elastic scattering of two spin-$\frac{1}{2}$ particles, there are three different possibilities for the initial- and final-state helicities. The particles may start and end with the same helicity ($++ \rightarrow ++$), start and end

with opposite helicities ($+- \rightarrow +-$), or start with opposite helicities and change helicities in the scattering ($+- \rightarrow -+$). Linear combinations of these three helicity configurations in the scattering can be formed, corresponding to the momentum (q), helicity (Δq), and transversity (δq) distribution functions given in Eq. 2.14.

$$\begin{aligned} q &: (++ \rightarrow ++) + (+- \rightarrow +-) \\ \Delta q &: (++ \rightarrow ++) - (+- \rightarrow +-) \\ \delta q &: (+- \rightarrow -+) \end{aligned} \tag{2.14}$$

Transversity is therefore a chiral-odd, or "helicity-flip," distribution. In a transverse basis, it represents the difference in probability of scattering off a quark with transverse spin parallel versus antiparallel to a transversely polarized proton. This interpretation is directly analogous to the meaning of helicity distributions in a helicity basis. The transversity distribution was first discussed in [133]. The Soffer bound, given by Eq. 2.15, relates the transversity, helicity, and momentum distributions of the nucleon [142].

$$|2\delta q(x)| \leq q(x) + \Delta q(x) \tag{2.15}$$

Analogous to the longitudinal spin sum rule (Eq. 2.10), there is also a transverse spin sum rule [54], given in Eq. 2.16, in which L_{S_T} is the transverse component of the partonic orbital angular momentum.

$$\frac{1}{2} = \frac{1}{2} \sum_{a=q,\bar{q}} \int dx \delta q_a(x, Q^2) + \sum_{a=q,\bar{q},g} \langle L_{S_T} \rangle_a (Q^2) \tag{2.16}$$

Note the absence of a gluon spin contribution; there is no transversity distribution for gluons at leading twist because there is no mechanism to flip the helicity of (spin-1) gluons in the scattering.

While transversity is a non-perturbative object as any other pdf, the nucleon tensor charge, related to transversity ($\int_0^1 dx(\delta q(x) - \delta \bar{q}(x))$), can be calculated in lattice QCD. For a description of recent work, see [128].

In pQCD, chiral-odd functions must appear in pairs because hard scattering processes conserve helicity. One possibility is to look for observables that represent the convolution of two transversity distributions, i.e. double transverse-spin asymmetries, A_{TT}. Another possibility is to convolute transversity with a chiral-odd fragmentation function, one example of which will be discussed below.

2.2.5.2 Observation of large transverse single-spin asymmetries

The measurement of transverse single-spin asymmetries (SSA's), for example in proton-proton collisions or DIS, represents one way of probing the quark and gluon structure of transversely polarized nucleons and is the approach exploited for the measurement in this thesis. Interest in these measurements is heightened by the large transverse SSA's observed in spin-dependent proton-proton scattering experiments spanning a wide range of energies. The experimental observation of large asymmetries, with the first measurements being in the late 1970's, was initially a surprise. The leading-twist pQCD expectation was that transverse SSA's should be suppressed as $\frac{\alpha_s m_q}{\sqrt{s}}$, where m_q is the quark mass [112].

Striking asymmetries were seen at a number of spin-dependent $p+p$ scattering experiments at energies ranging from $\sqrt{s} = 5 - 10$ GeV. Asymmetries approaching 30% were observed in inclusive pion production at large Feynman-x ($x_F = 2p_L/\sqrt{s}$, where p_L is the component of particle momentum in the beam direction) and p_T up to 2 GeV/c [94, 29]. In a different kinematic region at mid-rapidity and large $x_T = 2p_T/\sqrt{s}$, asymmetries were also observed in inclusive π^0 and π^+ production but not in π^- production [40, 136, 42]. At a higher center-of-mass energy of 19.4 GeV where pQCD may be applicable, asymmetries at large x_F persisted [7, 6]; however, the asymmetry in π^0 production at mid-rapidity at this energy was found to be zero up to p_T of 4 GeV/c [8]. Non-zero transverse single-spin asymmetries were also observed in semi-inclusive DIS [19, 20, 72].

The results for neutral and charged pions at high x_F from the E704 experiment at Fermilab [6] are shown in Figure 2.8. The observed asymmetries are strikingly large, reaching a magnitude of $\sim 40\%$ for charged pions at $x_F \approx 0.8$. There is a clear

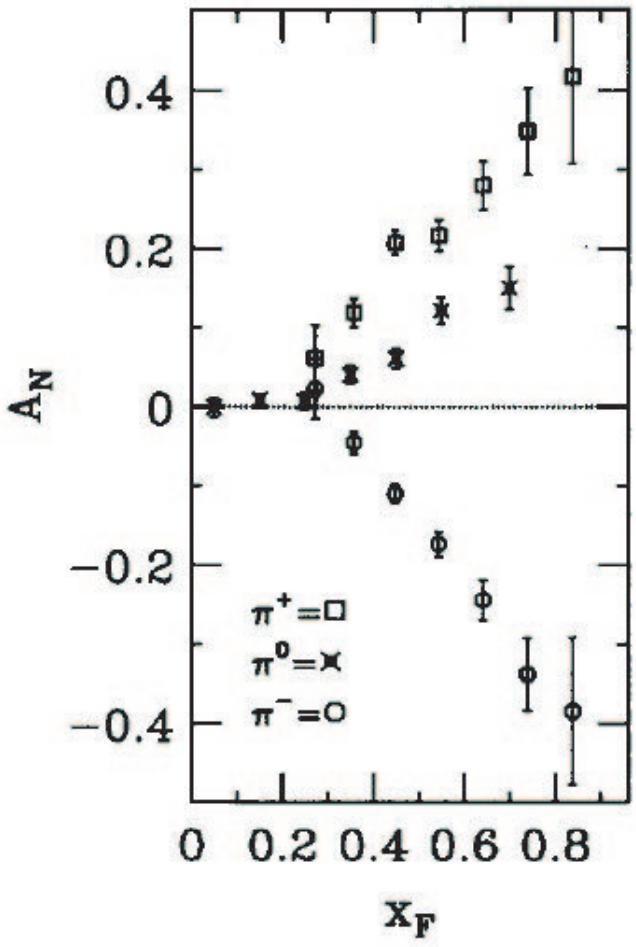

Figure 2.8: Transverse SSA of high-x_F neutral and charged pions at $\sqrt{s} = 19.4$ GeV, taken from [6].

sign dependence of the asymmetry on the pion charge, with $A_N^{\pi^+} > 0$ and $A_N^{\pi^-} < 0$ and both of approximately equal magnitude and exhibiting the same dependence on x_F. The π^0 asymmetry is also positive but with smaller magnitude.

Generally, transverse SSA's can be described by spin-momentum correlations having the form $\overrightarrow{S} \cdot (\overrightarrow{p_1} \times \overrightarrow{p_2})$, in which there are different possibilities for the spin and momentum three-vectors. Three different mechanisms, originating from different spin-momentum correlations, have been studied extensively as the possible origin of transverse SSA's in high-energy hadron collisions.

1. Transversity distributions can give rise to SSA's in combination with spin-

dependent, chiral-odd FF's, which serve as analyzers for the transverse spin of the struck quark. The Collins function [78] is an example of such a FF.

2. Quark and gluon distributions that are asymmetric in the intrinsic transverse momentum of the parton within the proton, k_T, can lead to SSA's. This idea was first suggested by Sivers [140]. The Sivers pdf can exist both for quarks and gluons, and a relation to orbital angular momentum of partons in the nucleon has been suggested [140, 76].

3. Interference between quark and gluon fields in the initial or final state can generate SSA's [132, 111].

2.2.5.3 Non-collinear pdf's and FF's

The polarized pdf's and FF's relevant to collinear factorization given in Section 2.2.3 are integrated over all possible values of k_T. In a pdf, k_T represents the transverse momentum of the parton within the proton; in a FF, it indicates the transverse momentum of the fragmenting hadron with respect to the scattered quark, or jet axis. Transverse-momentum-dependent (TMD) pdf's relate naturally to the orbital angular momentum of partons within a proton; however, a precise understanding of this relation remains unclear. If one does not assume collinearity but rather takes k_T-dependent pdf's and FF's, a rich variety of new possibilities emerges.

There are a total of eight leading-twist (twist-two) k_T-integrated and k_T-dependent quark distribution functions, as shown in Figure 2.9. Only three of these pdf's are independent of k_T. Parton distributions denoted by f indicate unpolarized quarks, g longitudinally polarized quarks, and h transversely polarized quarks. The subscript 1 signifies leading twist; the subscripts L and T denote longitudinal and transverse proton polarization, respectively. The superscript $\perp$ indicates explicit dependence on transverse momenta with a non-contracted index, as described in [125]. Note that h_{1T} is the transversity distribution, an alternative notation for δq. The field of transverse spin physics has been plagued for many years by confusing and inconsistent notation in the literature for relevant structure functions, pdf's, and FF's,

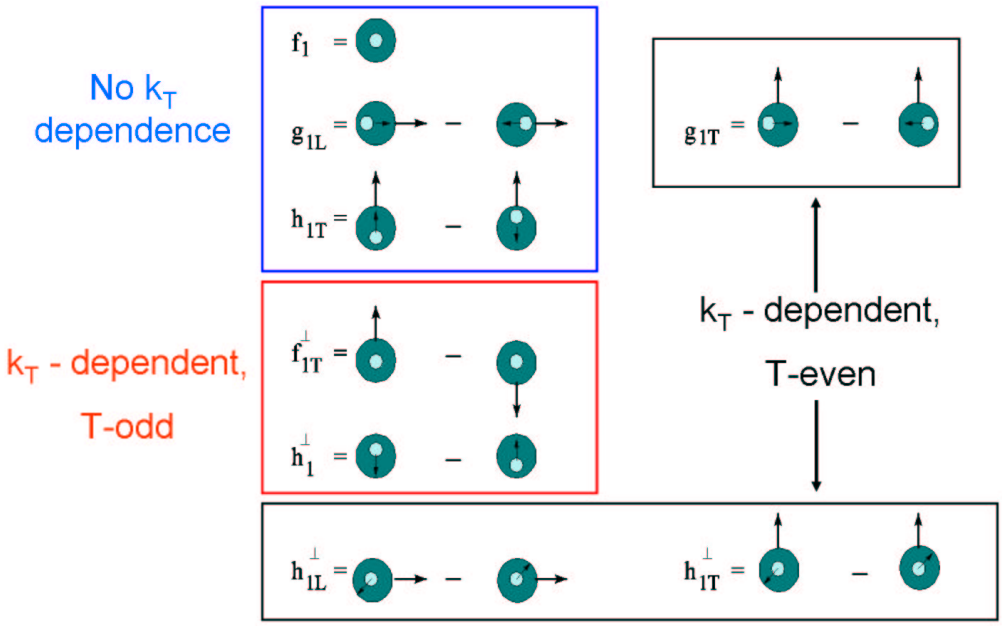

Figure 2.9: The eight leading-twist quark distribution functions, including collinear as well as k_T-dependent distributions.

as well as sign conventions for azimuthal angles in semi-inclusive DIS. One of the outcomes of the Transversity 2004 workshop in Trento, Italy was an examination and comparison of what existed in the literature and a set of recommended notation and sign conventions [49].

It should be pointed out that the factorization theorem has not been proven generally for the case of non-collinear partons. It has so far only been proven for the Drell-Yan process ($q + \overline{q} \rightarrow \ell^+ + \ell^-$) [87], with notable work also in $e^+ + e^- \rightarrow 2h + X$ and semi-inclusive DIS [83, 84, 85]. k_T-dependent factorization is therefore strictly speaking an assumption, albeit a well-accepted one in the field. Efforts are ongoing to establish the theoretical basis more firmly. Recent work considering gauge invariance in the cases of semi-inclusive DIS and Drell-Yan appears in [109, 108, 82]. Discussions of the universality and the evolution of TMD pdf's can be found in [80, 122, 67, 69] and [66, 103, 115, 105], respectively. In general, the role of k_T in hard-scattering processes is a vibrant area of research in pQCD.

2.2.5.4 Sivers effect

One of the pdf's that emerges if k_T is left unintegrated is known as the Sivers pdf, denoted as $f_{1T}^{\perp}$ and first proposed by Sivers in 1989 [140, 141]. It represents the spin-dependent asymmetry in the intrinsic k_T of the (unpolarized) partons in a transversely polarized proton. The Sivers function was for some time believed to be forbidden because it is time-reversal odd (T-odd), but it was finally realized in 2002 that final-state interactions via a soft gluon can create the necessary interference of amplitudes for the Sivers function to exist [74]. The T-odd nature of the Sivers function is now commonly referred to as "naive T-odd" to express the fact that it is not in fact forbidden in QCD.

The Sivers function plays a central role in the phenomenological Sivers effect, which has its origin in correlations of the form $\overrightarrow{S} \cdot (\overrightarrow{P} \times \overrightarrow{k_T})$, where $\overrightarrow{S}$ is the proton spin, $\overrightarrow{P}$ the proton momentum, and $\overrightarrow{k_T}$ the intrinsic transverse parton momentum in the proton. In a simplistic picture of the Sivers effect, the transverse polarization of the proton can be viewed as originating from the orbital angular momentum of the partons. A spin-dependent final-state azimuthal asymmetry is then generated by preferential scattering off of the orbiting partons in the "front" or "back" of the proton, with scattering off of the front of a proton with spin up generating particle production preferentially to the left of the polarized beam. The mechanism responsible for scattering off of a particular "side" of the proton is not entirely clear. Additional study of the Sivers effect has been performed by Burkardt as well as Hwang [75, 76].

The absolute value of the Sivers function would provide a lower bound on parton OAM. The Sivers function was originally investigated for quarks; that for gluons was first discussed only in 2003 [138]. Asymmetry calculations based on the Sivers effect to describe the E704 data and other results can be found for example in [38, 39].

2.2.5.5 Collins effect

As mentioned above, chiral-odd functions in pQCD must come in pairs because helicity is conserved in hard scattering processes. Therefore transversity, as a chiral-odd distribution, needs to be convoluted with another chiral-odd function in order to be relevant in physical processes. For production of final-state hadrons, a chiral-odd fragmentation function is one possibility. Such a FF was proposed in the early 1990's by Collins, Heppelmann, and Ladinsky [78, 79, 81].

The Collins FF, denoted $H_1^\perp$, represents the correlation between the transverse polarization of the fragmenting quark and the orientation of the hadron production plane, given by $\overrightarrow{S} \cdot (\overrightarrow{k} \times \overrightarrow{P}_h)$, in which $\overrightarrow{S}$ is the transverse polarization of the scattered quark, $\overrightarrow{k}$ is its three-momentum, and $\overrightarrow{P}_h$ is the three-momentum of the final-state hadron.

The Collins mechanism, a phenomenological mechanism incorporating the Collins FF, describes a spin-dependent azimuthal asymmetry in the distribution of hadrons within a jet. A relatively intuitive model of the Collins mechanism for the production of pseudoscalar mesons has been proposed by Artru *et al.* [45]. In this model, a transversely polarized quark is scattered out of a transversely polarized proton, with the probability of the direction of the scattered quark spin given by the transversity distribution. In order to produce a pseudoscalar (spin-0) meson such as a pion, the fragmenting quark must acquire an oppositely polarized (anti-)quark from the vacuum. If the quark-antiquark pair from the vacuum is assumed to have a total spin angular momentum of 1, conservation of angular momentum requires one unit of orbital angular momentum in the opposite direction. This orbital angular momentum of the (anti-)quark from the vacuum which subsequently binds to the scattered quark then produces a preference in azimuthal direction in the production of the final-state pion.

While it was originally believed that it was possible to explain the large transverse SSA's observed entirely in terms of the Collins effect (see for example [45]), recent work has suggested that this might not be the case [36, 120]. As yet, no consensus

has been reached.

2.2.5.6 Higher-twist effects

It has been shown that higher-twist contributions and non-zero k_T can produce the same effects in hard-scattering processes [130]. As such, there have been studies of how twist-three effects rather than TMD distributions can give rise to the large SSA's observed.

Qiu and Sterman have examined higher-twist asymmetry contributions in the initial state system, i.e. interference between quark and gluon fields in the polarized proton [132]. Similar studies have been performed by Kanazawa and Koike for quark-gluon interference in the final state, a parton fragmenting to a hadron [111]. In the initial-state case, both chiral-even and chiral-odd components are possible. It is believed that a relation of the chiral-odd twist-three initial-state effect of [132] to the Sivers mechanism may exist, but this is not completely understood.

2.2.6 Recent experimental results in transverse spin physics

RHIC data for polarized-proton collisions at $\sqrt{s} = 200$ GeV first became available in late 2001. In addition to the results from the PHENIX experiment presented in this thesis, transverse spin measurements have been made by the STAR and BRAHMS experiments at RHIC. At STAR it was discovered that large transverse SSA's persist even at RHIC energies, an order of magnitude higher than the energy for previous results [9]. They found asymmetries of up to $\sim 30\%$ in the forward production of neutral pions, as can be seen in Figure 2.10. The theoretical curves represent different fits to the E704 results discussed above [6], scaled in energy from 19.4 to 200 GeV. The general agreement of the scaled fits with the 200-GeV data suggests that the asymmetries are generated by similar mechanisms at the two energies; however, further study is needed before any definitive conclusion can be made. STAR also has preliminary asymmetry results for the production of neutral pions in the backward direction with respect to the polarized beam, for $-0.6 < x_F < -0.2$,

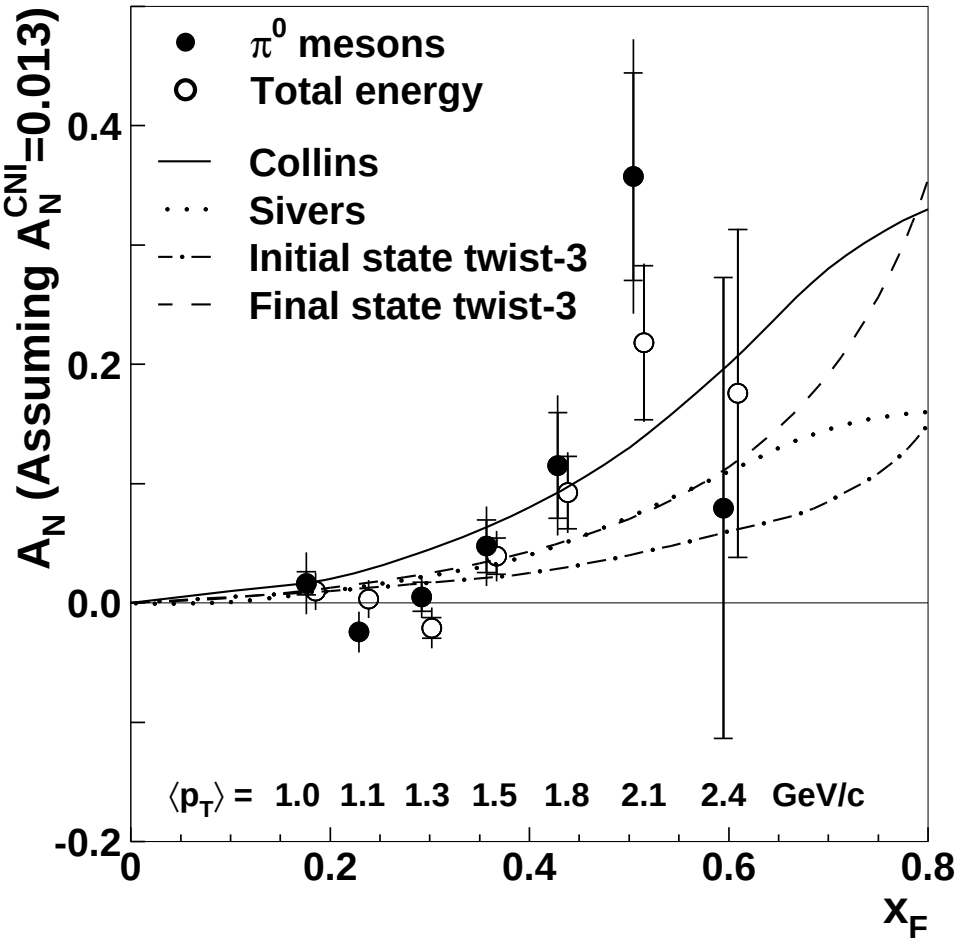

Figure 2.10: Transverse SSA of high-x_F neutral pions at $\sqrt{s} = 200$ GeV, taken from [9]. See text for more details.

which are consistent with zero [123].

BRAHMS has preliminary results for the transverse SSA's of charged pions as well as protons [146]. The charged pion asymmetries are shown in Figure 2.11. The charge dependence of the sign of the asymmetry clearly follows that observed by E704 [6]; however, the results are for low transverse-momentum values ($p_T <$ 3 GeV/c), so pQCD-based interpretations such as the Sivers and Collins effects may not be applicable. The results are in reasonable agreement with extrapolations of initial-state twist-three calculations by Qiu and Sterman.

The HERMES experiment at DESY has measured non-zero Collins and Sivers

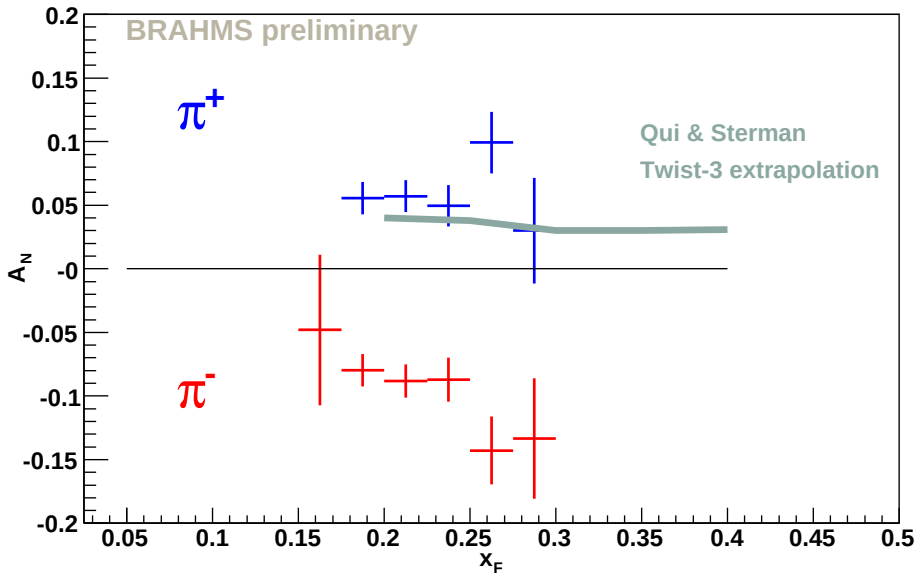

Figure 2.11: Transverse SSA's of moderate-x_F charged pions at $\sqrt{s} = 200$ GeV, taken from [146]. The theoretical curve is an extrapolation of initial-state twist-three calculations by Qiu and Sterman.

moments via semi-inclusive deep-inelastic scattering of positrons off of a hydrogen target [22]. The COMPASS experiment at CERN made a similar measurement with a muon beam on a deuteron target and found results consistent with zero [27]. The COMPASS observation is now understood to be because of asymmetry cancelations due to the isospin symmetry of the deuteron target at COMPASS. For an interpretation of the recent HERMES and COMPASS results and related predictions for transverse SSA's at RHIC, see [147].

The Collins FF for pions was recently measured by the BELLE $e^+ + e^-$ annihilation experiment at KEK [1]. The analyzing power of the Collins FF was determined to be significantly non-zero, as can be seen in Figure 2.12. This important measurement will provide vital input for factorized calculations, allowing pion production processes sensitive to the Collins mechanism to put constraints on the transversity distribution.

Despite much progress within both the experimental and theoretical arenas in

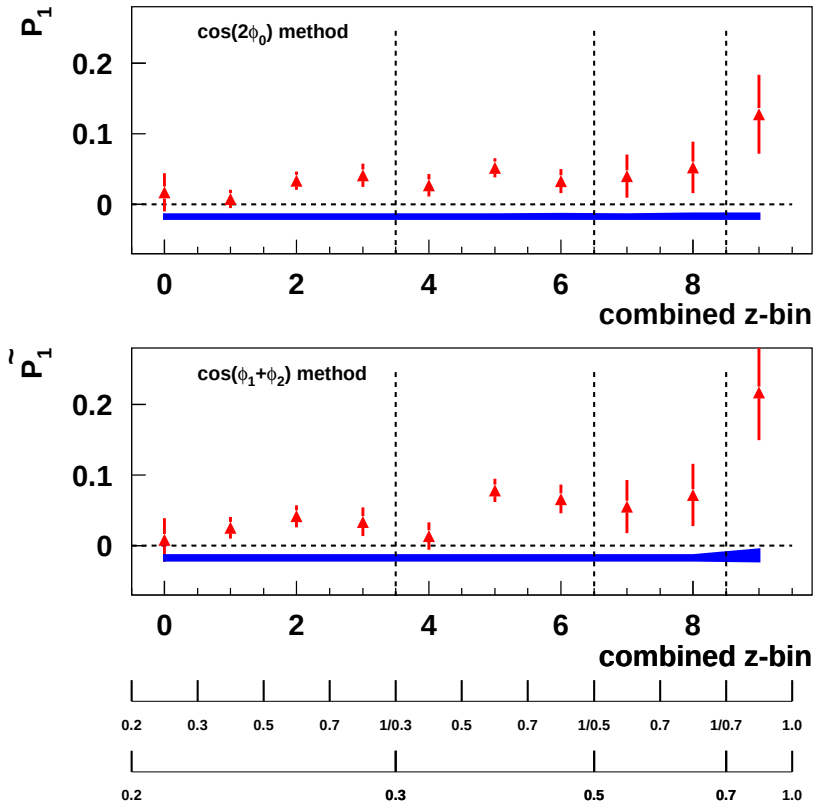

Figure 2.12: Analyzing power of the Collins FF for pions as a function of z, measured by the BELLE experiment via two different methods. See [1] for details.

recent years, no single, clear formalism has emerged in which to interpret the notable transverse spin effects that have been observed. A number of mechanisms remain as possible origins for the large transverse single-spin asymmetries, and a variety of further experimental measurements in different kinematic regions and sensitive to different partonic processes will be necessary in order to disentangle them.

Chapter 3

QCD at RHIC

RHIC was designed to study numerous aspects of QCD. The most flexible hadron collider in the world, it has so far produced gold-gold, copper-copper, deuteron-gold, and polarized proton-proton collisions at a variety of energies. Such a machine provides a rich environment for the study of QCD. The goal of colliding heavy ions at high energies is to create nuclear matter at extreme temperatures and densities, high enough that the quarks and gluons are (momentarily) not bound as hadrons but may co-exist rather as a quark-gluon plasma (QGP). Variations in collision species size and collision energy provide information on how the properties of the created matter are related to the initial conditions. Studies of small systems colliding with large nuclei (e.g. deuteron-gold) permit distinction between cold and hot nuclear effects. For a summary and review of what has been learned in the first few years of the RHIC heavy-ion program, see the evaluations from the four RHIC experiments published after the fourth year of running [44, 51, 10, 13].

The nucleon structure program at RHIC, with unique access to high-energy polarized-proton collisions, seeks to measure the helicity distributions of the partons within the proton, in particular gluon and sea-quark distributions, and to improve knowledge of the transverse spin structure of the proton. Through W boson production in eventual 500-GeV running, it will not only be possible and of interest to measure the flavor-separated helicity distributions of the sea quarks ($\Delta\bar{u}(x)$, $\Delta\bar{d}(x)$), but also the flavor-separated unpolarized pdf's ($\bar{u}(x)$, $\bar{d}(x)$). As stated in

Section 2.1.4, a large difference in the $\bar{u}$ and $\bar{d}$ content of the (unpolarized) proton has been observed and is still not well understood.

3.1 Cross section measurements and NLO pQCD

The goal of this thesis is to demonstrate how proton structure can be investigated via proton-proton collisions at RHIC. It is essential to understand how well factorized pQCD can be used to describe and interpret the RHIC data.

A number of polarization-averaged cross section measurements have been made at RHIC and compared to NLO pQCD calculations [16, 9, 15, 18]. Comparisons of data to NLO pQCD calculations are shown in Figures 3.1, 3.2, and 3.3. The most spectacular example of agreement between theory and data is seen in the mid-rapidity neutral pion measurement (Fig. 3.1) [16], which spans eight orders of magnitude and covers $1 < p_T < 15$ GeV/c. The data are compared to NLO pQCD calculations utilizing the CTEQ6M pdf's [131] and two different FF sets, differing principally in the gluon-to-pion FF. While both calculations describe the data well down to what are perhaps surprisingly low values of p_T (~ 1.5 GeV/c), the calculation incorporating the FF set of Kniel, Kramer, and Pötter (KKP) [113] is in better agreement with the data than that of Kretzer [114]. This is consistent with a larger gluon-to-pion FF. The bottom two panels in Fig. 3.1 indicate the sensitivity of the calculations to the choice of factorization and renormalization scales. The calculations have been performed using equal factorization and renormalization scales of p_T, $2p_T$, and $p_T/2$. The KKP FF set in particular exhibits relatively little scale dependence. For comparison, the renormalization and factorization scale dependence of current DIS fixed-target experiments performing spin physics measurements is several times larger. An alternative theoretical calculation is compared to these neutral pion results in [71].

There is similar agreement and similarly little scale dependence when studying the mid-rapidity production of inclusive charged hadrons, shown in Fig. 3.2 [15]. Here the calculations use the KKP FF set. As in the case of the neutral pions, the

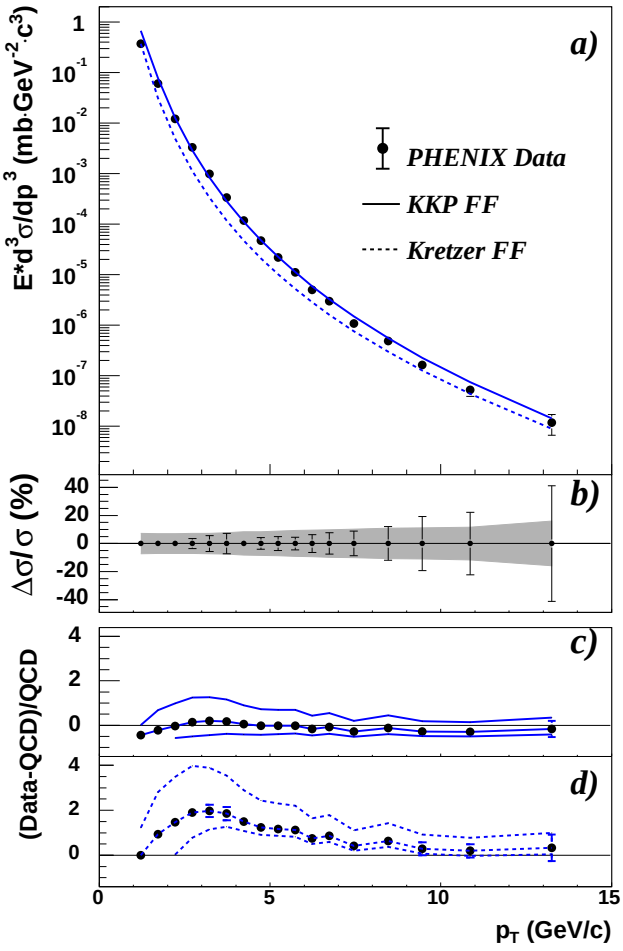

Figure 3.1: Invariant cross section versus transverse momentum for mid-rapidity neutral pion production at PHENIX, taken from [16]. The data are compared to NLO pQCD calculations using two different gluon-to-pion fragmentation functions. See text for further details.

bottom panel shows the difference between data and theory for three different scales of p_T, $2p_T$, and $p_T/2$.

Even the forward production of neutral pions at RHIC, potentially susceptible to soft (non-perturbative) contributions, has been described by pQCD with relative success, as shown in Fig. 3.3 from the STAR collaboration [9]. The two calculations given in this figure utilize the KKP and Kretzer FF sets, and similar to the mid-rapidity data, the forward data, at least for $p_T \gtrsim 1.7$ GeV/c, are in better agreement with the KKP set.

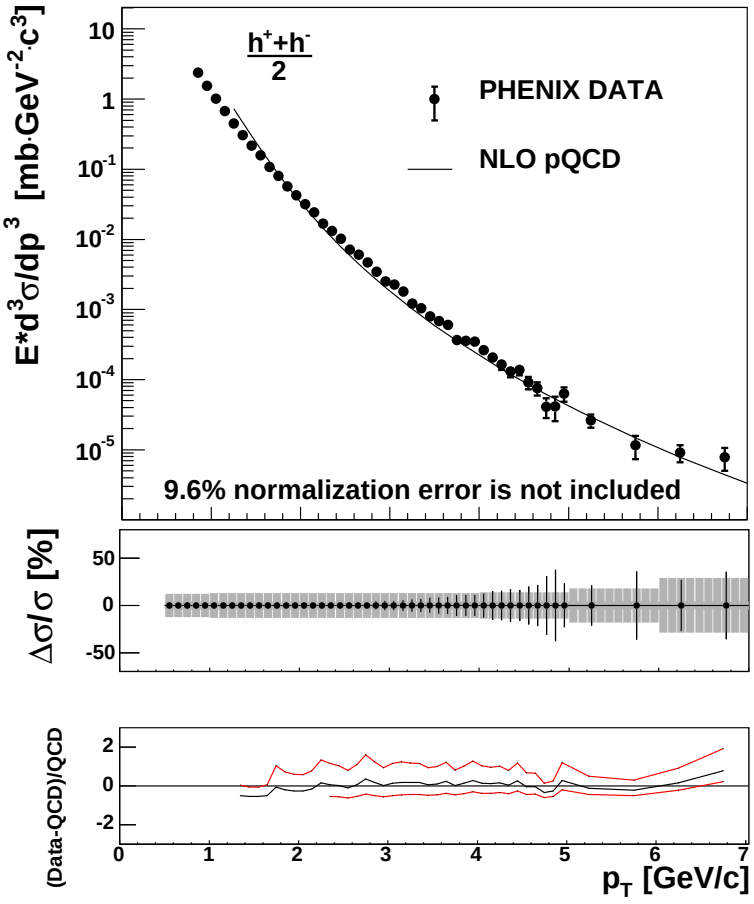

Figure 3.2: Invariant cross section versus transverse momentum for mid-rapidity charged hadron production at PHENIX, compared to NLO pQCD, taken from [15]. See text for further details.

The establishment of the ability of NLO pQCD to describe RHIC cross section data well and with little dependence on the choice of factorization and renormalization scales provides a solid foundation for using NLO pQCD to interpret in turn the *polarized* data at RHIC.

3.2 Spin asymmetries in factorized QCD

Generally, a spin asymmetry is the ratio of the difference to the sum of the spin-dependent cross sections for a particular process, given for example by Eq. 3.1 in

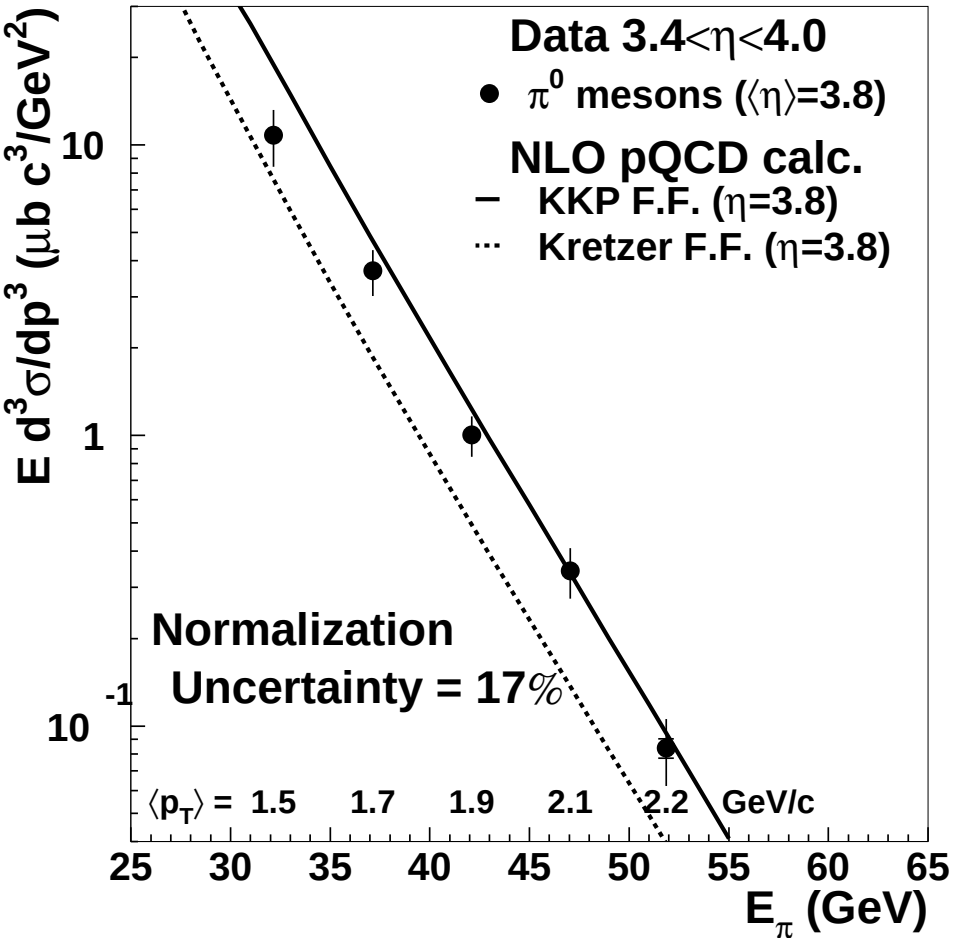

Figure 3.3: Invariant cross section versus transverse momentum for forward neutral pion production at STAR, compared to NLO pQCD calculations using two different fragmentation functions, taken from [9]. See text for further details.

the case of a double-spin asymmetry, with the arrow combinations representing same-spin and opposite-spin collisions which could be transverse or longitudinal.

$$\varepsilon = \frac{\sigma^{\uparrow\uparrow} - \sigma^{\uparrow\downarrow}}{\sigma^{\uparrow\uparrow} + \sigma^{\uparrow\downarrow}} \tag{3.1}$$

The denominator is simply the total unpolarized cross section and as such is calculable in factorized QCD as described above. The numerator is instead the difference of a convolution of spin-dependent pdf's, a spin-dependent partonic hard scattering cross section, and spin-independent FF's. As in the polarization-averaged case, the

partonic hard scattering cross section is calculable directly from perturbative theory, while the pdf's and FF's must be obtained from experimental measurements. The goal of the spin program at RHIC is to extract spin-dependent, or polarized, pdf's from asymmetry measurements. A particularly clean example is the extraction of the polarized gluon distribution, Δg, from the longitudinal double-spin asymmetry in direct photon production. At mid-rapidity and over a wide p_T range at RHIC energies, about 75% of direct photon production comes from quark-gluon Compton scattering, $q + g \rightarrow q + \gamma$. Equation 3.2 gives the asymmetry in direct photon production from this process.

$$A_{LL}^{q+g\rightarrow q+\gamma}(p_T) = \frac{\sum_q \Delta q(x_1) \bigotimes \Delta g(x_2) \bigotimes \Delta\sigma^{q+g\rightarrow q+\gamma}(\hat{s})}{\sum_q q(x_1) \bigotimes g(x_2) \bigotimes \sigma^{q+g\rightarrow q+\gamma}(\hat{s})} \tag{3.2}$$

Assuming the polarized quark distributions have already been well measured, e.g. in DIS experiments, it is relatively straightforward to extract Δg from Eq. 3.2. In practice, it is slightly more complicated, given that gluon Compton scattering is not the only process that contributes to direct photon production and the exact x values of the scattered partons are not known (see related discussion in Chapter 6). But generally, the longitudinal double-spin asymmetry in direct photon production at RHIC is expected to give a relatively clean measurement of Δg once enough statistics are available.

The above example illustrates how factorized QCD can be used to extract polarized pdf's from experimental spin asymmetries. In the future, once a variety of well-constrained measurements are available from RHIC, a global analysis of both DIS and RHIC results will be performed in order to obtain the spin-dependent pdf's that best describe all world data.

Chapter 4

Experimental setup

4.1 The Relativistic Heavy Ion Collider

The Relativistic Heavy Ion Collider (RHIC) is located at Brookhaven National Laboratory on Long Island, New York. The RHIC storage ring is 3.83 km in circumference and is designed with six interaction points (IP's), at which beam collisions are possible. Up to 112 particle bunches per ring can be injected, in which case the time between bunch crossings at the IP's is 106 ns. The design luminosity for Au+Au collisions is 2×10^{26} cm^{-2} s^{-2}; for $p+p$ collisions it is 2×10^{32} cm^{-2} s^{-2}. The design polarization for proton beams is 70%.

RHIC was built to collide heavy ions at a center-of-mass energy of up to 200 GeV per colliding nucleon pair and polarized protons at energies ranging from 50 to 500 GeV. Collision of asymmetric species, i.e. different species in the two beams, is also possible due to independent rings with independent steering magnets. The first physics run took place in 2000, with Au+Au collisions at 130 GeV per nucleon. The following four running periods included Au+Au collisions at 200, 62.4, and 19.6 GeV/nucleon, Cu+Cu collisions at 200, 62.4, and 22.4 GeV/nucleon, d+Au collisions at 200 GeV/nucleon, and polarized $p+p$ collisions at 200 GeV.

There were four major experiments developed for RHIC, three of which will continue to take data after 2005. There are two large experiments, STAR [3] and PHENIX [12], each of which have more than 500 collaborators, and two smaller

experiments, BRAHMS [5] and PHOBOS [50], having fewer than 100 collaborators each. PHENIX, STAR, and BRAHMS all have a spin-physics program as well as a heavy-ion program, while PHOBOS only studies heavy-ion physics. PHOBOS finished taking data in 2005. The four experiments were designed with some overlap and some complementarity in the physics processes they could measure. In this way it is frequently possible for one experiment to cross-check the results of another, yet each experiment has its own area of specialization. The PHENIX experiment, through which the measurement for this thesis was made, is described in detail in Section 4.3 below.

4.2 RHIC as a polarized $p + p$ collider

RHIC is the first and only polarized proton-proton collider in the world. Figure 4.1 shows a diagram of the RHIC complex including all equipment relevant for polarized proton beams. A number of technological developments and advances have made it possible to create a high-current polarized source, maintain the beam polarization throughout acceleration and storage, and obtain accurate measurements of the degree of beam polarization at various stages from the source to full-energy beams in RHIC. For an overview of RHIC as a polarized-proton collider, refer to [25].

4.2.1 RHIC-AGS complex

In the case of polarized-proton running at RHIC, a pulse of polarized H^- ions from the source (see Section 4.2.2) is accelerated to 200 MeV in the Linac, then stripped of its electrons as it is injected and captured as a single bunch of polarized protons in the Booster, which accelerates the protons to 1.5 GeV. The bunch of polarized protons is then transferred to the Alternating Gradient Synchrotron (AGS) and accelerated to 24 GeV before injection into RHIC. Each bunch is accelerated in the AGS and injected into RHIC independently, with the two RHIC rings being filled one bunch at a time. The direction of the spin vector is selected for each bunch separately.

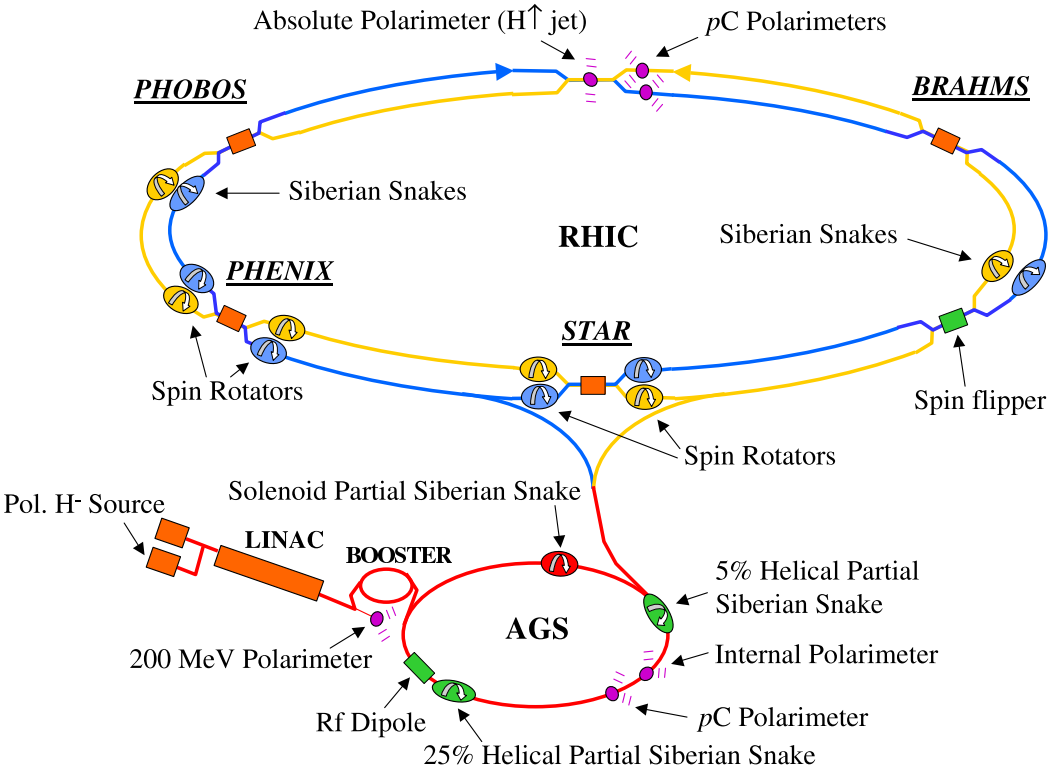

Figure 4.1: The RHIC-AGS complex as a polarized proton facility.

4.2.2 Polarized source

Polarized proton injection uses an optically-pumped polarized H^- ion source (OPPIS) constructed at TRIUMF in Canada from an OPPIS source previously used at KEK in Japan [148]. Polarization of 85% has been reached. In order to achieve a polarized proton beam, there are several steps. Unpolarized protons first pick up polarized electrons from an optically pumped rubidium vapor in a high magnetic field, forming hydrogen atoms with polarized electrons. The electron polarization is then transferred to the nucleus via static magnetic fields, creating nuclear-spin-polarized atoms. These atoms pick up a second unpolarized electron in a sodium vapor negative-ionizer cell. A pulse of polarized H^- ions is then accelerated to 200 MeV in the Linac and injected as a single bunch of polarized protons in the Booster.

4.2.3 Siberian snakes

The precession of the spin vector of a proton in a planar circular accelerator ring is given by the Thomas-BMT equation [144, 57] (Eq. 4.1),

$$\frac{d\overrightarrow{P}}{dt} = -(\frac{e}{\gamma M})(G\gamma\overrightarrow{B}_{\perp} + (1+G)\overrightarrow{B}_{\parallel}) \times \overrightarrow{P} \tag{4.1}$$

in which e is the proton charge, M is the proton mass, $\gamma = E/M$ is the relativistic boost, $G = 1.7928$ is the anomalous magnetic moment of the proton, $B_{\perp}$ indicates the magnetic field perpendicular to the plane of proton motion, typically the vertical guide field, and $B_{\parallel}$ is the longitudinal field. $\overrightarrow{P}$ here is in the frame of the proton. Note that for highly energetic protons (γ large), the $B_{\perp}$ term dominates.

Comparing the spin evolution equation to the Lorentz force equation of motion for a particle orbit in a magnetic field (Eq. 4.2),

$$\frac{d\overrightarrow{v}}{dt} = -(\frac{e}{\gamma M})\overrightarrow{B}_{\perp} \times \overrightarrow{v} \tag{4.2}$$

it becomes evident that for highly energetic protons or in a purely vertical field, the spin precesses a factor of $G\gamma$ faster than the orbital motion, meaning that the spin precesses $G\gamma$ times in a single revolution around the RHIC ring. This number is referred to as the spin tune, ν_{sp}.

There are two principal types of depolarizing resonances that may be encountered during acceleration, imperfection and intrinsic resonances. Imperfection resonances refer to those due to errors in magnet currents or alignments; intrinsic resonances are due to the (desired) beam focusing fields. A depolarizing resonance is encountered whenever the spin precession frequency is equal to the frequency with which a depolarizing field is crossed, leading to additive depolarization effects. Imperfect fields exist with a more or less random distribution around each ring. As such, resonances occur when $\nu_{sp} = G\gamma = n$, an integer, and the spin vector is at the same phase in its precession every time it encounters the same imperfect field. Intrinsic resonances occur when $\nu_{sp} = G\gamma = kP \pm \nu_y$, where k is an integer, P is the superperiodicity, or degree of regularity in the focusing-defocusing lattice, and ν_y is the vertical betatron

tune, the number of oscillations around the stable beam orbit per beam revolution, in the vertical plane. (The z-axis is taken to be in direction of proton motion, in the frame of the proton.)

Siberian snakes [92], a series of spin-rotating dipoles, so named because of the beam trajectory through the magnets and the fact that they were developed at Novosibirsk, are used to overcome both imperfection and intrinsic resonances in RHIC. There are two snakes installed in each RHIC ring at diametrically opposite points along the rings. The two snakes in each ring rotate the spin vector 180° about perpendicular horizontal axes, without perturbing the stable spin direction and with only local distortion of the beam orbit. In this way, all additive depolarizing effects from resonances are avoided.

In the AGS there is not enough space to permit a full snake. Only a partial snake [134], which rotates the spin vector by less than 180°, is possible, and complete reversal of the spin direction only occurs over the course of multiple revolutions. A partial snake of less than 10% is sufficient to overcome imperfection resonances but not intrinsic resonances in the AGS; a partial snake of 20% or more is expected to overcome both types of resonances. In the 2001-02 run, a solenoidal "warm" (non-superconducting) snake was available in the AGS. This magnet was a 5% snake; therefore, it rotated the spin direction by 9° each revolution. In order to handle intrinsic resonances, the technique used was to artificially enhance the resonances such that they were tuned to produce a complete spin flip each time one is encountered, rather than depolarization. An AC dipole magnet was used to achieve this. In 2004 the solenoidal snake was upgraded to a warm helical snake, which aided in decoupling the snake's effects on the x and y motion of the beam.

In 2005 a superconducting "cold" snake was installed in the AGS and partially commissioned; this final piece of equipment should allow achievement of the RHIC design polarization of 70%. Superconducting magnets allow a larger magnetic induction, thus a larger $\int B \cdot dl$ and greater spin rotation per revolution. The cold snake is a 25% snake, rotating the spin vector 45° each time. In 2006 the plan

is to use both the warm and cold snakes in conjunction, rotating the spin by 5% and 15% respectively, achieving the minimum rotation of 20% required to handle all resonances in the AGS. A description of the technique of using multiple partial snakes in conjunction can be found in [135].

The first polarized-proton run in 2001-2002 achieved an average beam polarization in RHIC of $\sim$ 15%. Improvements in both available hardware and machine understanding led to measured polarization values in excess of 50% in 2005. In addition, significant polarization ($\sim$ 30%) at a center-of-mass energy of 410 GeV was achieved in 2005. Further high-energy commissioning in preparation for eventual running at $\sqrt{s} = 500$ GeV will be done in 2006.

4.2.4 Polarimeters

For RHIC to provide full-energy polarized beams, the polarization must be measurable at various stages of acceleration in order to identify and address possible origins of depolarization at each step. Only RHIC polarimetry will be discussed here and not the various techniques used to measure the beam polarization further upstream in the process of acceleration. The RHIC polarimetry fulfills a three-fold purpose: (1) beam polarization measurements to provide feedback for the accelerator physicists; (2) beam polarization measurements to provide polarization values as input for the various experiments; and (3) experimental study of polarized elastic scattering.

There are two types of polarimeters installed in RHIC, designed to measure the beam polarization in the vertical direction. The proton-carbon (pC) polarimeter takes advantage of a known analyzing power, $A_N^{p\mathrm{C}} \approx 0.01$, in the elastic scattering of polarized protons with carbon atoms ($p^\uparrow + \mathrm{C} \rightarrow p^\uparrow + \mathrm{C}$) in order to measure the beam polarization. This analyzing power originates from interference between electromagnetic and hadronic elastic scattering amplitudes, which are finite due to the anomalous magnetic moment of the proton. Thus the term "Coulomb-nuclear interference" (CNI) is used to describe the process. Refer for example to [70] for a

discussion of CNI in hadronic reactions at high energies. For the pC polarimeter at RHIC, the left-right (azimuthal) asymmetry of the recoil carbon atoms is measured using an array of silicon detectors, allowing calculation of the beam polarization as in Eq. 4.3,

$$P_{\text{beam}} = \frac{1}{A_N^{p\text{C}}} \frac{\sqrt{N_L^{\uparrow} N_R^{\downarrow}} - \sqrt{N_L^{\downarrow} N_R^{\uparrow}}}{\sqrt{N_L^{\uparrow} N_R^{\downarrow}} + \sqrt{N_L^{\downarrow} N_R^{\uparrow}}} \tag{4.3}$$

where $N_L^{\uparrow}$ ($N_R^{\downarrow}$) indicates the number of recoil carbons scattering to the left (right) of the proton beam from bunches polarized up (down). (Compare to Eq. 5.8 in Section 5.6.1.)

The analyzing power in the process now utilized by the pC polarimeter to measure the RHIC beam polarization was initially measured by AGS experiment E950 [26]. However, the AGS measurement was only made to $\pm 30\%$, at a beam energy of 22 GeV, and further calibration is necessary to understand the RHIC beam polarization at 100 GeV.

Calibration of the pC polarimeter to within an absolute beam polarization of $\sim 5\%$ can be provided by a polarized hydrogen-jet-target polarimeter [149]. Such a device was commissioned at RHIC in 2004. The measurement is in some ways similar to that of the pC polarimeter. The left-right transverse single-spin asymmetry of elastically scattered *protons* due to the CNI process is measured using silicon strip detectors. However, the analyzing power for this process of elastic proton-proton scattering is not known. Instead, the hydrogen-jet-target polarization, $> 90\%$, is known to better than 2% in absolute polarization. The beam polarization can be obtained by measuring first the asymmetry due to the polarized target (ε_{tgt}), averaging over the spin states of the beam, and then similarly measuring the asymmetry due to the polarized beam (ε_{beam}), averaging over spin states of the target, which are varied in time. The same (unknown) analyzing power, A_N, applies to both cases,

and the beam polarization, P_{beam}, can be calculated as in Eq. 4.4.

$$A_N = \frac{\varepsilon_{tgt}}{P_{tgt}} = \frac{\varepsilon_{beam}}{P_{beam}} \Rightarrow P_{beam} = P_{tgt}\frac{\varepsilon_{beam}}{\varepsilon_{tgt}} \tag{4.4}$$

Once the beam polarization is determined, Eq. 4.3 can be rearranged and used in turn to measure the analyzing power of the process. Results on the measurement of the analyzing power of the jet polarimeter can be found in [127].

Low rates for this process mean that measurements performed over a long time are necessary. Because of this, the pC polarimeter, which can make measurements in less than ten seconds and provide immediate information on the stability or decay of the beam polarization from a few data points taken over the several hours of a fill, remains essential. Results obtained from the two different polarimeters can be compared offline, and in this way the pC polarimeter can be calibrated.

In order to check the *absolute* sign of the spin direction for each bunch, it is possible to measure bunch-by-bunch asymmetries, making left-right asymmetry measurements from events coming from only a single bunch number, and then take advantage of the fact that the sign of the CNI asymmetry is known from theory.

Note that if bunch-by-bunch polarimeter information were not available, as was the case in 2002, and a few individual bunches had the incorrect spin direction assigned to them, this would make the beam polarization appear to be less than its true value. The experiments in turn would utilize these same, incorrect spin assignments, diluting any raw asymmetry in particle production they may observe. However, the larger beam polarization correction would exactly compensate for the diluted raw asymmetry, and a true physics asymmetry would still result. If instead all bunches were assigned the incorrect spin direction, the measured CNI asymmetry would have the opposite sign with respect to theoretical predictions.

4.2.5 Spin rotators

The naturally stable spin direction through acceleration and storage is transverse to the proton's momentum, in the vertical direction. Spin rotator dipole magnets,

commissioned in 2003, have been used to achieve both radial and longitudinal spin [121]. The spin vector is rotated away from vertical immediately before the collision point and then back to vertical immediately afterwards. The rotators are located outside the interaction regions of the PHENIX and STAR experiments, giving both experiments the ability to choose independently whether they want longitudinally or transversely polarized collisions. The BRAHMS experiment, having no spin rotators available, focuses on transverse spin measurements. The local nature of the spin rotator magnets means that the STAR and PHENIX experiments must each have their own way of checking the direction of the spin vector at their respective interaction regions. In PHENIX this ability is provided by the local polarimeter, described in Section 4.3.3.

4.2.6 Spin flippers

In addition, RHIC is equipped with a "spin flipper," an AC dipole with a radial magnetic field installed in an area common to both beams, which flips the spin 180° bunch by bunch [52]. Spin flipping involves detuning one of the two snakes to alter the spin tune and then sweeping the spin flipper frequency of the AC dipole through the resonance to effect a controlled spin reversal. The ability to flip all the spin vectors bunch by bunch is important in order to reduce potential systematic errors from any correlations that may exist between a bunch and its spin direction. An example of such possible correlations would be a systematically larger bunch length for bunches of a particular spin sign, which could lead to subtle differences in the effective luminosity seen by the luminosity detectors and the final-state-particle detectors (e.g. the PHENIX central arms, see Section 4.3.2). Frequent or carefully timed use of the spin flipper throughout a machine fill could also facilitate balancing the relative luminosity at all interaction regions; any bunch crossings later discarded for any reason from offline analysis would represent the various spin configurations in an approximately balanced way, and the relative luminosity would not be greatly affected.

Preliminary commissioning of the spin flippers was performed in 2002 [53] but was not continued in subsequent years. Final commissioning and the beginning of regular usage is planned for 2006 or 2007.

4.3 The PHENIX experiment and detector

The PHENIX collaboration, one of the two large collaborations at RHIC, is comprised of more than 500 people from over 60 institutions around the world. The PHENIX experiment was designed to specialize in the measurement of photons, electrons, and muons as well as high-p_T probes in general over a limited acceptance, with good mass resolution and particle identification capabilities. It has an extremely high rate capability as well as sophisticated trigger systems, allowing measurement of rare processes. PHENIX produced a wealth of physics results from the first years of RHIC running and anticipates the ability to continue taking advantage of improvements in machine luminosity to further develop its program to measure rare probes.

The PHENIX detector consists of two mid-rapidity ($|\eta| < 0.35$, $\eta = -\ln\tan\frac{\theta}{2}$) spectrometer arms, primarily for identifying and tracking charged particles as well as measuring electromagnetic probes, forward spectrometer arms for identifying and tracking muons, and interaction detectors. An overview of the PHENIX detector is given in [12].

4.3.1 Interaction and vertex detectors

PHENIX has two detectors used to determine when a collision occurs and to measure the position of the event vertex in the beam direction. The beam-beam counters (BBC's) are quartz Čerenkov detectors, located at ± 1.44 m from the nominal interaction point, which measure charged particles over 2π and cover a pseudorapidity range of $3.0 < |\eta| < 3.9$. The zero-degree calorimeters (ZDC's) are hadronic calorimeters sensitive primarily to forward neutrons. They also cover 2π in azimuth, are located at ± 18 m, and extend over $4.7 < |\eta| < 5.6$. The ZDC's were

developed for RHIC rather than specifically for PHENIX and are used by all four RHIC experiments.

A minimum-bias (MB) trigger occurs when there is a minimum of one photomultiplier tube (PMT) fired in each of the two BBC's. In 200-GeV proton-proton collisions, the BBC's see approximately 50% of the total inelastic $p+p$ cross section and provide a vertex resolution of $\sim$ 2 cm. The ZDC's are sensitive to a much smaller fraction of the interactions and are not used as part of the MB trigger in $p+p$. The primary roles of the ZDC's in proton-proton collisions are in local polarimetry (see Section 4.3.3) and for systematic studies of the relative luminosity between bunch crossings with different spin configurations (see Appendix A). In gold-gold collisions both the BBC's and ZDC's observe a significant fraction of the inelastic cross section (the BBC's observe 92%), and correlations in the measured ZDC energy and BBC charge are used to determine the centrality (degree of overlap) of the heavy-ion collisions.

In the 2001-02 $p+p$ run at RHIC, when the data for the present work were taken, there was an additional interaction detector installed, the normalization trigger counter (NTC). The NTC consisted of two scintillation counters located at $\pm$40 cm from the center of the interaction diamond and covering the full azimuth. This detector was installed to improve cross section measurements in $p+p$ collisions; it was sensitive to $\sim$ 85% of the total inelastic cross section. For further discussion of the PHENIX BBC's and NTC, see [28]; for a more detailed description of the RHIC ZDC's, see [14].

4.3.2 PHENIX central arms

The PHENIX central arms cover a pseudorapidity range of $|\eta| < 0.35$ and two 90-degree intervals in azimuth, offset 33.75 degrees from vertical. See Figure 4.2 for a schematic diagram of the PHENIX central arms as instrumented in the 2001-02 RHIC run.

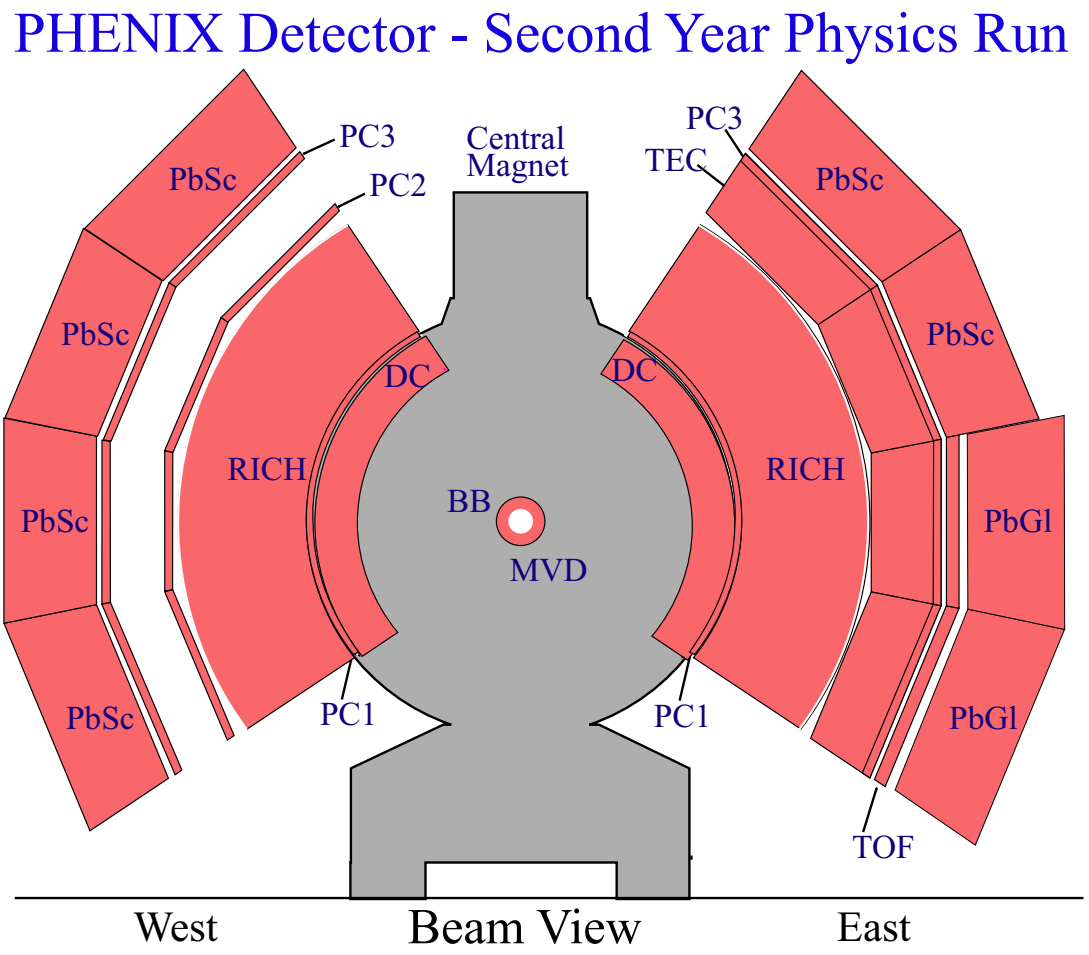

Figure 4.2: PHENIX central arms in 2001-02.

4.3.2.1 Tracking detectors

The PHENIX central tracking system is comprised of a drift chamber (DC) and pad chambers (PC's). The DC is located at $r = 2.0 - 2.4$ m from the beam pipe and covers 2 m along the beam direction. It measures the trajectories of charged particles in the $r - \phi$ direction, providing the p_T of the particle as well as ϕ information, necessary for invariant-mass reconstruction of particle pairs. The innermost plane of the PC is located immediately outside the DC; the outermost plane is immediately in front of the electromagnetic calorimeter (EMCal, see below). There is a middle PC plane located behind the ring-imaging Čerenkov detector (see below) in the West arm only. The PC's provide three-dimensional spatial point information for pattern

recognition. The outermost plane of the PC is particularly effective in providing a charged veto for particles that shower in the EMCal.

The tracking detectors are placed outside the magnetic field; there is only a residual field of < 0.6 kG present in the DC. With no inner tracking available, tracks are assumed to point back to the event vertex, provided by the BBC's. Thus charged particles that do not originate at the vertex have incorrectly reconstructed momentum, leading to low-momentum, long-lived particle decays and conversion electrons as sources of background in high-p_T charged particle analysis. The tracking detectors are described in more detail in [11].

4.3.2.2 Ring-imaging Čerenkov detector

A ring-imaging Čerenkov detector (RICH) is placed between the layers of tracking subsystems. Its main purpose is electron-pion discrimination. It has been filled with CO_2 gas in the first five years of RHIC running. The momentum threshold for production of Čerenkov radiation by charged pions in CO_2 is 4.7 GeV/c, while for electrons it is 0.017 GeV/c. In the p_T range between these two values, there is excellent e/π separation. Further discussion of the RICH can be found in [23].

4.3.2.3 Electromagnetic calorimeter

The EMCal is designed to measure the energy and position of electrons and photons. It also contributes significantly to particle identification through energy-position measurements as well as timing information. It is the outermost subsystem in the central arms, located at $\sim$ 5 m in r. The EMCal in the West arm is divided into four sectors of a lead-scintillator (PbSc) sampling calorimeter; in the East arm there are two sectors of PbSc and two of a lead-glass (PbGl) Čerenkov calorimeter. The two kinds of detectors rely on significantly different physics processes and as such can be useful in making systematic comparisons. The PbGl excels in energy measurements and is less sensitive to hadrons, while the PbSc has better timing resolution. The nominal energy resolution of the PbSc is $8.1\%/\sqrt{E\ (\mathrm{GeV})} \oplus 2.1\%$; the PbGl has a nominal energy resolution of $6\%/\sqrt{E\ (\mathrm{GeV})}$. The intrinsic timing

resolution is $\sim$ 200 ps for the PbSc and $\sim$ 300 ps for the PbGl. While designed as an electromagnetic calorimeter, the EMCal is approximately 1 nuclear interaction length and offers some sensitivity to hadrons. Detailed description of the EMCal is available in [41].

4.3.3 Local polarimeter

In order to provide local polarimetry, a shower maximum detector (SMD) was added to the PHENIX ZDC's. The ZDC/SMD combination measures both the energy and position of forward neutrons. A large ($\sim -11\%$) transverse single-spin azimuthal asymmetry for neutrons with $p_T < 0.5$ GeV/c has been observed [60]. This asymmetry can be exploited to measure the degree to which the beam polarization is vertically transverse, radially transverse, or longitudinal. Maxima and minima of particle production are expected at right angles in ϕ to the spin vector. For longitudinal polarization, no azimuthal asymmetry is expected; a non-zero longitudinal single-spin asymmetry would violate parity and is forbidden in particle production via strong and electromagnetic processes. Figure 4.3 shows the observed asymmetry as a function of ϕ for the cases of vertical and longitudinal beam polarization. The expected maxima and minima at $\pm\frac{\pi}{2}$ can be seen for vertical polarization, and the asymmetry is approximately consistent with zero in the case of longitudinal polarization.

4.3.4 Muon arms

The forward spectrometer arms in PHENIX are designed to identify and measure prompt and decay muons. They cover 2π in azimuth and a pseudorapidity range of $1.2 < |\eta| < 2.4$. A high-resolution tracker in a radial magnetic field is followed by alternating layers of absorber and low-resolution tracking for muon identification. The tracker magnet also serves as a hadron absorber. The design is to reject pions and kaons at a level of 10^{-3}. In Figure 4.4, the muon arms are shown as instrumented for the 2001-02 RHIC run. Note that only the south arm was available for data

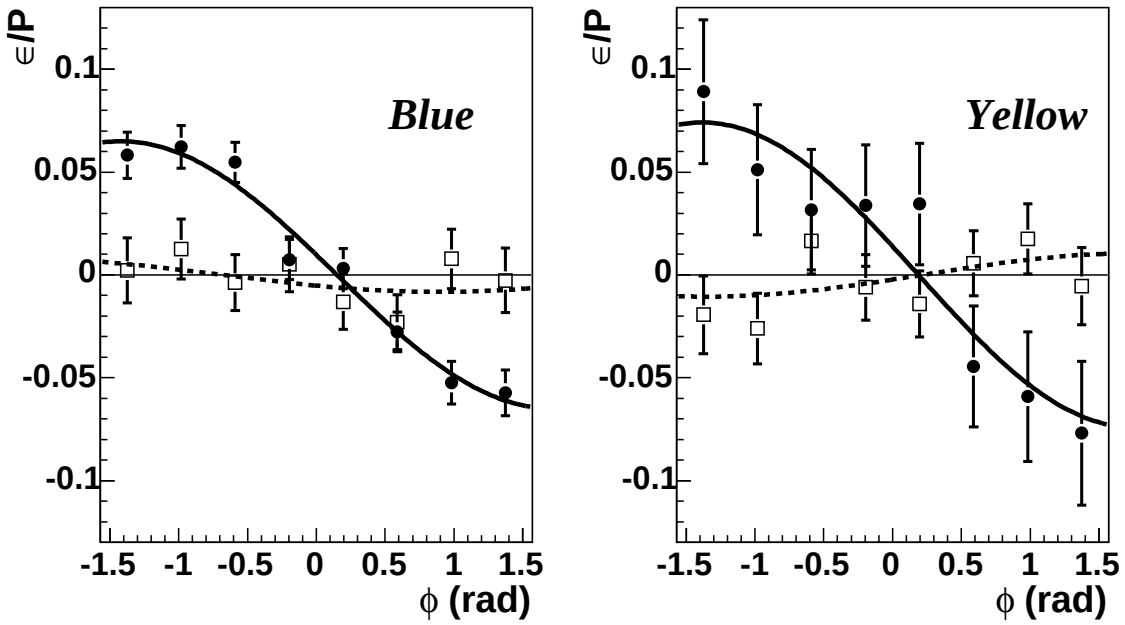

Figure 4.3: PHENIX local polarimeter measurement. The raw asymmetry in neutron production divided by the degree of beam polarization is shown vs. azimuthal angle. The solid points are with the spin rotators off (vertical polarization); the open points are with the spin rotators on (longitudinal polarization).

taking in this year; the north arm was completed in 2003. See [24] for further information regarding the muon arms.

4.3.5 Detectors and triggers used in the analysis for this thesis

To measure the energy and position of photons from neutral pion decays, the present analysis utilized both the PbSc and PbGl electromagnetic calorimeters. The central arm tracking detectors were used to eliminate EMCal clusters associated with charged tracks. The BBC's were used to provide a MB trigger. The EMCal-RICH trigger (ERT, described below) was used to select events with high-p_T photons.

4.3.5.1 EMCal-RICH trigger

The hardware-level rare-event triggers implemented in PHENIX include an EMCal-RICH trigger (ERT). The ERT can be used as a high-energy photon trigger or in con-

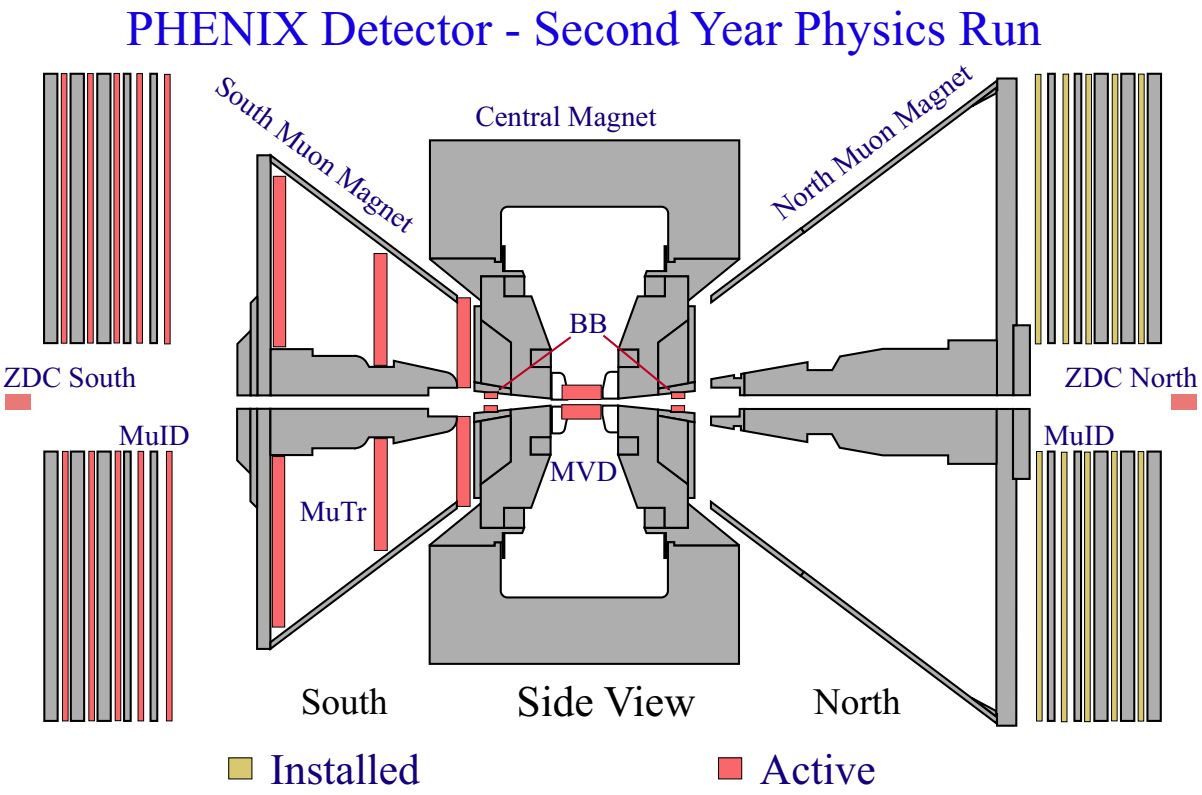

Figure 4.4: PHENIX muon arms in 2001-02.

junction with the RICH as an electron trigger. The EMCal towers are grouped into trigger tiles, over which the deposited energy is summed, and an event is recorded if the total energy in a tile is above a preset threshold. The tiles are configured to be non-overlapping sets of 2×2-tower regions and overlapping sets of 4×4-tower regions. Up to three different energy thresholds may be set for the 4×4-tower tile size. The electron trigger utilizes the 2×2-tower tile size.

4.3.5.2 EMCal calibration

There was an initial series of EMCal calibrations performed, both before detector installation and *in situ* in the PHENIX interaction region, descriptions of which can be found in [41]. During regular data taking, a pulsed UV laser is utilized to provide EMCal calibration information. In offline analysis, three major techniques used to calibrate the EMCal energy are examining the location of the π^0 mass peak position,

the energy-momentum ratio for electrons, and the location of the minimum-ionizing peak.

Chapter 5

Data and analysis

5.1 Overview

The left-right transverse single-spin asymmetry, A_N, of mid-rapidity neutral pions was measured from the data taken during the first polarized proton run at RHIC, in late 2001 and early 2002. To make a single-spin measurement with two polarized beams, the spin states of only one beam at a time were taken into account, averaging over the spin states of the other. Neutral pions were reconstructed via their decay to two photons. The general procedure was to obtain the spin-dependent π^0 yields for each machine fill, calculate the raw (uncorrected) asymmetries for each fill as a function of p_T, make fill-by-fill polarization corrections, and then average the asymmetries over all fills. The results were corrected for estimated contributions to the asymmetry from the background under the π^0 invariant-mass peak by measuring and subtracting the asymmetry of the background immediately around the peak in mass. Various studies were subsequently performed as checks. The final results of this analysis have been published in *Physical Review Letters* [15].

5.2 Data selection and quality

Prior to this spin-asymmetry analysis, a polarization-averaged cross section measurement was made for neutral pion production at PHENIX and published in [16]. The analysis completed for this thesis started with the data sample utilized in the

cross section analysis, and then additional quality cuts relevant to a spin-dependent analysis were made.

The data used were from ERT 2×2-triggered events. The 2×2 energy threshold was ~ 0.8 GeV in the 2001-02 run. The triggered sample had much better statistics at higher transverse momenta than the MB sample, but the MB sample was also analyzed for comparison purposes. 18.7 million triggered events were analyzed, corresponding to approximately 880 million sampled MB events. The detector subsystems involved were the BBC and the EMCal, including both the lead scintillator (PbSc) and lead glass (PbGl). Additionally, the drift chamber and pad chambers were used to veto clusters in the EMCal produced by charged particles. Basic checks on the quality of output from all involved subsystems were performed.

5.2.1 Fill and run selection

In making $\pi^0 \rightarrow \gamma + \gamma$ spin-asymmetry or cross section measurements, it is essential to ascertain that the EMCal was working properly when the analyzed runs were taken. The uppermost sector of PbSc in the West arm had been omitted from the cross section analysis due to problems with electronics noise during data taking. A number of runs had been eliminated from that analysis because of EMCal towers with unusually high or low numbers of hits that were not among the known and understood hot or dead EMCal towers. In addition, a sequence of runs had been omitted because of the ERT. The energy threshold for the ERT 2×2 trigger had been adjusted in the early part of the data-taking period, and only runs taken after the threshold was stable at ~ 0.8 GeV were included. Runs from a total of twenty machine fills were included in the final cross section analysis.

For the present analysis, six of the twenty fills used in the cross section analysis were removed. Two were removed because no polarization measurement was available. Three additional fills were removed because a number of bad runs from these fills were found in a study investigating the stability of the MB trigger. One fill was removed because it had an unusual spin pattern.

5.2.2 Event and crossing selection

An offline BBC event vertex within ±30 cm of the nominal interaction point was required for all events. The acceptance of the central arms is approximately constant for collisions taking place in this region. The BBC vertex resolution was $\sim$ 2 cm. The online vertex cut for the MB trigger in the 2001-02 run was ±75 cm.

Spin-sorting the events requires keeping track of the direction of the spin vector for the polarized bunch in the bunch crossing that produced the event (simply the term *crossing* will be used henceforth). Note that the same pairs of bunches in the two rings collide at the same interaction points each time, but the same pairs of bunches do not necessarily collide at the different interaction points, i.e. at different experiments. Data quality was checked on a crossing-by-crossing basis. For the entire 2001-02 $p+p$ data set, four crossings out of a nominal 60 were consistently removed from this analysis. These four crossings had unusually low luminosities because they were regularly affected by either injection or steering activities in the ring. In addition, the ten crossings in which only one beam had filled bunches while the other had a five-crossing beam-abort gap were removed from all fills. Any events occurring in these crossings were beam-background collisions rather than beam-beam collisions.

There were two bunch-by-bunch spin patterns utilized in the 2001-02 run, one in the initial period of data taking and the other in the latter period. The second pattern included bunches with zero polarization so that they would be available for systematic checks, in particular for the pC polarimeter. For fills with the second polarization pattern, one additional crossing was eliminated from this analysis because it had zero polarization. The other zero-polarization crossings corresponded to two of the low-luminosity bunches that had already been eliminated. A schematic illustration of the first spin pattern is given in Figure 5.1. Note that the spin patterns are selected to provide approximately equal numbers of same-spin and opposite-spin crossings for each experiment. They are also chosen so that the spin combinations are different every crossing. This rapid change in spin combinations, occurring on

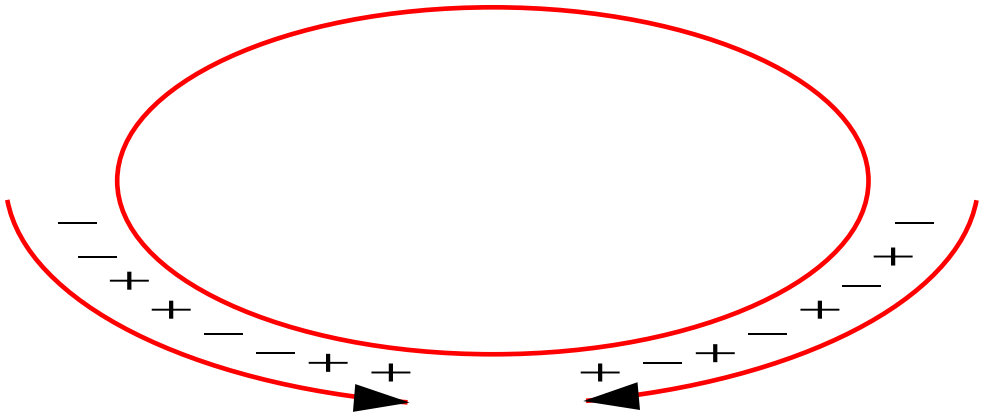

Figure 5.1: Schematic illustration of the first spin pattern, with no zero-polarization crossings. In one beam, alternate bunches have opposite spin directions; in the other beam, the spin direction changes every two bunches.

the order of every hundred nanoseconds, greatly reduces potential time-dependent systematic uncertainties.

Crossing-by-crossing luminosity measurements from the pC polarimeter provided a fill-dependent bad crossing list. A total of four individual crossings from two fills were discarded from the analysis based on this information.

5.3 EMCal-RICH trigger

All data used for the final asymmetry results were from events accepted by the 2×2-tower tile trigger for high-p_T (high energy at mid-rapidity) photons. The 2×2 trigger had an average rejection factor of 47, i.e. only accepted on average one in 47 MB events. It had a 78% efficiency for neutral pions above $p_T \approx 3.5$ GeV/c, as can be seen in Fig. 5.2.

The effects of the trigger on the mean p_T of the photon pairs falling under the π^0 peak can be seen in Table 5.1. The trigger raised the mean p_T in the 1-2 GeV/c bin significantly because it was still well below its maximum efficiency in this transverse momentum range. The trigger had little effect on the mean p_T of higher p_T bins.

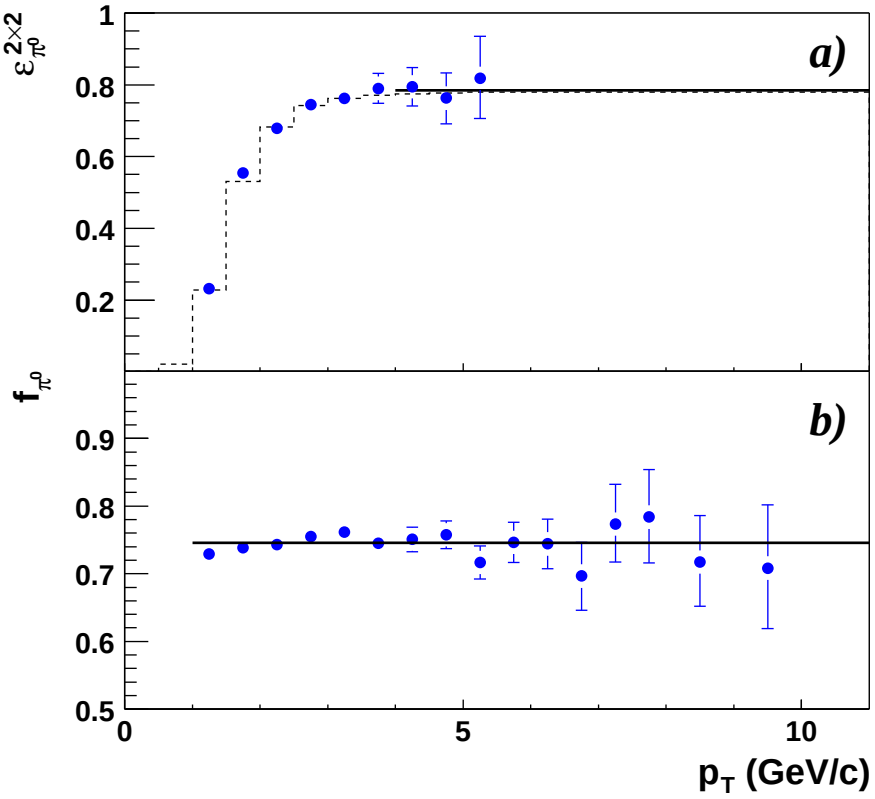

Figure 5.2: a) The 2×2 trigger efficiency for neutral pions, as a function of pion transverse momentum. The dashed line shows a Monte Carlo simulation based on trigger tile efficiencies, and the solid line indicates an upper limit on the π^0 efficiency based on the number of active trigger tiles. b) The fraction of the π^0 yield satisfying the MB trigger condition. The solid line is the fit of the data to a constant. The figure is taken from [16].

p_T bin (GeV/c)	$< p_T >$ MB (GeV/c)	$< p_T > 2 \times 2$ (GeV/c)
1-2	1.27	1.38
2-3	2.32	2.33
3-4	3.33	3.35
4-5	4.39	4.36

Table 5.1: Mean p_T of photon pairs under the π^0 mass peak for MB and 2×2-triggered data.

p_T (GeV/c)	π^0 yield	Peak width (MeV/c^2)
1-2	658k	13.2
2-3	143k	11.2
3-4	22k	10.4
4-5	4k	10.6

Table 5.2: π^0 yields obtained after background subtraction; 1σ π^0 peak widths from a Gaussian fit.

5.4 Reduction of background

In order to understand the background contribution to the π^0 mass peak and obtain π^0 yields, the invariant-mass spectrum for photon pairs was fitted. The mass peak was fitted to a Gaussian and the combinatorial background to a second-degree polynomial. The π^0 yields per p_T bin, given in Table 5.2, were obtained by subtracting the background from the total number of pairs in the peak. An example fitted and subtracted invariant-mass spectrum for $1 < p_T < 2$ GeV/c is shown in Figure 5.3. Mass bins of 10 MeV/c^2 were used in this analysis.

The 1σ peak widths from a Gaussian fit to the 120-160 MeV/c^2 mass region are shown in Table 5.2. The transverse momentum spectrum for the pairs falling under the π^0 mass peak can be seen in Figure 5.4.

Several cuts were made in order to reduce the background in the photon pair sample. Mismatched true photons, coming from two different particles, were the main source of background. Other sources of background included electrons, hadrons that deposited energy in the EMCal, or secondary particles not coming from the event vertex, all of which could lead to false combinatorial pairs whose mass fell under the π^0 mass peak, either in combination with each other or with true photons from neutral pions. The cuts were:

- Minimum energy cut of 0.1 GeV in the PbSc, 0.2 GeV in the PbGl. This cut effectively eliminated pairs in which one photon carried nearly all the energy and the other very little. The same minimum energy cut was used for the π^0 A_{LL} analysis, the results of which were published in [17].

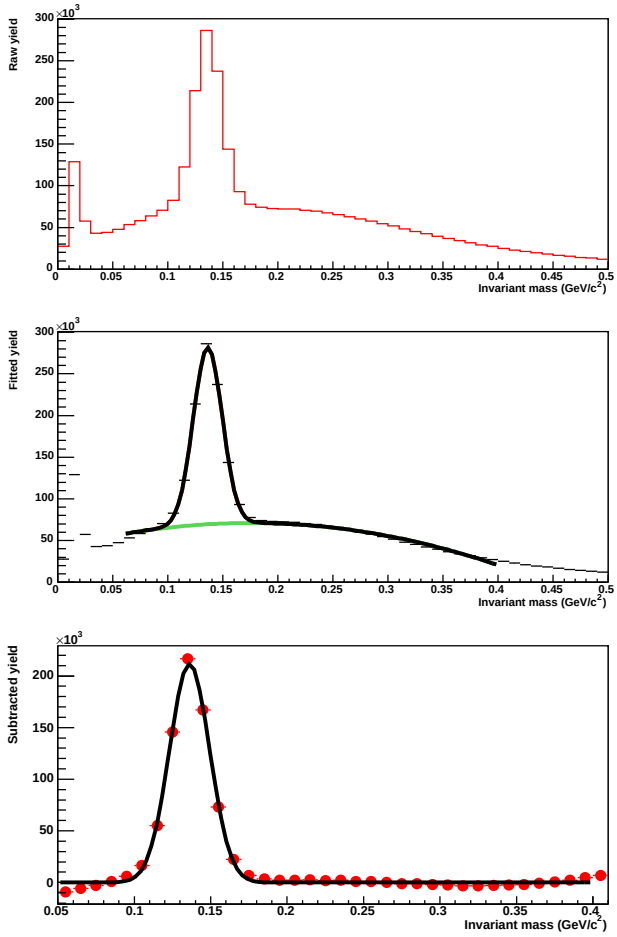

Figure 5.3: Top panel: Invariant-mass spectrum for $1 < p_T < 2$ GeV/c photon pairs. Middle panel: Fitted spectrum. Bottom panel: Subtracted spectrum.

- Charged veto cut. All EMCal clusters within a 10-cm radius of a projected charged-track position onto the EMCal were excluded.

- Shower shape cut in the PbSc to select clusters displaying the expected shape for energy deposits from photon hits. The analogous information for the PbGl was not available.

While a time-of-flight (TOF) cut could have potentially offered additional hadron-photon discrimination, the EMCal TOF was not well calibrated in the 2001-02 data set, so no timing cut was performed.

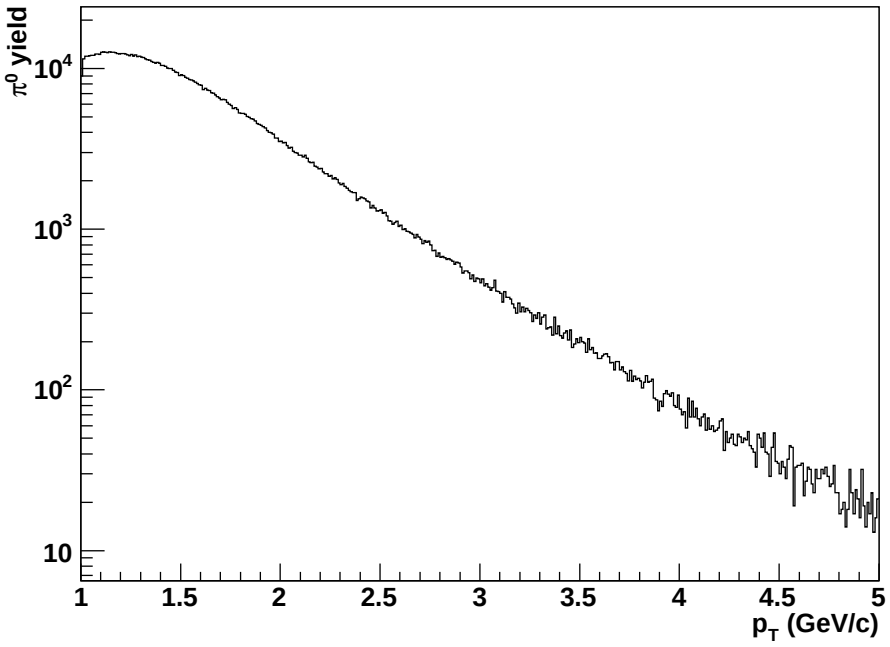

Figure 5.4: Raw transverse momentum spectrum for photon pairs falling under the π^0 mass peak.

p_T (GeV/c)	Background fraction (%)	
	Before cuts	After cuts
1-2	58	34
2-3	23	12
3-4	12	6
4-5	9	5

Table 5.3: Reduction of background contribution to the π^0 mass peak, taken as 120-160 MeV/c^2, before and after background-removal cuts.

The background fraction, r, was obtained by taking the ratio of the fitted background to the total number of pairs falling within the mass peak. This fraction before and after the extra cuts were performed is shown in Table 5.3. Significant reduction was achieved in the lowest two p_T bins.

5.5 Asymmetry calculation

5.5.1 Overview

The two counter-circulating RHIC beams are frequently referred to as "blue" and "yellow," named after the colored stripes painted on the respective magnet systems. The blue beam orbits clockwise, the yellow beam counter-clockwise. Both beams are typically polarized, as they were in the 2001-02 data-taking period. In order to make a single-spin asymmetry measurement, the spin direction of the bunches in only one beam was considered at a time, averaging over the spin direction of the bunches in the other. Results from the blue and yellow beams were obtained separately and subsequently combined.

The formula used to calculate asymmetry values is given in Eq. 5.1,

$$A_N = \frac{1}{P_{\text{beam}}} \frac{1}{\langle |\cos\varphi| \rangle} \frac{N^{\uparrow} - \mathcal{R} N^{\downarrow}}{N^{\uparrow} + \mathcal{R} N^{\downarrow}} \tag{5.1}$$

in which P_{beam} is the beam polarization, $\frac{1}{\langle |\cos\varphi| \rangle}$ is an azimuthal acceptance correction factor (see below), $N^{\uparrow}$ ($N^{\downarrow}$) is the neutral pion yield from crossings with the polarized bunch spin up (down), and $\mathcal{R} = \mathcal{L}^{\uparrow}/\mathcal{L}^{\downarrow}$ is the relative luminosity between crossings having the polarized bunch with spin up versus down. As A_N is a left-right asymmetry, Eq. 5.1 must be used separately for the two detector arms. As given, it applies to yields to the left of the polarized beam; an overall minus sign is required for yields observed to the right of the polarized beam. Asymmetry results for the left and right detector arms were obtained separately and then combined. The correction factors and relative luminosity are discussed further below.

The beam polarization varies fill by fill. Thus the asymmetry is determined for every fill, then averaged over all fills. An example of fill-by-fill asymmetries is given in Figure 5.5; this figure also gives an indication of the fill-by-fill stability of the measured asymmetry. Large observed variation among fills could indicate systematic errors. (Note that all uncertainties given in figures and tables are statistical unless stated otherwise.) Table 5.4 shows results obtained from Eq. 5.1 for the two

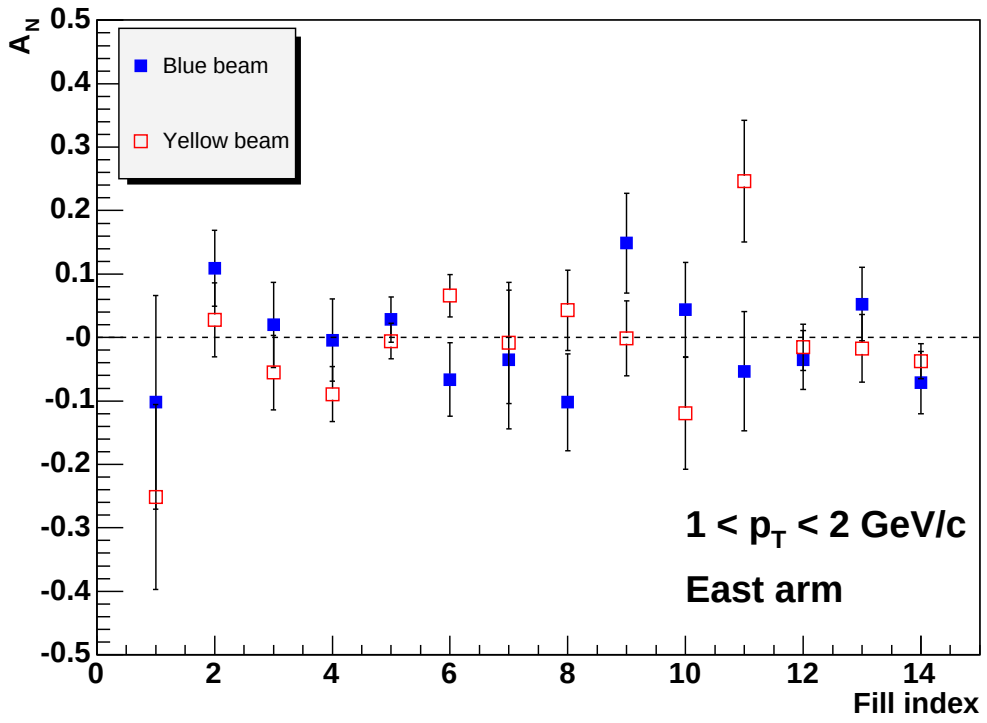

Figure 5.5: Fill-by-fill asymmetry results for the two beams.

detector arms for triggered events. Note that the uncertainties are slightly smaller for the yellow beam due to higher average polarization. Combined results for both detector arms are shown in Figure 5.6, and the values for both arms and beams combined are given in Table 5.5. All results given in this section are before correction to the asymmetries for the asymmetry of the background, which is described in Section 5.5.5.

5.5.2 Determination of relative luminosity

The relative luminosity between crossings with spin-up bunches and crossings with spin-down bunches for the polarized beam in consideration was obtained from the number of MB events recorded by the BBC. A typical value in this analysis was $\mathcal{R} = \mathcal{L}^{\uparrow}/\mathcal{L}^{\downarrow} = 1.09$ for the yellow beam, $\mathcal{R} = 0.92$ for the blue beam. Error in the relative luminosity as measured in this case for azimuthal transverse single-spin asymmetries

p_T (GeV/c)	Beam	Left		Right	
		A_N	σ_{A_N}	A_N	σ_{A_N}
1-2	Blue	-0.008	0.015	-0.012	0.019
	Yellow	-0.005	0.015	0.003	0.011
2-3	Blue	0.028	0.035	-0.066	0.039
	Yellow	-0.016	0.030	-0.003	0.028
3-4	Blue	-0.101	0.094	0.106	0.099
	Yellow	0.033	0.077	-0.092	0.073
4-5	Blue	-0.02	0.23	0.16	0.22
	Yellow	0.01	0.17	0.14	0.18

Table 5.4: Asymmetry results for particles observed in the left detector arm (west arm for blue, east arm for yellow) and right detector arm (east for blue, west for yellow).

p_T (GeV/c)	A_N	σ_{A_N}
1-2	-0.006	0.008
2-3	-0.014	0.017
3-4	-0.013	0.043
4-5	0.070	0.101

Table 5.5: Combined asymmetry results for the two beams and particle production on the two sides of the polarized beam.

could potentially come from an azimuthal dependence of the BBC efficiencies. The error would be proportional to the physics asymmetry of the particles hitting the BBC (measured to be $\lesssim 1\%$) times the difference in the efficiency of the left and right halves of the detector. There is no current measurement of this value, but it is expected to be small, also at the level of a few times 10^{-2} or less. This would lead to a potential systematic error on $\mathcal{R}$ on the order of a few times 10^{-4}, but this is only a rough estimate. Rather than providing a quantitative error directly on the relative luminosity measurement, an alternative method of asymmetry calculation that does not rely upon measurement of the relative luminosity is used to estimate the uncertainty on the asymmetry values calculated using Eq. 5.1. See Section 5.6.1 for a description of this alternative method. Refer to Appendix A for a discussion of potential sources of error in the determination of the relative luminosity for different single- and double-spin asymmetry measurements.

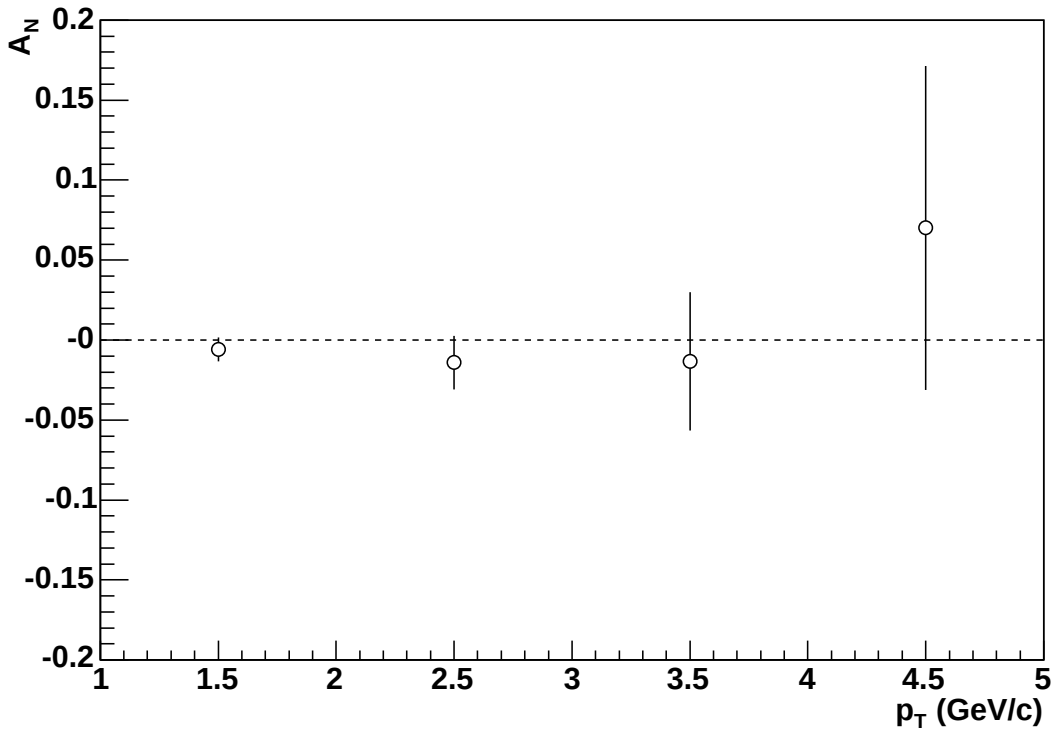

Figure 5.6: Combined asymmetry results for the two beams and particle production to the left and right.

5.5.3 Fill-by-fill polarization correction

The average beam polarization in the 2001-02 run was $15 \pm 5\%$, with the 5% representing a systematic scale uncertainty, discussed below. Unpolarized protons in the beam act to dilute the physics asymmetries being measured. It is necessary to correct for this dilution, which is done by the factor of $\frac{1}{P_{\rm beam}}$ in Eq. 5.1.

The beam polarization varies fill by fill and is typically different for the two beams. In the 2001-02 run, the yellow beam frequently had slightly higher polarization than the blue beam. The polarization values for both beams for all fills included in this analysis are given in Table 5.6. Statistical uncertainties on the beam polarization were on the order of 10^{-3} in absolute polarization. These uncertainties were negligible compared to the statistical uncertainties on the yields as well as compared to the systematic uncertainty on the polarization (see separate discussion

Fill	P_{blue}	P_{yellow}
2222	0.12	0.14
2226	0.22	0.23
2233	0.17	0.19
2235	0.16	0.24
2244	0.14	0.18
2251	0.09	0.16
2266	0.09	0.10
2275	0.12	0.14
2277	0.08	0.11
2281	0.13	0.11
2289	0.15	0.15
2290	0.17	0.21
2301	0.15	0.17
2304	0.09	0.16

Table 5.6: Fill-by-fill beam polarization values for the 14 RHIC fills used.

below) and were not incorporated into the final error on the asymmetry values.

5.5.4 Acceptance correction

The transverse single-spin asymmetry, A_N, is an azimuthal or "left-right" asymmetry. One can consider only particle production to the left or right of the polarized beam and calculate the asymmetry in production from spin-up versus spin-down bunches, as in Eq. 5.1. Performing the calculation in this way, detector acceptance effects cancel. Alternatively, one can consider only particle production from up- or down-polarized bunches and calculate the asymmetry in production to the left versus the right, as given in Eq. 5.2

$$A_N = \frac{1}{P_{\text{beam}}} \frac{1}{\langle |\cos\varphi| \rangle} \frac{N_L - \mathcal{R}_{\text{acc}} N_R}{N_L + \mathcal{R}_{\text{acc}} N_R} \tag{5.2}$$

for bunch polarization in the upward direction. Here N_L and N_R are the number of neutral pions produced in the left and right detector arms with respect to the polarized beam direction, and $\mathcal{R}_{\text{acc}} = \frac{\alpha_L}{\alpha_R}$ is the relative acceptance of the left and right detector arms. In this way, luminosity effects cancel. From Eq. 5.2, the left-right nature of the asymmetry is clear. However, maximal effects, i.e. the greatest

$\langle \lvert\cos\varphi\rvert \rangle$	Ideal	Actual: MB	Actual: 2×2
West Arm	0.943	0.955	0.949
East Arm	0.883	0.880	0.874
Both Arms	0.909	0.920	0.913

Table 5.7: Comparison of results for the average value of $|\cos\varphi|$ for ideal and actual detector acceptances. Results for the west and east arms are significantly different because the uppermost sector was not included in the west. Differences between the MB and triggered data are due to the distribution of dead or masked tiles in the ERT.

and least particle production, are at 90° from the direction of the spin vector, which was vertical in the entire 2001-02 run. Thus integrating particle yields over the entire azimuthal coverage of the central arm spectrometers would lead to a dilution of the true physics asymmetry. The factor of $\frac{1}{\langle |\cos\varphi| \rangle}$ in both Eq. 5.1 and 5.2 corrects for this dilution. Note that $\varphi = 0°$ is in the horizontal plane, implying no dilution at $\varphi = 0°$ or $\varphi = 180°$.

The value of $\langle |\cos\varphi| \rangle$ over the idealized azimuthal coverage of the detector arms can be calculated analytically by Eq. 5.3.

$$\langle |\cos\varphi| \rangle = \frac{\int |\cos\varphi| d\varphi}{\int d\varphi} \tag{5.3}$$

To account more carefully for dead areas in the EMCal and in the ERT, which would require detailed attention to the distribution of these areas in order to make an analytical calculation, the average values of $|\cos\varphi|$ used in the analysis were calculated directly from the data using Eq. 5.4, where j is a sum over all photon pairs with an invariant mass which fell under the π^0 mass peak. A comparison of results for $\langle |\cos\varphi| \rangle$ determined analytically and from the data is given in Table 5.7.

$$\langle |\cos\varphi| \rangle = \frac{\sum_{j=1}^{N} |\cos\varphi_j|}{N} \tag{5.4}$$

5.5.5 Subtraction of background asymmetry

Subtraction of the asymmetry of the background is performed as given in Eq. 5.5, taking into account the fraction of background under the π^0 mass peak. A_N^{peak} indicates the asymmetry of all photon pairs falling under the π^0 peak; note that it has generally been written simply as A_N up until this point. Equation 5.6 gives the prescription for calculation of the final statistical uncertainty on the π^0 asymmetry after subtraction of the background asymmetry.

$$A_N^{\pi^0} = \frac{A_N^{\text{peak}} - r A_N^{\text{bg}}}{1 - r} \tag{5.5}$$

$$\sigma_{A_N^{\pi^0}} = \frac{\sqrt{\sigma^2_{A_N^{\text{peak}}} + r^2 \sigma^2_{A_N^{\text{bg}}}}}{1 - r} \tag{5.6}$$

The same technique to handle background in a π^0 asymmetry analysis was used for the longitudinal double-spin asymmetry [17]. Refer back to Table 5.3 for the fraction of background in each p_T bin. After cuts to reduce the background, it ranged from 34% in the 1-2 GeV/c p_T bin to 5% in the 4-5 GeV/c bin.

It is not possible to measure the asymmetry of the background under the peak directly. Differentiation between true neutral pions and combinatorial background is only possible statistically and not on an event-by-event basis. Therefore it must be estimated in order to correct for it. The asymmetries of two different background invariant-mass regions were studied as estimates of the asymmetry of the background under the π^0 peak: 50-MeV/c^2 regions immediately around the π^0 mass peak (60-110 MeV/c^2 and 170-220 MeV/c^2), and the invariant-mass region above the π^0 but below the η (250-450 MeV/c^2). The final results published in [15] subtracted the asymmetry of the two 50-MeV/c^2 regions. It was felt that this invariant-mass region, being closer to that directly under the peak, was likely to reflect the asymmetry of background under the peak more accurately. However, the background region used was found to have little effect on the final results. The similarity in the background asymmetries for the two different invariant-mass regions lent confidence to their

p_T (GeV/c)	A_N^{bg}	$\sigma_{A_N^{\mathrm{bg}}}$
1-2	-0.007	0.009
2-3	-0.031	0.034
3-4	0.036	0.123
4-5	0.42	0.39

Table 5.8: Asymmetry results of background photon pairs falling within 50-MeV/c^2 regions around the π^0 mass peak.

p_T (GeV/c)	$A_N^{\pi^0}$	$\sigma_{A_N^{\pi^0}}$
1-2	-0.005	0.012
2-3	-0.012	0.020
3-4	-0.016	0.047
4-5	0.052	0.109

Table 5.9: Background-subtracted π^0 asymmetries, using 50-MeV/c^2 mass regions around the π^0 peak as the background.

validity in estimating the asymmetry of the background under the π^0 peak. See Section 5.6.5 for further comparison of the results obtained from the two different background regions.

The asymmetries measured for photon pairs falling in the background invariant-mass region immediately surrounding the peak are shown in Table 5.8. The asymmetries after background-asymmetry subtraction for the two 50-MeV/c^2 regions are given in Table 5.9. The asymmetry results before and after subtraction of the background asymmetry are shown in Figure 5.7. It can be seen that correction for the background asymmetry made only a small difference in the results. The mean p_T in each bin was adjusted to account for possible differences between the mean p_T of the true neutral pions and the background pairs under the peak. The final value is calculated by Eq. 5.7

$$p_T^{\pi^0} = \frac{p_T^{\mathrm{peak}} - r p_T^{\mathrm{bg}}}{1 - r} \tag{5.7}$$

and given for each p_T bin in Table 5.10.

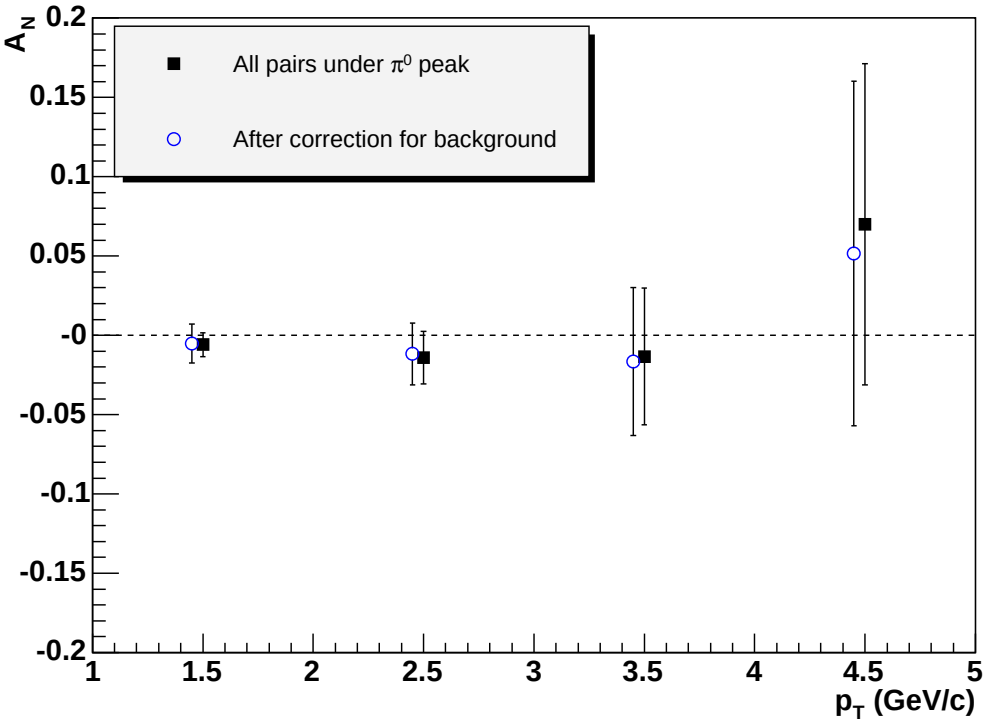

Figure 5.7: Asymmetry results before and after correction for the asymmetry of the background in the invariant-mass regions immediately surrounding the π^0 peak. Background-corrected points are shifted down by 50 MeV/c from the center of the bin for readability.

$\langle p_T \rangle$ (GeV/c)		
π^0 peak	Background	Final
1.40	1.31	1.45
2.34	2.28	2.34
3.35	3.33	3.36
4.38	4.37	4.38

Table 5.10: Mean p_T values of the background and of neutral pions after correction for background.

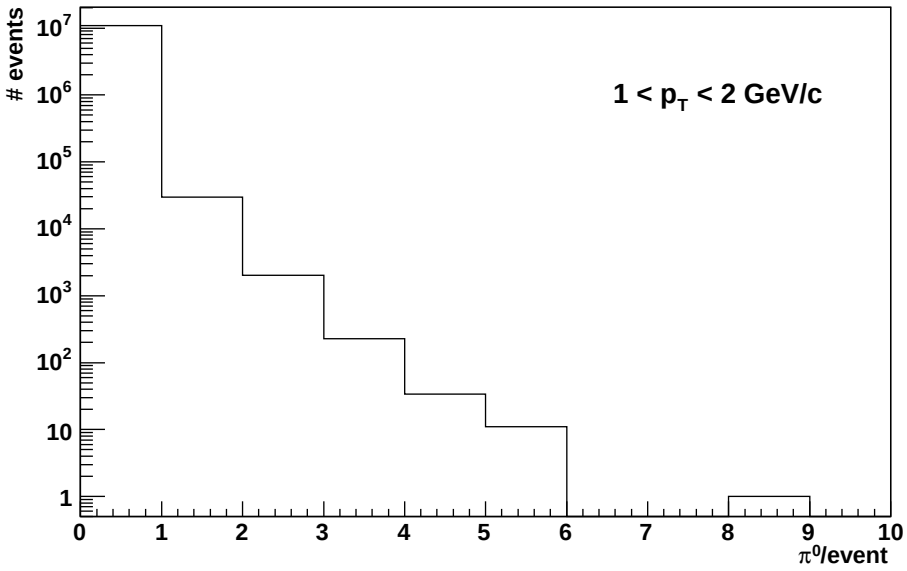

Figure 5.8: Number of photon pairs per MB event in π^0 invariant-mass range, $1 < p_T < 2$ GeV/c, west arm.

5.5.6 Calculation of statistical uncertainties

In order to calculate the statistical error, accounting for the fact that multiple neutral pions could be produced per collision, the multiplicity distributions of π^0's per event for the different detector arms were determined. See Figures 5.8 and 5.9 for sample multiplicity distributions in the west arm. Note that these distributions in fact indicate the multiplicity per event of photon pairs with an invariant mass between 120 and 160 MeV/c^2, thus including both real π^0's as well as false combinatorial pairs. From these multiplicity distributions, the degree to which the distribution is non-Poisson was calculated in a simplistic way by taking the ratio of the distribution's RMS to the square root of its mean. For a Poisson distribution, this ratio would be 1.

Table 5.11 shows the degree to which the photon pair yield is non-Poisson, calculated as $\sigma_k/\sqrt{< k >}$, where $< k >$ is the mean number of pairs per triggered event and σ_k is the RMS of this multiplicity distribution. These values were determined for the MB data, and then the uncertainty on each individual yield, N, was taken

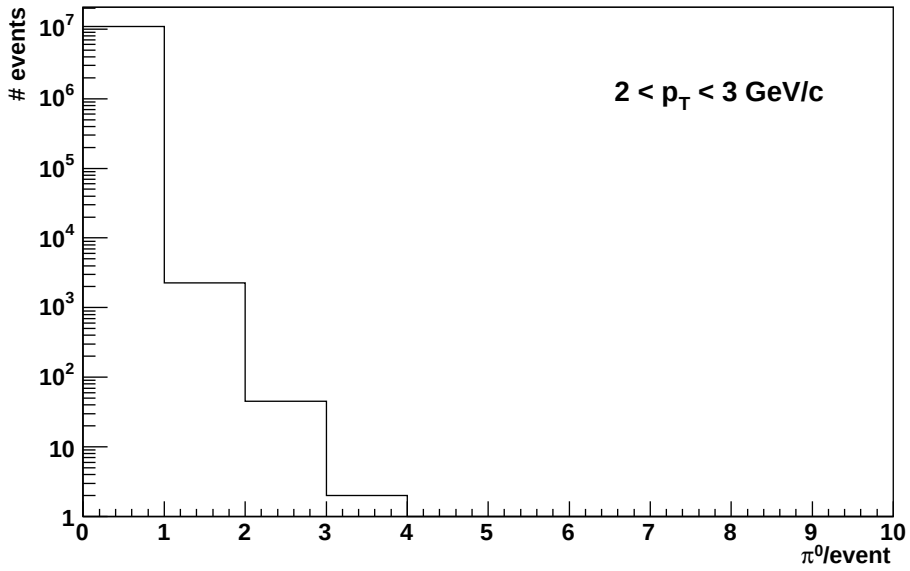

Figure 5.9: Number of photon pairs per event in π^0 invariant-mass range, $2 < p_T < 3$ GeV/c, west arm.

p_T (GeV/c)	π^0 peak		Background	
	West	East	West	East
1-2	1.08	1.06	1.16	1.11
2-3	1.02	1.02	1.08	1.05
3-4	1.01	1.01	1.04	1.02
4-5	1.02	1.00	1.41	1.00

Table 5.11: Degree to which the yield is non-Poisson for MB photon pairs falling in the 120-160 MeV/c^2 and (60-110 or 170-220 MeV/c^2) invariant-mass regions.

to be $\frac{\sigma_k}{\sqrt{<k>}}\sqrt{N}$. The 4-5 GeV/$c$ background bin suffers from very low statistics. Rather than using the calculated value of 1.41 for the west arm, 1.04, the same as for the 3-4 GeV/c background bin, was used.

5.5.7 Asymmetry scale uncertainty

In the 2001-02 run, only the pC polarimeter was available in RHIC. As stated in Section 4.2.4, the analyzing power in the process utilized by the pC polarimeter to measure the beam polarization was originally measured by AGS experiment E950 to

±30% [26]. The total systematic error on the measurement of the beam polarization was derived from a relative systematic uncertainty on the RHIC beam measurement of 15%, the 30% relative uncertainty on the analyzing power of the process, and a relative uncertainty of 10% in the change in analyzing power from a beam energy of 22 GeV at the AGS to 100 GeV at RHIC [110]. Adding these uncertainties in quadrature gave a total relative systematic uncertainty on the beam polarization of ±35%. This uncertainty is a scale uncertainty; it affects asymmetry values and statistical errors, generally proportional to $\frac{1}{P_{\text{beam}}}\frac{1}{\sqrt{N}}$, in the same way, preserving the significance of each point from zero.

5.6 Studies and checks

5.6.1 Alternative asymmetry calculation

As described above in Section 5.5.4, azimuthal transverse single-spin asymmetries can be considered for a single polarization direction comparing particle production to the left and right of the beam, or for particle production on a single side of the beam comparing different polarization directions. Equation 5.8 combines yields from up- and down-polarized bunches and from the left and right halves of the detector such that systematic errors are reduced.

$$A_N = \frac{1}{P_{\text{beam}}}\frac{1}{\langle|\cos\varphi|\rangle}\frac{\sqrt{N_L^{\uparrow}N_R^{\downarrow}}-\sqrt{N_L^{\downarrow}N_R^{\uparrow}}}{\sqrt{N_L^{\uparrow}N_R^{\downarrow}}+\sqrt{N_L^{\downarrow}N_R^{\uparrow}}} \tag{5.8}$$

In particular, the acceptance and luminosity asymmetries cancel out to several orders. See [143] for a detailed discussion of this and other methods of calculation for transverse single-spin asymmetries. It should be noted that while Eq. 5.1 is mathematically exact, Eq. 5.8 is an approximation, albeit an excellent one for the purposes of this analysis. It should also be noted that Eq. 5.8 is only suitable for transverse single-spin analysis, while Eq. 5.1 has an equivalent for longitudinal double-spin analysis (see Eq. A.1).

The asymmetry is determined for every fill, then averaged over all fills, as in the

p_T (GeV/c)	Beam	A_N	σ_{A_N}
1-2	Blue	-0.010	0.012
	Yellow	-0.001	0.009
2-3	Blue	-0.017	0.026
	Yellow	-0.009	0.020
3-4	Blue	-0.002	0.068
	Yellow	-0.032	0.053
4-5	Blue	0.06	0.16
	Yellow	0.08	0.12

Table 5.12: Asymmetry results as determined by Eq. 5.8.

calculations using Eq. 5.1. Table 5.12 shows the results obtained from Eq. 5.8 for triggered events.

The results of the asymmetry calculations obtained using Eq. 5.1 and Eq. 5.8 can be seen together in Figure 5.10. The figure is for the yellow beam; results for the blue beam are similar. The two methods agree extremely well. The dominant systematic uncertainty in the results from Eq. 5.1 is expected to be from the determination of the relative luminosity; therefore, systematic uncertainties are calculated from a direct quantitative comparison of the asymmetry results obtained from these two methods of calculation.

A systematic uncertainty, σ_{sys}, was calculated for each bin from $A_N^1 - A_N^2 \equiv \Delta$, $\sigma_{A_N^1}$, and $\sigma_{A_N^2}$. The index '1' refers to results from Eq. 5.1; '2' to results from Eq. 5.8. The uncertainty on the difference was calculated following a prescription for results obtained by applying two different methods to data sets that are 100% correlated (exactly the same data) [58]. In this case, $\sigma_\Delta = \sqrt{|\sigma^2_{A_N^1} + \sigma^2_{A_N^2} - 2\rho\sigma_{A_N^1}\sigma_{A_N^2}|}$, with the correlation $\rho = 1$. $\sigma_{sys} = |\Delta| - \sigma_\Delta$ was taken in cases where $|\Delta| > \sigma_\Delta$, and $\sigma_{sys} = 0$ was taken in cases where $|\Delta| < \sigma_\Delta$. See Tables 5.13 and 5.14 for the values used in the calculation and the results. The systematic error was also calculated as the square root of the difference of the squares, $\sigma_{sys} = \sqrt{|\Delta|^2 - \sigma^2_\Delta}$, to see if it affected the results. At the level of 10^{-3}, which is the precision quoted in [15], it did not. Final systematic uncertainties calculated using this method, averaged over the two beams, are shown in Table 5.15.

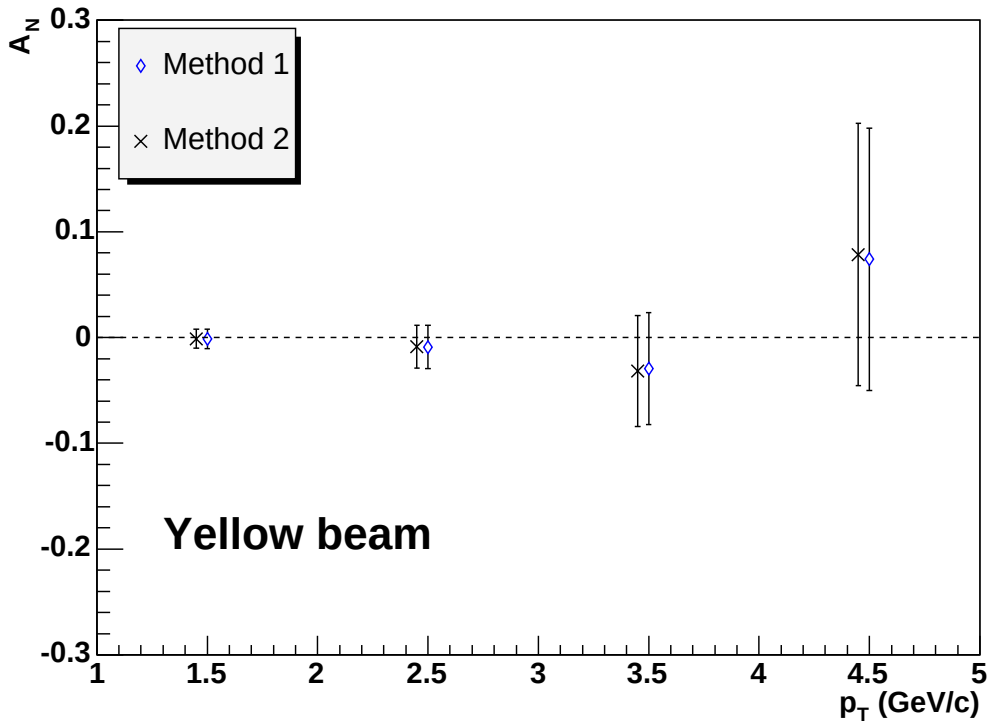

Figure 5.10: Comparison of asymmetry results obtained using Eq. 5.1 (Method 1) and Eq. 5.8 (Method 2), shown here for the yellow beam. Points for Method 2 are shifted down by 50 MeV/c from the center of the bin for readability.

p_T (GeV/c)	A_N^1 ($\times 10^2$)	A_N^2 ($\times 10^2$)	Δ ($\times 10^2$)	$\sigma_{A_N^1}$ ($\times 10^2$)	$\sigma_{A_N^2}$ ($\times 10^2$)	σ_Δ ($\times 10^2$)	σ_{sys} ($\times 10^2$)
1-2	-0.291	-0.292	0.001	0.816	0.816	0.000	0.001
2-3	-1.79	-1.79	0.00	2.07	2.07	0.00	0.00
3-4	1.61	1.61	0.00	5.51	5.51	0.00	0.00
4-5	4.23	4.17	0.06	13.0	13.0	0.00	0.06

Table 5.13: Agreement of asymmetry results from the two methods of calculation, blue beam. Note that these values were obtained before final cuts were performed. See text for further explanation.

p_T (GeV/c)	A_N^1 ($\times 10^2$)	A_N^2 ($\times 10^2$)	Δ ($\times 10^2$)	$\sigma_{A_N^1}$ ($\times 10^2$)	$\sigma_{A_N^2}$ ($\times 10^2$)	σ_Δ ($\times 10^2$)	σ_{sys} ($\times 10^2$)
1-2	-0.974	-0.975	0.001	0.636	0.635	0.001	0.000
2-3	-2.50	-2.50	0.00	1.61	1.61	0.00	0.00
3-4	-3.29	-3.30	0.01	4.27	4.28	0.01	0.00
4-5	6.81	6.99	-0.18	10.0	10.1	0.1	0.1

Table 5.14: Agreement of asymmetry results from the two methods of calculation, yellow beam. The data samples are 100% correlated, so agreement at better than the statistical level is expected. Note that these values were obtained before final cuts were performed. See text for further explanation.

p_T (GeV/c)	Avg σ_{sys} ($\times 10^2$)
1-2	0.000
2-3	0.00
3-4	0.00
4-5	0.1

Table 5.15: Systematic uncertainty on the neutral pion asymmetry, calculated for each bin and averaged over both beams.

While the comparison of the asymmetry results from the two different methods of calculation provided a strong check on the relative luminosity, the main identified potential source of systematic error present in the asymmetries as calculated by Eq. 5.1, a number of other checks on the results were performed. These other checks are described in the following sections.

5.6.2 Left and right detector arms

Calculating the asymmetry using Eq. 5.1 necessarily gives separate results for the left and right sides of the polarized beam. There is no overlap in the particle yields from the two detector arms; therefore, the expected agreement between the two results is that for uncorrelated samples. The uncertainty on the difference in results is taken to be $\sigma_\Delta = \sqrt{|\sigma^2_{A_N^{\text{left}}} + \sigma^2_{A_N^{\text{right}}} - 2\rho\sigma_{A_N^{\text{left}}}\sigma_{A_N^{\text{right}}}|}$, with the correlation $\rho = 0$. As can be seen from Table 5.16, the difference in the results from the two detector arms was within the uncertainty on the difference, and the results were in agreement.

p_T (GeV/c)	A_N^{left}	A_N^{right}	Δ	σ^{left}	σ^{right}	σ_Δ
1-2	-0.014	-0.007	-0.007	0.011	0.009	0.0142
2-3	-0.034	-0.021	-0.013	0.026	0.024	0.0354
3-4	0.002	-0.072	0.074	0.068	0.065	0.0941
4-5	0.01	0.13	-0.12	0.15	0.16	0.219

Table 5.16: Evaluation of agreement of asymmetry results from particle production to the left and right of the polarized beam, shown for the yellow beam. Δ is the difference between the asymmetries for the two arms. σ_Δ is the uncertainty on the difference.

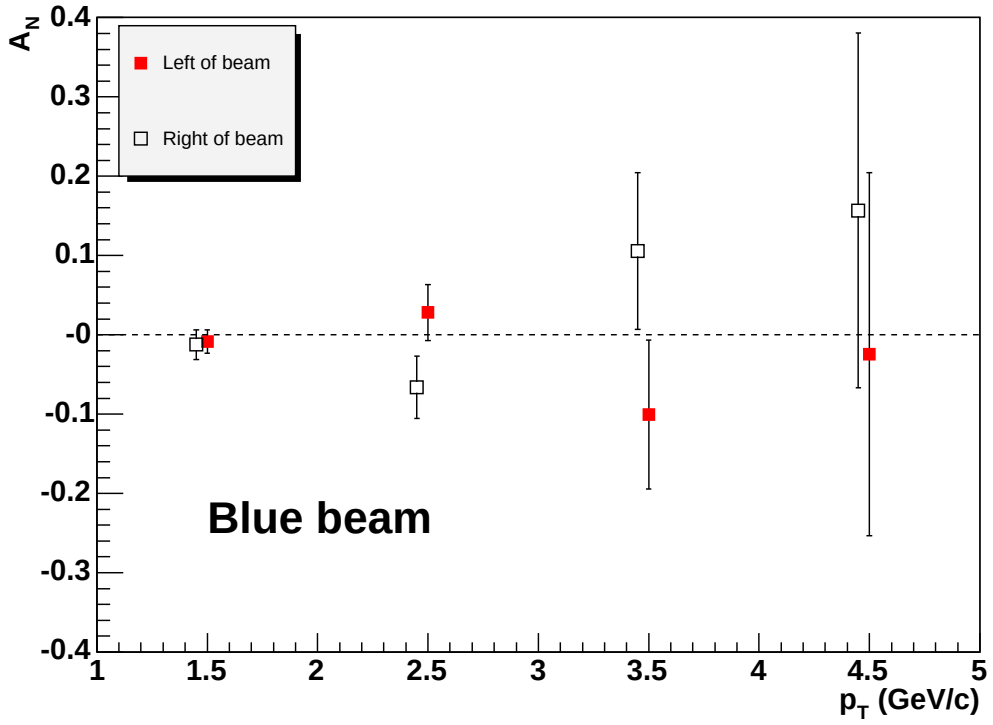

Figure 5.11: Comparison of results for particle production to the left and right side, blue beam polarized. Points for the right of the beam are shifted down by 50 MeV/c from the center of the bin for readability. Statistical agreement is expected.

Results for both detector arms can be seen together for the blue and yellow beams in Figures 5.11 and 5.12, respectively.

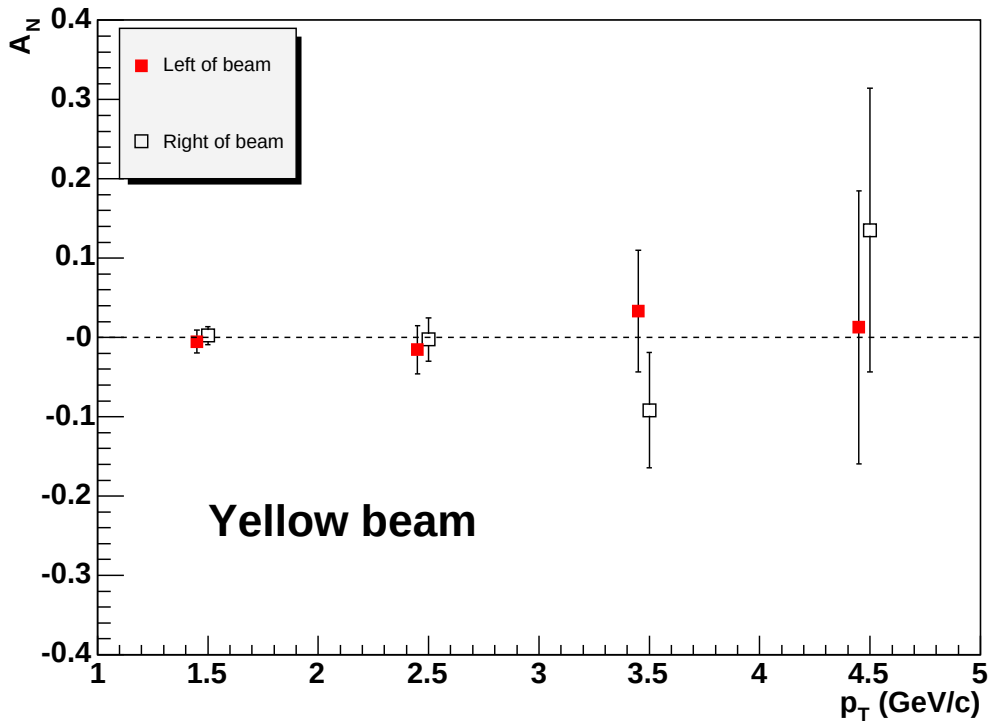

Figure 5.12: Comparison of results for particle production to the left and right side, yellow beam polarized. Points for the right of the beam are shifted down by 50 MeV/c from the center of the bin for readability. Statistical agreement is expected.

5.6.3 Two independent beams

While the results for the blue and yellow beams use the same events and yields, they are combined in a different way, taking into account the spin direction of either one beam or the other, leading to (nearly) statistically independent measurements. As the correlation between results from the two beams is believed to be small but is unknown, it is assumed to be zero in evaluating the agreement of the results. Thus as for the case of comparing results from the two detector arms, the uncertainty on the difference of the results from the two beams is taken to be $\sigma_\Delta = \sqrt{|\sigma^2_{A_N^{\rm blue}} + \sigma^2_{A_N^{\rm yellow}} - 2\rho\sigma_{A_N^{\rm blue}}\sigma_{A_N^{\rm yellow}}|}$, with $\rho = 0$. It can be seen in Table 5.17 that the results from the two beams agree as expected. Results for both beams can be seen together and evaluated by eye in Figure 5.13.

p_T (GeV/c)	A_N^{blue}	A_N^{yellow}	Δ	σ^{blue}	σ^{yellow}	σ_Δ
1-2	-0.01035	-0.00129	-0.00906	0.01184	0.00922	0.01501
2-3	-0.0190	-0.0090	-0.0100	0.0264	0.0205	0.03342
3-4	0.0026	-0.0292	0.0318	0.0681	0.0529	0.08623
4-5	0.0662	0.0741	-0.0079	0.160	0.124	0.20243

Table 5.17: Evaluation of agreement of asymmetry results from blue and yellow beams. Δ is the difference between the asymmetries for the two beams. σ_Δ is the uncertainty on the difference.

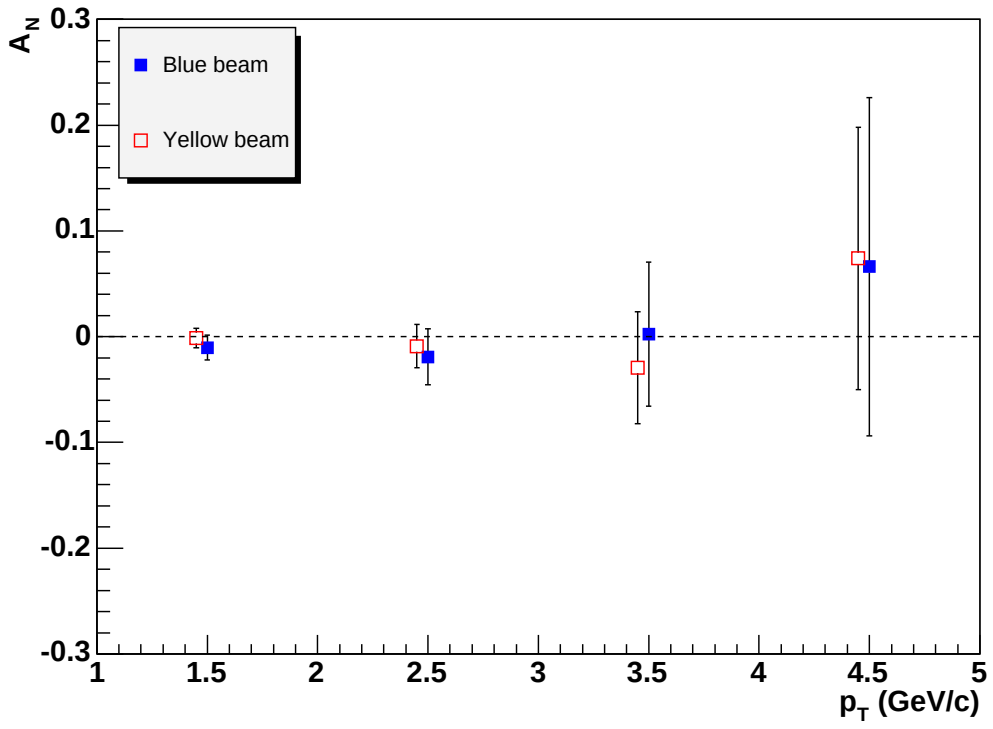

Figure 5.13: Comparison of results obtained for the two polarized beams. Points for the yellow beam are shifted down by 50 MeV/c from the center of the bin for readability. Statistical agreement or better is expected.

p_T (GeV/c)	A_N		σ_{A_N}	
	bg 1	bg 2	bg 1	bg 2
1-2	-0.008	-0.014	0.005	0.004
2-3	-0.006	0.008	0.020	0.013
3-4	-0.012	0.015	0.079	0.055
4-5	0.00	0.03	0.21	0.14

Table 5.18: Asymmetry results of photon pairs falling within the two 50-MeV/c^2 regions around the mass peak (bg 1) and within 250-450 MeV/c^2 (bg 2). Note that this check was performed before the final cuts on the data sample; thus, the results from bg 1 shown here differ from the final background results.

5.6.4 Triggered and minimum-bias data

Results for the physics asymmetry, A_N, can also be compared for the triggered and minimum-bias data samples. In this case the correlation between the samples is poorly understood. In the higher p_T bins, where the trigger was more efficient, nearly all pions in the MB sample should have fired the trigger and been present in the triggered sample as well, making the MB sample nearly a direct subset of the triggered sample. In the lower p_T bins, this correlation should be lower but still significant. Because of the unknown correlation and the fact that the MB sample is severely statistically inferior to the triggered sample, no direct evaluation of their agreement was performed. However, it can be seen in Figure 5.14 that the MB and triggered results do not exhibit notable disagreement.

5.6.5 Different background regions in invariant mass

As described above, the asymmetry of two different background mass regions in invariant mass was investigated: 50-MeV/c^2 regions around the π^0 mass peak (60-110 MeV/c^2 and 170-220 MeV/c^2) and the mass region between the π^0 and η (250-450 MeV/c^2). Table 5.18 shows the background asymmetries as calculated by Eq. 5.1 for the two background regions. The asymmetries are similar. The background asymmetries are consistent with zero for both background regions for $2 < p_T < 5$. In the 1-2 GeV/c p_T bin, both regions suggest a slightly negative asymmetry.

In Figure 5.15 a direct comparison of the asymmetry results after subtraction of

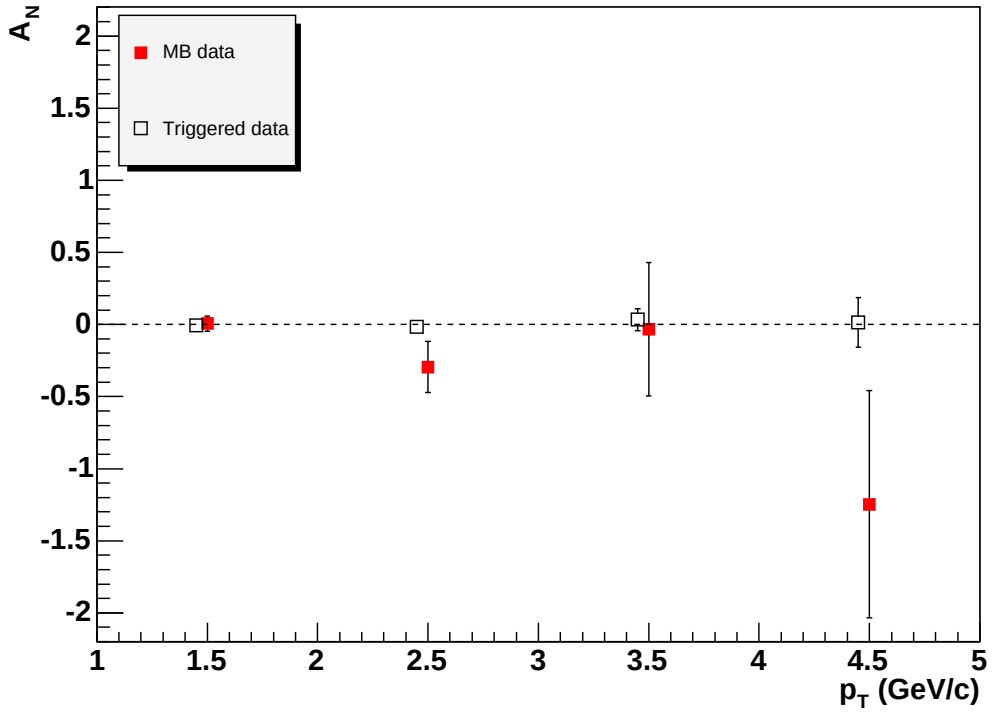

Figure 5.14: Comparison of results for minimum-bias and triggered events, shown here for the yellow beam and east detector arm. Points for the triggered data are shifted down by 50 MeV/c from the center of the bin for readability. The correlation between the samples is unknown.

the two background asymmetries is shown. The background region used has little effect on the final asymmetry.

5.6.6 Different π^0 invariant-mass integration regions

As an additional check on the sensitivity of A_N to the background under the π^0 peak, three different integration regions for the π^0 mass were examined: 120-160 MeV/c^2, 110-170 MeV/c^2, and 100-180 MeV/c^2. Figure 5.16 shows a comparison of asymmetries obtained for peak integration from 120-160 MeV/c^2 and 100-180 MeV/c^2. There is little effect on the result from the amount of background included, providing additional evidence that the background under the peak does not affect the asymmetry greatly.

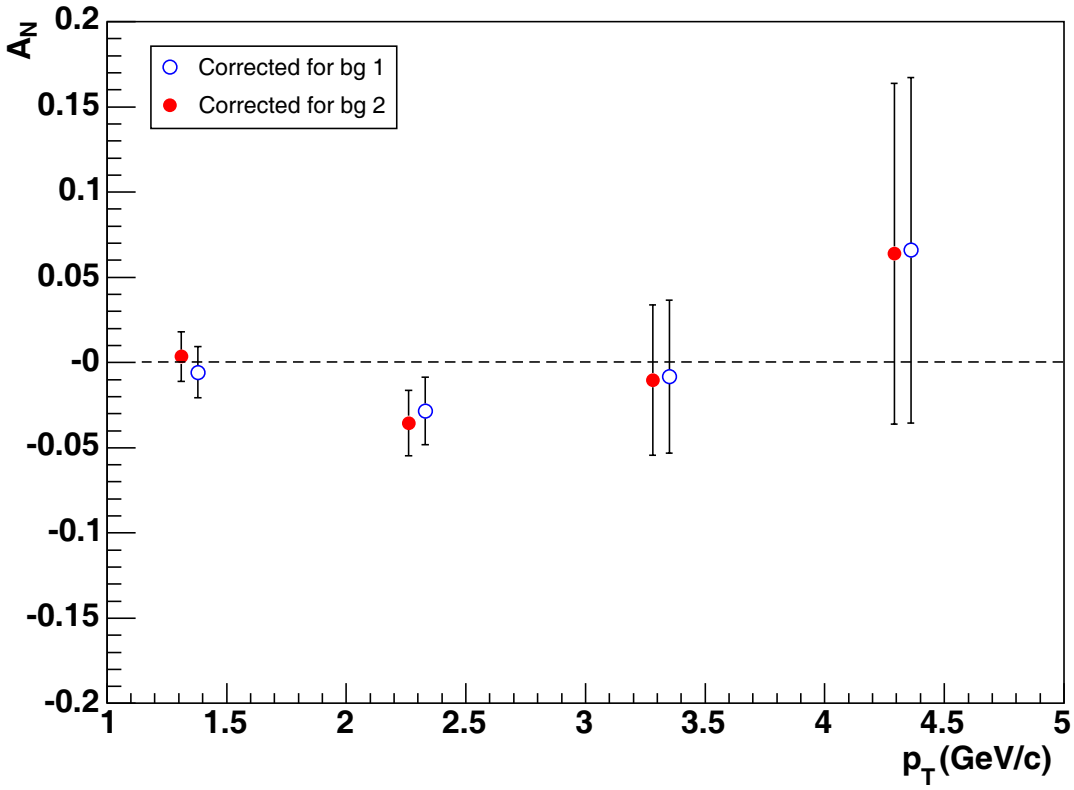

Figure 5.15: Comparison of asymmetries obtained after subtracting the asymmetry of two different background invariant-mass regions. "bg 1" indicates the asymmetry after subtraction of the asymmetry around the peak; "bg 2" is after subtraction of the asymmetry of the 250-450 MeV/c^2 background region. Points for bg 2 are shifted down by 50 MeV/c from the center of the bin for readability. Note that this check was performed before the final cuts on the data sample; thus the results differ from the final ones.

5.6.7 Bunch shuffling

A technique called "bunch shuffling" can be utilized to check for uncorrelated bunch-to-bunch and fill-to-fill systematic errors. For each bunch crossing the spin direction is reassigned randomly, and then the new asymmetry with false spin dependence is recalculated. This procedure is repeated many times. With random reassignment of the spin direction to each crossing, a Gaussian asymmetry distribution centered around zero is expected. One must take care in choosing the exact procedure used for this study. If done correctly, the root-mean-square (RMS) width of the "shuffled"

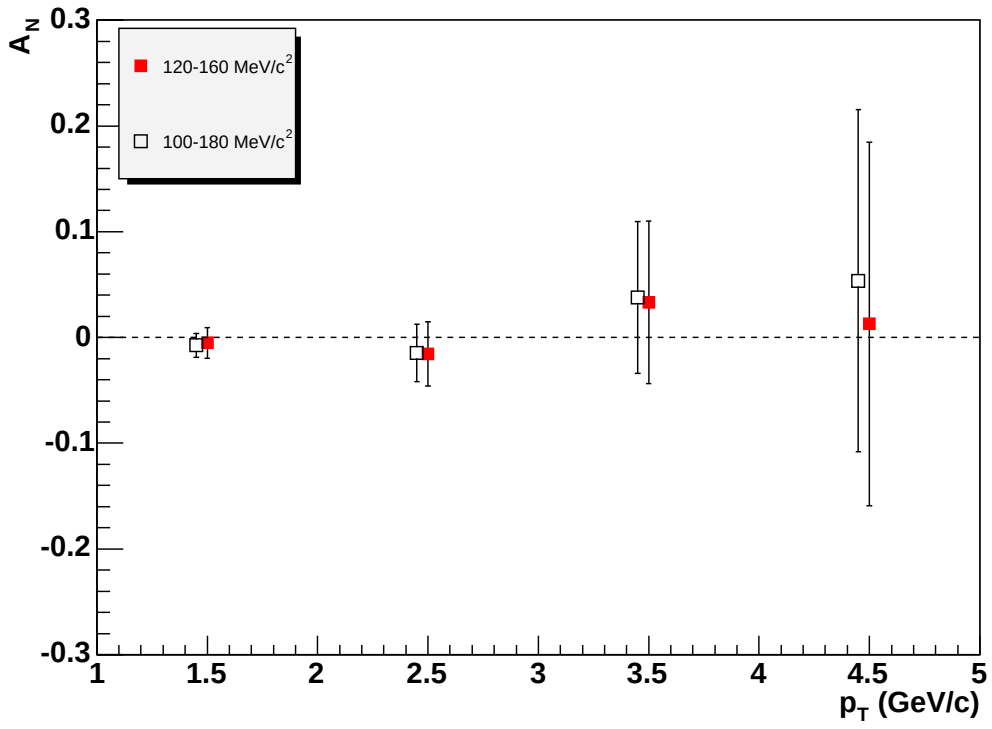

Figure 5.16: Comparison of results for different π^0 peak integration regions. Points for the wider integration region are shifted down by 50 MeV/c from the center of the bin for readability.

(non-physics) asymmetry distribution should correspond to the statistical uncertainty on the physics asymmetry, since fluctuations in the calculated asymmetry should not be due to any spin dependence but rather to statistical fluctuations in event-by-event particle production. If the RMS width of the shuffled asymmetry distribution is larger than the statistical uncertainty on the physics asymmetry, it should reflect the presence of elements that broaden the distribution beyond statistical fluctuations in particle production, e.g. some source of bunch-to-bunch systematic error in the physics asymmetry. It should be noted, however, that the expected quantitative agreement between the statistical uncertainty and RMS width of the shuffled distribution is not entirely understood. As is discussed in Section 5.6.7.1, a study done for this thesis found that it is also possible to obtain widths smaller

than the statistical uncertainties.

It is easier to consider the validity of various procedures assuming large asymmetries, for example 1 (100%) . Taking one bunch at a time and randomly assigning its spin direction to be up or down, with no further constraints, it is theoretically possible to make the spin assignments exactly as the true, original spin directions ($\mathrm{up}_{\mathrm{phys}} \rightarrow \mathrm{up}_{\mathrm{shuf}}$, $\mathrm{down}_{\mathrm{phys}} \rightarrow \mathrm{down}_{\mathrm{shuf}}$), or exactly opposite ($\mathrm{up}_{\mathrm{phys}} \rightarrow \mathrm{down}_{\mathrm{shuf}}$, $\mathrm{down}_{\mathrm{phys}} \rightarrow \mathrm{up}_{\mathrm{shuf}}$), yielding a shuffled asymmetry distribution that can range from -1 to +1, even with a wealth of statistics. This method would generally give distribution widths wider than the statistical uncertainties on the physics asymmetry values. Selecting any half of the bunches to be assigned up and the other half to be assigned down creates a similar situation for true relative luminosity values close to 1, i.e. a nearly equal number of events coming from bunches with spin up and spin down: it is possible to assign the shuffled spins to be nearly the same as the original physics spin directions.

The procedure utilized in this analysis was to assign half of the original up spins to down and keep the others as up, and similarly assign half of the original down spins to up while keeping the others down. Thus the particle production gets redistributed evenly, at the *crossing* (not event) level, between up and down spins, and even for large physics asymmetries, shuffled asymmetry will always be (nearly) zero. Repeating this procedure many times should yield a distribution around zero that is due to *event-by-event* statistical fluctuations in particle production (i.e. 0, 1, 2, etc. neutral pions produced in a given event, with a certain probability distribution).

For this analysis, Eq. 5.8 was used to calculate the shuffled asymmetries, as it avoided the complication of recalculating the relative luminosity for each iteration. The bunch shuffling procedure was performed 1000 times. Refer to Figure 5.17 for examples of shuffled asymmetry distributions from the data set used for this analysis; the expected increase of the distribution width for the smaller-statistics (higher-p_T) bins can be clearly seen. In Table 5.19 it can be seen that the mean of the shuffled asymmetry distributions was zero at the level of 10^{-4} or better. The χ^2

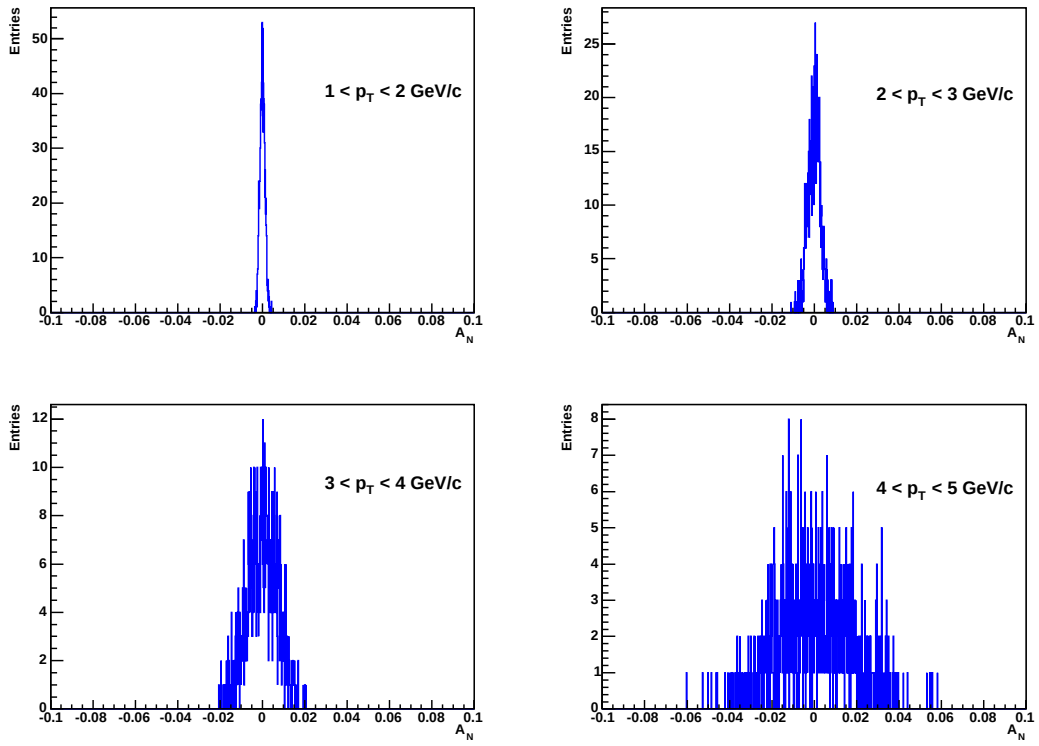

Figure 5.17: Bunch-shuffled asymmetry distributions for triggered data, shown here for the blue beam.

p_T (GeV/c)	Beam	$\overline{A}_N^{\text{shuf}}$
1-2	Blue	-9.3×10^{-6}
	Yellow	-2.2×10^{-5}
2-3	Blue	-7.8×10^{-7}
	Yellow	-2.2×10^{-5}
3-4	Blue	3.8×10^{-5}
	Yellow	1.0×10^{-4}
4-5	Blue	3.0×10^{-4}
	Yellow	-4.3×10^{-4}

Table 5.19: Mean values of shuffled asymmetry distributions.

distributions for a fit to a constant asymmetry across all shuffled fills can be seen in Figure 5.18. The dotted line shows the expected χ^2 distribution for 13 degrees of freedom (asymmetry values for 14 fills, fit to a constant), which are in agreement with the data.

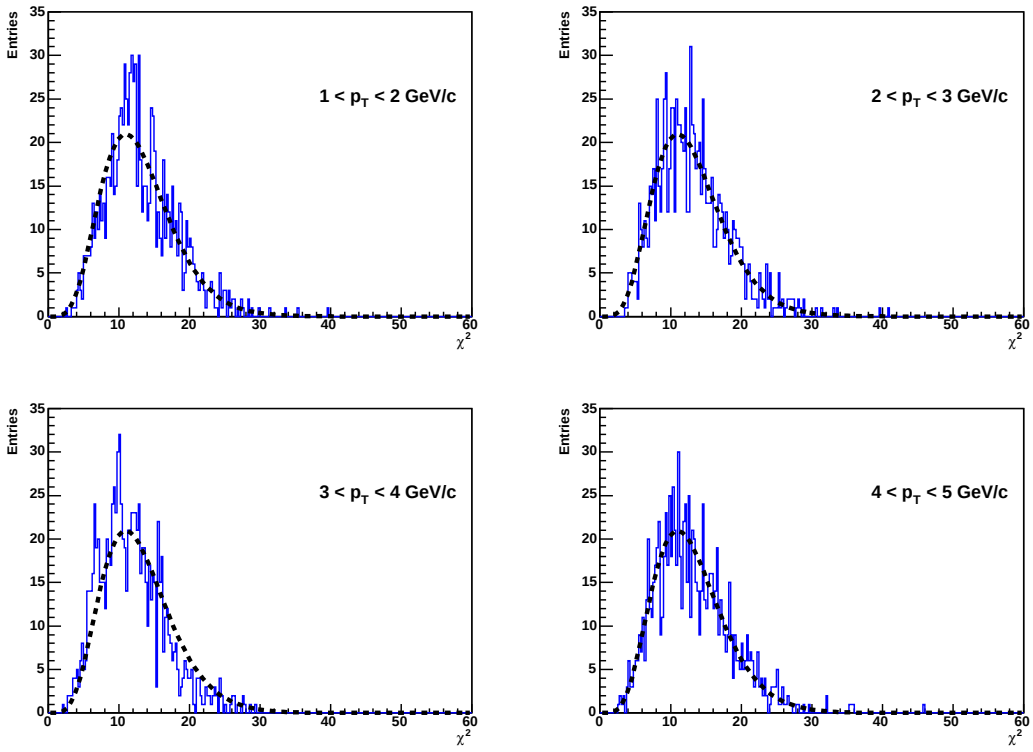

Figure 5.18: Bunch-shuffled χ^2 distributions from triggered data, shown here for the blue beam. The dashed lines indicate the expected distributions.

Table 5.20 shows the statistical uncertainties on the physics asymmetries compared to the RMS widths of the shuffled asymmetry distributions for the blue and yellow beams. In order for the uncertainties on the physics asymmetries to reflect simply statistical distributions in particle production, the beam polarization was not factored in. For this reason, the statistical uncertainties are exactly the same for the blue and yellow beams, the results for each using the same total set of events. The % difference is calculated as $100 \times (\sigma_{A_N^{\rm shuf}} - \sigma_{A_N^{\rm phys}})/\sigma_{A_N^{\rm phys}}$.

The shuffled widths are systematically *smaller* than the statistical uncertainties calculated for the physics asymmetry. This outcome was at first a surprise, as the expectation was that the RMS width should have been the same as or greater than the physics statistical uncertainty. However, a subsequent Monte-Carlo study of the bunch shuffling technique, discussed below, corroborated the tendency for the

p_T (GeV/c)	Beam	$\sigma_{A_N^{\text{phys}}}$	$\sigma_{A_N^{\text{shuf}}}$	% difference
1-2	Blue	0.0014	0.0012	-14
	Yellow	0.0014	0.0012	-14
2-3	Blue	0.0032	0.0030	-6.3
	Yellow	0.0032	0.0028	-13
3-4	Blue	0.0082	0.0070	-15
	Yellow	0.0082	0.0069	-16
4-5	Blue	0.0191	0.0179	-6.3
	Yellow	0.0191	0.0179	-6.3

Table 5.20: Comparison of statistical uncertainties on the physics asymmetries ($\sigma_{A_N^{\text{phys}}}$) and RMS widths of shuffled asymmetry distributions ($\sigma_{A_N^{\text{shuf}}}$).

width of shuffled distributions for a zero physics asymmetry to be narrower than the statistical uncertainty.

5.6.7.1 Bunch shuffling Monte Carlo

A Monte Carlo study of the bunch shuffling technique was performed to better quantitatively understand the expected agreement between the RMS widths of shuffled asymmetry distributions and the statistical uncertainties of the physics asymmetry values, for different simulated physics asymmetry values.

In the Monte Carlo study, 14 fills were assumed, the same number as in the actual data set. In order to simulate the variation in the total particle yield per fill, the actual total π^0 yields per fill for the 1-2 GeV/c p_T bin were used as the simulated yields per fill. The number of bunches per beam was taken to be 48, selected because it was very close to the typical value of 46 in the actual data set, and because it was divisible by four, so that it was possible to assume half of the bunches were spin up and half were spin down, then easily reassign exactly half in each spin group to the wrong spin direction. The desired physics asymmetry to simulate was selected, which determined the average yield per bunch with spins up and down in each fill. Simulated yields for each bunch crossing were produced by sampling from Poisson distributions around these asymmetry-dependent averages. In this way, the uncertainty on the yields themselves was purely Poisson and well

understood. The uncertainty on the simulated asymmetry was purely statistical and calculated by performing straightforward error propagation on the asymmetry formula assuming only uncertainties on the yields; there were no effects due to detectors, triggers, polarization measurements, or any other factors incorporated. The simulated yields were then input into the same software program written to handle the bunch shuffling of the data. The RMS width of the resulting shuffled asymmetry distribution was then compared to the statistical error on the simulated "physics" asymmetry.

The effects of varying the simulated physics asymmetry, the total statistics, and the number of bunches per beam were studied. In Table 5.21 the results for two different statistical sample sizes as well as three different simulated asymmetry values are shown. There are several items to note here. Despite incorrectly assigning the spin direction for exactly one half of the bunches, the width of the shuffled distribution increases noticeably as a function of the simulated physics asymmetry. The statistical uncertainty on the physics asymmetry is itself weakly but *inversely* dependent on the physics asymmetry, leading to a shuffled width that is more than double the simulated uncertainty for a 90% simulated asymmetry. For the case of a zero simulated asymmetry, corresponding to the results of the present analysis (see Section 5.7), a shuffled width smaller than the simulated uncertainty is obtained for a statistical sample equivalent to the π^0 yield in the 1-2 GeV/c p_T bin in the present analysis. For ten times this statistical sample, the study suggests that the shuffled widths tend to increase with respect to the smaller sample, for at least the zero and 30% simulated asymmetry values. In order to investigate the possibility that the smaller width for zero simulated asymmetry was due to correlations in obtaining shuffled asymmetries many times for a limited number of bunch crossings, a study with only 10 bunches per beam was performed, the results of which are given in Table 5.22. Performing 10,000 reassignments of the spin direction of five out of ten bunches should have led to many duplicate reassignments and thus duplicate shuffled asymmetry values in the distribution. (Note that the difference in the number of

Statistics	A_N^{sim}	$\sigma_{A_N^{\text{sim}}} \times 10^4$	$\sigma_{A_N^{\text{shuf}}} \times 10^4$	% difference
1	0	9.70	9.16	-5.5
1	0.3	9.20	9.18	-0.2
1	0.9	4.20	9.37	123
10	0	3.05	3.09	1.3
10	0.3	2.91	3.09	6.2
10	0.9	1.33	2.99	125

Table 5.21: Bunch shuffling results for two different statistical sample sizes and three different simulated asymmetry values, assuming 48 bunches per beam. The "Statistics" column indicates the factor times the 1-2 GeV/c p_T bin π^0 yields in the actual data sample. 10,000 shuffles were performed.

iterations in the data versus the simulation was due simply to technical reasons.) For the smaller statistical sample size, the shuffled distribution width was only slightly smaller for 10 bunches per beam than 48 bunches; for the larger sample size the reduction was more significant. While the degree of correlation should not depend on the value of the physics asymmetry, it may be that the reduction of the shuffled distribution width due to correlations only makes it less than the statistical uncertainty in the case of zero asymmetry because for larger asymmetries, the dependence of the width on the asymmetry is a larger effect.

As an additional means of investigating correlations as the cause of shuffled distribution widths being smaller than the statistical uncertainties, an attempt was made to remove all correlations. To achieve this, the yield for each crossing was resampled for each iteration of the reassignment of spin directions. This procedure effectively incorrectly assigned the spin direction for the yields from the bunches in many different fills (♯ effective fills = ♯ shuffling iterations), all having the same physics asymmetry, rather than repeatedly reassigning the spin direction for the yields in a single fill or small number of fills. The results of this exercise are shown in Table 5.23; the shuffled width is within 1% of the statistical uncertainty on the simulated physics asymmetry, suggesting that the smaller shuffled distribution widths may be due to correlations. Note that this procedure is not applicable to real data, due to the fact that there is always a limited number of fills.

# bunches	Statistics	$A_N^{\rm sim}$	$\sigma_{A_N^{\rm sim}} \times 10^4$	$\sigma_{A_N^{\rm shuf}} \times 10^4$	% difference
10	1	0	9.65	9.01	-6.6
48	1	0	9.70	9.16	-5.5
10	10	0	3.05	2.89	-5.2
48	10	0	3.05	3.09	1.3

Table 5.22: Comparison of simulated shuffling results for 10 and 48 bunches per beam. 10,000 shuffles were performed.

Statistics	$A_N^{\rm sim}$	$\sigma_{A_N^{\rm sim}} \times 10^4$	$\sigma_{A_N^{\rm shuf}} \times 10^4$	% difference
1	0	9.66	9.74	0.9

Table 5.23: Modified bunch shuffling simulation with correlations removed (see text).

While the Monte Carlo investigation confirmed the pattern seen in applying the bunch shuffling technique to the actual data, the merits and limitations of the technique are still not completely understood. Improved procedures for randomly reassigning the spin direction of the bunches in order to obtain better agreement between statistical uncertainties on the physics asymmetries and shuffled asymmetry distribution widths may exist. A more thorough future study would be valuable. This method of checking for uncorrelated bunch-to-bunch and fill-to-fill systematic errors is particularly important for double-spin asymmetry measurements, in which many of the checks available to a single-spin analysis are not available.

5.7 Results

Final asymmetry results for mid-rapidity neutral pions from 200-GeV polarized $p+p$ collisions for $1 < p_T < 5$ GeV/c, as published in [15], are given in Figure 5.19 and Table 5.24. They utilized the triggered data sample and the 50-MeV/c^2 regions in invariant mass around the π^0 peak for the background correction. The asymmetries are consistent with zero within a few percent for all p_T bins. For further discussion of these results and their implications, see Chapter 7.

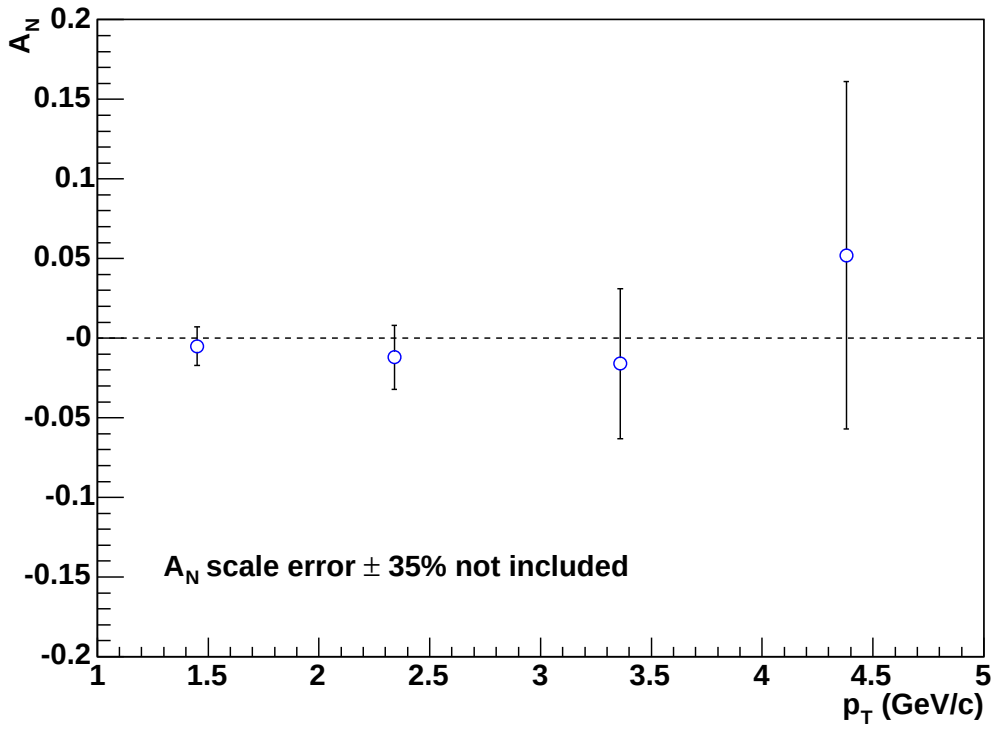

Figure 5.19: Final mid-rapidity neutral pion transverse single-spin asymmetry. The error bars represent statistical uncertainties.

p_T (GeV/c)	$\langle p_T \rangle$ (GeV/c)	r (%)	A_N^{peak} (%)	A_N^{bg} (%)	$A_N^{\pi^0}$ (%)
1-2	1.45	34	-0.6±0.8	-0.7± 0.9	-0.5± 1.2
2-3	2.34	12	-1.4±1.7	-3.1± 3.4	-1.2± 2.0
3-4	3.36	6	1.3±4.2	3.6±12.2	-1.6± 4.7
4-5	4.38	5	7.0±10.1	42 ±39	5.2±10.9

Table 5.24: Neutral pion transverse single-spin asymmetry values and statistical uncertainties for all photon pairs falling within the π^0 mass peak, for the background (bg), and for the π^0 background-corrected. The third column (r) indicates the background contribution under the π^0 peak. An A_N scale uncertainty of ±35% is not included.

p_T (GeV/c)	$\langle p_T \rangle$ (GeV/c)	$A_N^{h^-}$ (%)	$A_N^{h^+}$ (%)
0.5-1	0.70	-0.38±0.42	-0.09±0.41
1-2	1.32	-0.12±0.82	-0.54±0.78
2-5	2.56	-2.1±2.7	-3.1 ±2.6

Table 5.25: Charged hadron transverse single-spin asymmetry values and statistical uncertainties. An A_N scale uncertainty of ±35% is not included.

5.8 Comparison to charged hadron asymmetry results

A similar analysis of the transverse single-spin asymmetry, A_N, of inclusive charged hadrons at mid-rapidity for $0.5 < p_T < 5.0$ GeV/c was performed by F. Bauer for the 2001-02 data. The results of the neutral pion and charged hadron measurements have been published together in [15]. For more details on the charged hadron analysis, refer to the publication. Charged hadron asymmetry results were obtained separately for positively and negatively charged particles; they are presented in Table 5.25. While a clear charge dependence has been observed in transverse single-spin asymmetries for forward production (refer back to Section 2.2.5), the results for mid-rapidity neutral pions and both charges of hadron were all found to be similarly consistent with zero. Figure 5.20 shows the observed asymmetries for both neutral pions and charged hadrons together.

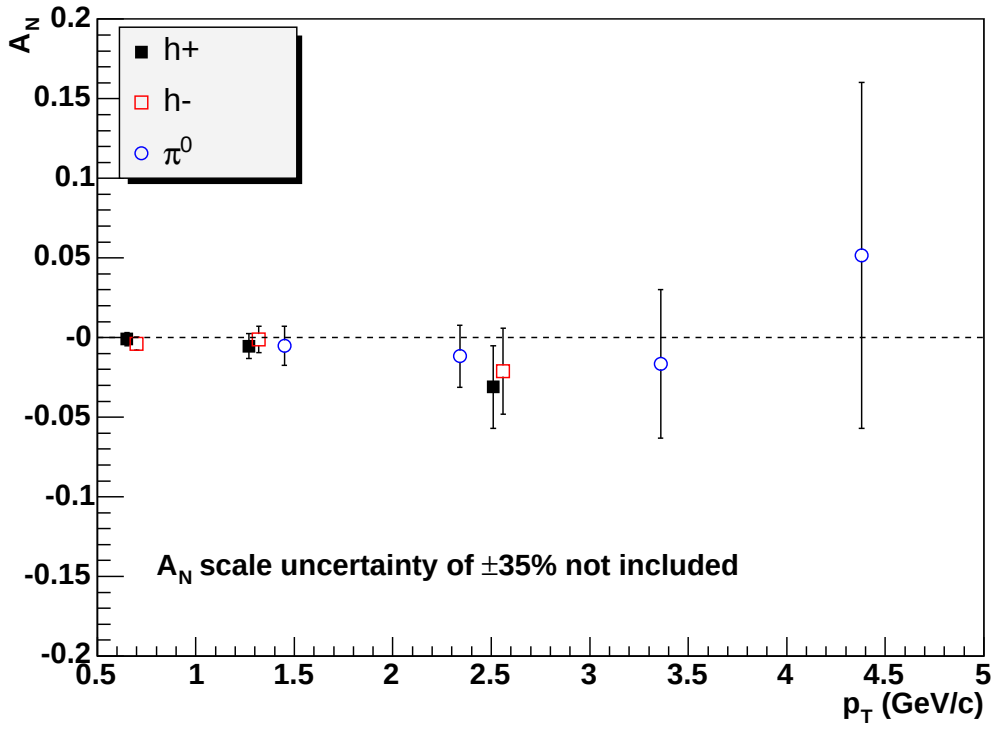

Figure 5.20: Mid-rapidity neutral pion and charged hadron transverse single-spin asymmetries versus mean p_T. Points for positive hadrons have been shifted down by 50 MeV/c to improve readability. The error bars represent statistical uncertainties.

Chapter 6

Future prospects for transverse spin physics

The experiments at RHIC have the potential to perform a wide variety of studies related to the transverse spin structure of the proton. Several measurements beyond those completed have already been planned, and others are being proposed and considered. Because there are currently a number of possible mechanisms under discussion that may contribute to the large transverse SSA's observed, seeking measurements sensitive to or dominated by a single mechanism is especially valuable. In this chapter, potential future measurements at RHIC are discussed, with particular focus on possible measurements by the PHENIX experiment.

6.1 BRAHMS

The BRAHMS experiment does not have spin rotator magnets around its IP and therefore does not have access to longitudinally polarized collisions. Consequently, its polarized proton program is completely focused on transverse spin physics. BRAHMS was designed to specialize in the measurement of identified charged particles at forward and mid-rapidity. It is in a unique position at RHIC to make a precision measurement of A_N for identified charged particles (π^+/π^-, K^+/K^-, $p/\bar{p}$) in the forward and backward directions with respect to the polarized beam. Preliminary results from pions and protons are already available from the 2004 data [146]; the

first kaon asymmetries as well as more accurate pion and proton asymmetries are expected from the data obtained in 2005. The kaon asymmetries and their charge dependence will provide additional information directly in support of or against the hypothesis that the large asymmetries observed are due to valence quarks. Assuming they are, positive kaons, with a quark content of $u\bar{s}$, would be expected to have a positive asymmetry, and negative kaons, comprised of $\bar{u}s$, would be expected to have an asymmetry of approximately zero or only slightly negative. More precise A_N measurements will also help to distinguish among various model calculations that are consistent with the present results and to put an upper bound on the Sivers distribution function. Now that the BELLE experiment has made a first measurement of the Collins FF [1], transverse SSA's will also be able to constrain transversity. The 2005 BRAHMS results for pions are expected to cover $0.15 < |x_F| < 0.35$; lower beam energies in future running would allow even higher x_F values to be reached. Current results from STAR suggest that the π^0 asymmetry may have a maximum at $x_F \approx 0.5$ or 0.6 and decrease quickly beyond that; see below. Lower-energy running would permit exploration of the behavior of the charged-particle asymmetries as a function of x_F and provide information on transversity at different x values. RHIC is capable of colliding polarized proton beams at center-of-mass energies as low as 50 GeV.

6.2 STAR

The STAR detector has the largest acceptance among the RHIC experiments. Its main barrel, a time-projection chamber for tracking charged particles surrounded by an electromagnetic calorimeter, has full azimuthal coverage for $|\eta| < 1$, making it particularly suitable for multi-particle correlation measurements and jet reconstruction. In 2003 Boer and Vogelsang proposed a single transverse-spin di-jet measurement that could isolate the Sivers effect and probe the gluon Sivers function [68]. A non-zero Sivers function implies a spin dependence in the k_T distributions of the partons within the proton, which would lead to an observable spin-dependent

asymmetry in $\Delta\varphi$ of (nearly) back-to-back jets. A discussion of how such an analysis would be performed by STAR is given in [97]; there will likely be a significant result after the 2006 run at RHIC.

As a follow-up to earlier neutral pion A_N measurements with a forward π^0 detector covering $3.3 < \eta < 4.2$ [9, 126], STAR intends to make a precision measurement of the π^0 transverse SSA over a large x_F range. The current results suggest that the asymmetry may decrease in magnitude for $x_F \gtrsim 0.6$; additional data should make this trend clearer, if it exists. As is the case for BRAHMS A_N measurements, further A_N results from STAR will be able to constrain the Sivers and transversity distributions.

Through recent upgrades, STAR now has electromagnetic calorimetry covering $-1 < \eta < 2$, allowing observation of neutral pions and direct photons within this acceptance. Measurement of A_N for direct photons has been proposed as a probe of the Sivers function for gluons [139]. As mentioned previously, direct photon production is dominated by quark-gluon Compton scattering ($q + g \rightarrow \gamma + X$) over a wide range in photon transverse momentum at RHIC. The fact that there is no fragmentation involved in direct photon production eliminates contributions to the asymmetry from the Collins effect. Alternatively or additionally, STAR could measure correlated photon-jet pairs, which would offer better understanding of the kinematics of the direct photon production, i.e. the x values of the two partons. Jet production, similar to direct photon production, does not consider fragmentation to particular hadrons and is insensitive to the Collins effect. SSA's of photons and jets in events with correlated photon-jet pairs would thus access the gluon and quark Sivers functions, respectively, with some ability to identify the x values at which these functions are probed.

6.3 PHENIX

As discussed in Section 4.3, PHENIX specializes in the measurement of leptonic and photonic probes and high-p_T particles over a limited acceptance. From the modest

transverse-spin data sample taken in 2005 (0.16 pb^{-1}, $\sim 48\%$ average polarization), PHENIX has already begun analysis to obtain improved mid-rapidity A_N results for neutral pions and charged hadrons, which are expected to provide tighter constraints on the gluon Sivers function. Future higher-statistics data samples for these particles at mid-rapidity will provide greater sensitivity to transversity and the Collins effect. See Chapter 7 for further relevant discussion.

There is also analysis underway to obtain first results for A_N of single muons, largely from open charm decay but with significant contributions from light-hadron decays. The current x_F reach for this measurement is ~ 0.15, lower than the x_F values at which significant asymmetries have been observed for other particle species; higher x_F values would become accessible with lower-energy running. A forward hadron A_N measurement using the PHENIX muon spectrometers ($1.2 < |\eta| < 2.4$) may also be possible using muons from hadron decays and the charged hadrons themselves that punch through the steel absorber in front of the muon tracker; however, careful studies will need to be done in order to understand the particle ratios in this sample.

In 2006, PHENIX intends to perform a transverse single -spin di-hadron measurement similar to the STAR di-jet measurement isolating the Sivers effect, following the proposal in [68]. This analysis would study the spin dependence of the azimuthal angle between nearly back-to-back π^0-hadron pairs, triggering on a decay photon from the π^0 in order to obtain a higher-statistics sample. Although dilution of the effect is anticipated for hadron rather than jet pairs, studies have shown that the effect should still be measurable. In examining back-to-back hadrons rather than jets, fragmentation to the final-state hadrons must be considered, and some sensitivity to the Collins mechanism is introduced. However, as described in Chapter 7, there is a large contribution from gluon fragmentation to π^0 production for $p_T \lesssim 5$ GeV/c, to which the Collins mechanism does not apply. The effect is expected to be maximized when the initial spin of the proton is in the same direction as the final-state jet axis; thus, to match the PHENIX central arm acceptance, data will be taken

with radially polarized collisions.

Also similar to possible measurements at STAR, PHENIX could measure A_N of direct photons, sensitive to the Sivers function. Future upgrades extending the azimuthal coverage for tracking to 2π in the inner region and adding forward electromagnetic calorimetry ($0.9 < |\eta| < 3.0$) are expected to expand the coverage for this measurement as well as make γ-jet and jet-jet measurements feasible.

It has been proposed to study the transverse SSA of D meson production at RHIC as a measurement of the gluon Sivers function [37, 34]. This measurement would be significant at any point over a wide range of x_F values ($-0.2 < x_F < 0.6$). D mesons are produced principally via the reaction $g+g \rightarrow c+\bar{c}$, with contributions from $q + \bar{q} \rightarrow c + \bar{c}$ becoming important only at very large x_F ($x_F \gtrsim 0.6$). In neither process is the final c or $\bar{c}$ polarized, excluding the Collins mechanism from contributing to any asymmetry that may be observed. Any transverse SSA seen for mid- to moderate rapidity D production would thus be a direct indication of a non-zero gluon Sivers function. PHENIX is currently capable of measuring open charm decays statistically via single electrons in the central arms and single muons in the muon spectrometers. In the future, a silicon vertex detector upgrade will make it possible to identify D mesons event-by-event. A silicon-pixel and silicon-strip barrel detector, covering the central arm pseudorapidity region and 2π in azimuth, is expected to be installed in 2009. A silicon-strip endcap detector, covering the muon arm acceptance, has been proposed for 2011.

The flavor separation of the Sivers function for u, d, $\bar{u}$, and $\bar{d}$ quarks via A_N of forward or backward W boson production has been suggested [137]. PHENIX already has a W physics program planned for the future, once 500-GeV polarized collisions are achieved by RHIC, making W measurements possible. The processes of interest will be:

$$\begin{aligned} u + \bar{d} &\rightarrow W^+ \rightarrow \mu^+ + \nu_\mu \\ d + \bar{u} &\rightarrow W^- \rightarrow \mu^- + \bar{\nu}_\mu \end{aligned}$$

PHENIX will observe the final-state muons; an upgrade to trigger on the highest-p_T

muons, which will come principally from W decays, is expected to be installed in 2009. The muon trigger upgrade will also improve the pattern recognition in the muon arms, reducing background and making measurements such as single muons from D decays, or muon pairs from resonance decays or the Drell-Yan process ($q + \bar{q} \rightarrow \ell^+ + \ell^-$), cleaner.

The double transverse-spin asymmetry, $A_{TT} = \frac{\sigma^{\uparrow\uparrow} - \sigma^{\uparrow\downarrow}}{\sigma^{\uparrow\uparrow} + \sigma^{\uparrow\downarrow}}$, is another observable sensitive to transverse spin quantities. A_{TT} for the Drell-Yan process provides direct access to the transversity distribution. The transversity distributions for the quark and the antiquark provide the necessary convolution of two chiral-odd functions to be an allowed process in QCD, with no fragmentation or final-state interactions involved. Although this asymmetry is expected to be at the sub-percent level for $\sqrt{s} = 200$ GeV, it could reach several percent for $\sqrt{s} < 100$ GeV. PHENIX already has an effective di-muon trigger that would be suitable for measuring Drell-Yan pairs; however, studies would need to be done to understand the current backgrounds. The muon trigger upgrade mentioned above would provide a cleaner sample. Investigation would be necessary to optimize the beam energy in order to obtain the best compromise between luminosity and the size of the predicted asymmetry. A first direct measurement of transversity would be an exciting milestone in the field of transverse nucleon spin structure.

Chapter 7

Conclusions

The transverse single-spin asymmetry, A_N, for neutral pion production at $x_F \approx 0.0$ for $1 < p_T < 5$ GeV/c from polarized proton-proton interactions at $\sqrt{s} = 200$ GeV has been presented. It is consistent with zero within statistical errors of a few percent. The measurement, together with a similar measurement for charged hadrons, represents the first mid-rapidity A_N result at high p_T and collider energies; both have been published in *Physical Review Letters* [15]. The measurement is in a kinematic regime where the theoretical framework of perturbative QCD has been demonstrated to describe the polarization-averaged cross sections for neutral pions and charged hadrons well for $p_T \gtrsim 1.5$ GeV/c. A pQCD framework is expected to be applicable in the interpretation of the polarized results down to similar transverse momentum values.

The present result is consistent with the mid-rapidity results for neutral pions from $p + p$ collisions at $\sqrt{s} = 19.4$ GeV [8]. The measurement is complementary to the measurement of A_N for forward neutral pion production in $p + p$ collisions at $\sqrt{s} = 200$ GeV [9], which observed asymmetries reaching $\sim 30\%$.

Neutral pion production at forward rapidity is expected to originate from partonic processes involving valence quarks ($x \gtrsim 0.1$), whereas the particle production at mid-rapidity presented here is dominated by gluon-gluon and quark-gluon processes ($x \lesssim 0.1$). Figure 7.1 shows the fractional contribution of different partonic scattering processes to the production of neutral pions at mid-rapidity at 200 GeV,

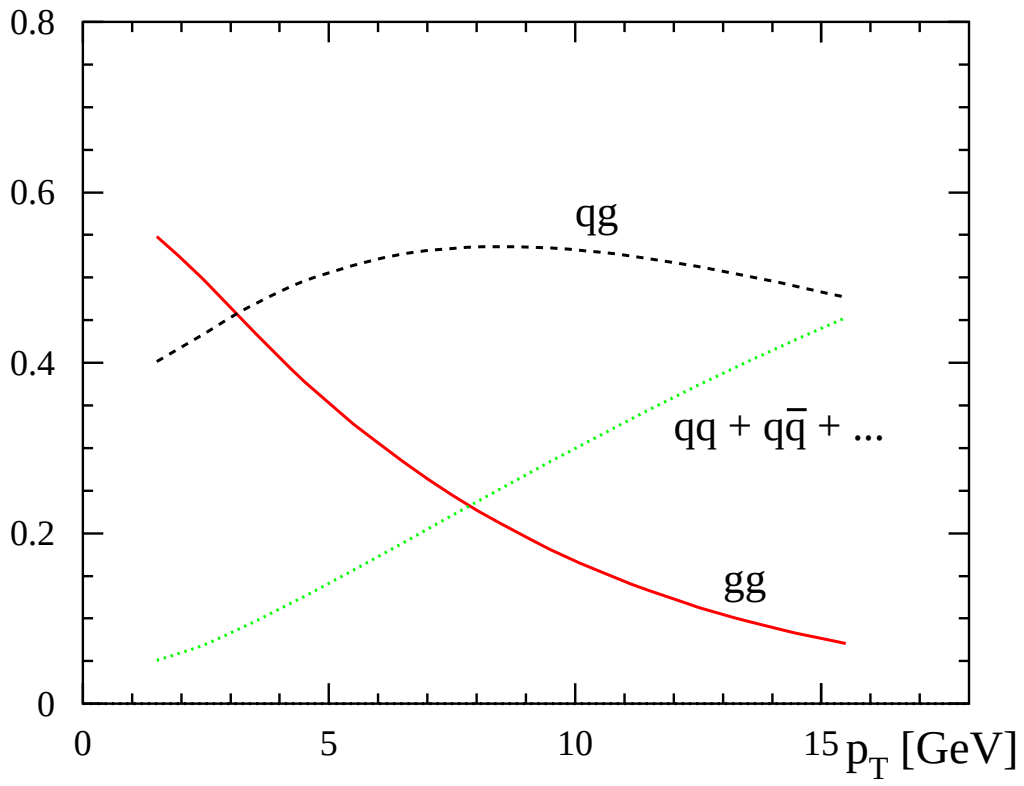

Figure 7.1: Relative fractional contributions of partonic processes to mid-rapidity π^0 production at $\sqrt{s} = 200$ GeV, calculated by W. Vogelsang.

calculated by W. Vogelsang. As evident from the figure, π^0 production in the transverse momentum range covered by the measurement presented here is approximately half from gluon-gluon scattering and half from gluon-quark scattering. As such, the asymmetry is not very sensitive to mechanisms involving quarks, e.g. the Collins effect.

Independently of the suppression or dilution of the Collins effect in the present results due to a dominance of gluon scattering, it has been stated by Anselmino *et al.* that the Collins effect is suppressed more generally [36, 35]. They argue that when all partonic intrinsic motion is taken into account in the formalism without sim-

plifications or approximations, the complicated azimuthal angle dependencies and numerous different phases involved in the Collins mechanism lead to strong suppression of the final asymmetry. They demonstrate that with saturated bounds on the non-perturbative components (the transversity distribution function and Collins FF), the Collins mechanism alone is insufficient to explain the large asymmetries observed in forward charged pion production at $\sqrt{s} = 19.4$ GeV [6]. There has been some criticism of the formalism on which their argument is based (see for example the alternative treatment presented in [48]), but a consensus in support of its validity or repudiating it has yet to be reached within the theoretical community. In the framework of Anselmino *et al.*, the PHENIX mid-rapidity A_N results, i.e. the π^0 measurement presented here as well as the charged hadron measurement discussed in Section 5.8, provide strong constraints on the Sivers distribution function for gluons and indicate that it is small. A publication providing a quantitative constraint on the gluon Sivers distribution from the PHENIX data is forthcoming [91].

Regardless of more detailed interpretations that may become available, the results are consistent with the naive pQCD expectation that transverse single-spin asymmetries are suppressed at high p_T and mid-rapidity [112, 132].

The transverse SSA results from the E704 experiment at Fermilab [6, 8] and from the RHIC experiments [9, 146, 15] are strikingly similar despite an order of magnitude difference in center-of-mass energy. In the forward direction ($x_F > 0$), significant asymmetries were observed at both energies for the production of charged and neutral pions. In both cases a similar, clear dependence of the asymmetry on the particle charge was observed: positive for positive and neutral pions and negative for negative pions, with $|A_N^{\pi^+}| \approx |A_N^{\pi^-}|$. Mid-rapidity ($x_F \approx 0$) neutral pion results are consistent with zero at both energies. Asymmetries consistent with zero have been measured not only at mid-rapidity but also in the backward direction ($x_F < 0$) at RHIC. The A_N results for forward, mid-rapidity, and backward particle production considered all together suggest that the large SSA's observed in the forward region are due to valence quarks.

Interest in transverse nucleon-spin structure and transverse SSA's rose sharply when the first large asymmetries were observed in the late 1970's, contradicting naive expectations from pQCD. Despite similar effects observed by more than one subsequent experiment in the 1980's, it was not until higher-energy data became available starting in the 1990's that a pQCD framework became potentially applicable in interpreting the effects, and the theoretical ideas most widely accepted today began to develop.

The study of transverse nucleon-spin structure has progressed rapidly both theoretically and experimentally over the course of the last several years. Notable experimental contributions have come from the HERMES and COMPASS polarized deep-inelastic scattering experiments, the BELLE experiment studying $e^+ + e^-$ annihilation, and the STAR, PHENIX, and BRAHMS collaborations studying polarized $p + p$ collisions at RHIC.

The recent measurement of the Collins FF for pions by BELLE [1] represents a turning point in the study of the transverse spin structure of the proton. The non-zero result means that the Collins mechanism remains as a possible origin of the large transverse single-spin asymmetries observed. Moreover, it allows access to the transversity distribution function through single-spin asymmetries for the first time. Non-zero asymmetries already measured by DIS and hadronic-collision experiments can now be revisited and reinterpreted to obtain first constraints on transversity, assuming the asymmetries contain contributions from the Collins effect.

The startup of RHIC as the world's first polarized-proton collider in late 2001 ushered in a new era in the study of nucleon spin structure. RHIC holds great potential for in-depth exploration of both the transverse and longitudinal spin structure of the proton. To date, two transverse spin publications [9, 15] and one longitudinal-spin publication [17] have come out of the major experiments at RHIC. Additional preliminary results are also available, as summarized in Section 2.2.

The transverse single-spin asymmetry for neutral pions presented here represents an early measurement in a rigorous program to study transverse proton spin struc-

ture at hard scales using a pQCD framework at RHIC. Conclusively explaining the large transverse single-spin asymmetries, which have been observed over an extensive range of energies, would help to link proton structure at soft and hard scales. A number of planned and proposed future transverse spin measurements have been described in Chapter 6. Some of the measurements proposed would be able to isolate particular mechanisms. These measurements will be essential in order to disentangle the several possible contributions to the large observed asymmetries currently under discussion and to begin to understand the transverse spin structure of the proton. It should be possible to measure transversity, the last remaining leading-twist, k_T-integrated distribution function that is completely unknown, and to start to measure the various transverse-momentum-dependent (TMD) distribution functions such as the Sivers function.

As discussed in Section 2.2.5, TMD distribution functions are related to the orbital angular momentum of partons within the proton. Thus measurement of the Sivers function could shed light on parton OAM, which remains to date nearly inscrutable. No proposal for a clear and direct experimental measurement of OAM has yet been set forth. Therefore, measurement of the Sivers function could provide a starting point for elucidating this still-opaque aspect of nucleon angular-momentum structure.

Despite the fact that the proton is one of the most commonplace and stable particles in existence, a fundamental component of ordinary matter, the path to unraveling proton structure has been a long one, and the journey is not yet finished. The final picture will not be complete without full description of its momentum, helicity, and transverse-spin structure. A comprehensive understanding of the proton, in many ways the embodiment of QCD, implies an understanding of the strong force, one of the four fundamental forces in nature and the foundation for all of nuclear physics.

Bibliography

[1] K. Abe et al. Measurement of azimuthal asymmetries in inclusive production of hadron pairs in e^+e^- annihilation at BELLE, 2005. Presented at 22nd International Symposium on Lepton-Photon Interactions at High Energy (LP 2005), Uppsala, Sweden, 30 Jun - 5 Jul 2005, hep-ex/0507063.

[2] H. Abramowicz and A. Caldwell. HERA collider physics. *Rev. Mod. Phys.*, 71:1275–1410, 1999.

[3] K. H. Ackermann et al. STAR detector overview. *Nucl. Instrum. Meth.*, A499:624–632, 2003.

[4] K. Ackerstaff et al. The flavor asymmetry of the light quark sea from semi-inclusive deep inelastic scattering. *Phys. Rev. Lett.*, 81:5519–5523, 1998.

[5] M. Adamczyk et al. The BRAHMS experiment at RHIC. *Nucl. Instrum. Meth.*, A499:437–468, 2003.

[6] D. L. Adams et al. Analyzing power in inclusive π^+ and π^- production at high x_F with a 200-GeV polarized proton beam. *Phys. Lett.*, B264:462–466, 1991.

[7] D. L. Adams et al. Comparison of spin asymmetries and cross-sections in π^0 production by 200-GeV polarized anti-protons and protons. *Phys. Lett.*, B261:201–206, 1991.

[8] D. L. Adams et al. Single spin asymmetries and invariant cross-sections of the high transverse momentum inclusive π^0 production in 200- GeV/c $p + p$ and anti-$p + p$ interactions. *Phys. Rev.*, D53:4747–4755, 1996.

[9] J. Adams et al. Cross sections and transverse single-spin asymmetries in forward neutral pion production from proton collisions at $\sqrt{s} = 200$ GeV. *Phys. Rev. Lett.*, 92:171801, 2004.

[10] J. Adams et al. Experimental and theoretical challenges in the search for the quark gluon plasma: The STAR collaboration's critical assessment of the evidence from RHIC collisions. *Nucl. Phys.*, A757:102–183, 2005.

[11] K. Adcox et al. PHENIX central arm tracking detectors. *Nucl. Instrum. Meth.*, A499:489–507, 2003.

[12] K. Adcox et al. PHENIX detector overview. *Nucl. Instrum. Meth.*, A499:469–479, 2003.

[13] K. Adcox et al. Formation of dense partonic matter in relativistic nucleus-nucleus collisions at RHIC: Experimental evaluation by the PHENIX collaboration. *Nucl. Phys.*, A757:184–283, 2005.

[14] C. Adler et al. The RHIC zero-degree calorimeters. *Nucl. Instrum. Meth.*, A499:433–436, 2003.

[15] S. S. Adler. Measurement of transverse single-spin asymmetries for mid-rapidity production of neutral pions and charged hadrons in polarized $p + p$ collisions at $\sqrt{s} = 200$ GeV. *Phys. Rev. Lett.*, 95:202001, 2005.

[16] S. S. Adler et al. Mid-rapidity neutral pion production in proton-proton collisions at $\sqrt{s} = 200$ GeV. *Phys. Rev. Lett.*, 91:241803, 2003.

[17] S. S. Adler et al. Double helicity asymmetry in inclusive mid-rapidity π^0 production for polarized $p + p$ collisions at $\sqrt{s} = 200$ GeV. *Phys. Rev. Lett.*, 93:202002, 2004.

[18] S. S. Adler et al. Mid-rapidity direct-photon production in $p + p$ collisions at $\sqrt{s} = 200$ GeV. *Phys. Rev.*, D71:071102, 2005.

[19] A. Airapetian et al. Observation of a single-spin azimuthal asymmetry in semi-inclusive pion electro-production. *Phys. Rev. Lett.*, 84:4047–4051, 2000.

[20] A. Airapetian et al. Single-spin azimuthal asymmetry in exclusive electroproduction of π^+ mesons. *Phys. Lett.*, B535:85–92, 2002.

[21] A. Airapetian et al. Quark helicity distributions in the nucleon for up, down, and strange quarks from semi-inclusive deep-inelastic scattering. *Phys. Rev.*, D71:012003, 2005.

[22] A. Airapetian et al. Single-spin asymmetries in semi-inclusive deep-inelastic scattering on a transversely polarized hydrogen target. *Phys. Rev. Lett.*, 94:012002, 2005.

[23] M. Aizawa et al. PHENIX central arm particle ID detectors. *Nucl. Instrum. Meth.*, A499:508–520, 2003.

[24] H. Akikawa et al. PHENIX muon arms. *Nucl. Instrum. Meth.*, A499:537–548, 2003.

[25] I. Alekseev et al. Polarized proton collider at RHIC. *Nucl. Instrum. Meth.*, A499:392–414, 2003.

[26] I. G. Alekseev et al. Analyzing power in CNI-region at AGS (experiment E950). *AIP Conf. Proc.*, 549:670–673, 2002.

[27] V. Yu. Alexakhin et al. First measurement of the transverse spin asymmetries of the deuteron in semi-inclusive deep inelastic scattering. *Phys. Rev. Lett.*, 94:202002, 2005.

[28] M. Allen et al. PHENIX inner detectors. *Nucl. Instrum. Meth.*, A499:549–559, 2003.

[29] C. E. Allgower et al. Measurement of analyzing powers of π^+ and π^- produced on a hydrogen and a carbon target with a 22-GeV/c incident polarized proton beam. *Phys. Rev.*, D65:092008, 2002.

[30] G. Altarelli and G. Parisi. Asymptotic freedom in parton language. *Nucl. Phys.*, B126:298, 1977.

[31] D. Amati, R. Petronzio, and G. Veneziano. Relating hard QCD processes through universality of mass singularities. *Nucl. Phys.*, B140:54, 1978.

[32] D. Amati, R. Petronzio, and G. Veneziano. Relating hard QCD processes through universality of mass singularities. 2. *Nucl. Phys.*, B146:29–49, 1978.

[33] P. Amaudruz et al. The Gottfried sum from the ratio $F_2(n)/F_2(p)$. *Phys. Rev. Lett.*, 66:2712–2715, 1991.

[34] M. Anselmino, M. Boglione, U. D'Alesio, E. Leader, and F. Murgia. Accessing Sivers gluon distribution via transverse single spin asymmetries in $p^\uparrow + p \to DX$ processes at RHIC. *Phys. Rev.*, D70:074025, 2004.

[35] M. Anselmino, M. Boglione, U. D'Alesio, E. Leader, and F. Murgia. Can the Collins mechanism explain the large transverse single spin asymmetries observed in $p^\uparrow + p \to \pi X$? In *Proceedings of the 16th International Spin Physics Symposium (SPIN 2004), Trieste, Italy, 10-16 Oct 2004*, pages 341–344. Trieste/Mainz, 2005. hep-ph/0412236.

[36] M. Anselmino, M. Boglione, U. D'Alesio, E. Leader, and F. Murgia. Parton intrinsic motion: Suppression of the Collins mechanism for transverse single spin asymmetries in $p^\uparrow + p \to \pi X$. *Phys. Rev.*, D71:014002, 2005.

[37] M. Anselmino, M. Boglione, E. Leader, U. D'Alesio, and F. Murgia. The gluon Sivers distribution in D production at RHIC. In *Proceedings of the 16th International Spin Physics Symposium (SPIN 2004), Trieste, Italy, 10-16 Oct 2004*, pages 345–348. Trieste/Mainz, 2005. hep-ph/0412022.

[38] M. Anselmino, M. Boglione, and F. Murgia. Single spin asymmetry for $p^{\uparrow}+p \rightarrow \pi X$ in perturbative QCD. *Phys. Lett.*, B362:164–172, 1995.

[39] M. Anselmino and F. Murgia. Single spin asymmetries in $p^{\uparrow} + p$ and anti-$p^{\uparrow}$ p inclusive processes. *Phys. Lett.*, B442:470–478, 1998.

[40] J. Antille et al. Spin dependence of the inclusive reaction $pp^{\uparrow} \rightarrow \pi^0 X$ at 24 GeV/c for high p_T π^0 produced in the central region. *Phys. Lett.*, B94:523, 1980.

[41] L. Aphecetche et al. PHENIX calorimeter. *Nucl. Instrum. Meth.*, A499:521–536, 2003.

[42] V. D. Apokin et al. Observation of significant spin effects in hard collisions at 40 GeV/c. *Phys. Lett.*, B243:461–464, 1990.

[43] M. Arneodo et al. A reevaluation of the Gottfried sum. *Phys. Rev.*, D50:1–3, 1994.

[44] I. Arsene et al. Quark-Gluon Plasma and Color Glass Condensate at RHIC? The perspective from the BRAHMS experiment. *Nucl. Phys.*, A757:1–27, 2005.

[45] X. Artru, J. Czyzewski, and H. Yabuki. Single spin asymmetry in inclusive pion production, Collins effect and the string model. *Z. Phys.*, C73:527–534, 1997.

[46] J. Ashman et al. A measurement of the spin asymmetry and determination of the structure function g_1 in deep inelastic muon proton scattering. *Phys. Lett.*, B206:364, 1988.

[47] J. Ashman et al. An investigation of the spin structure of the proton in deep inelastic scattering of polarized muons on polarized protons. *Nucl. Phys.*, B328:1, 1989.

[48] A. Bacchetta, C. J. Bomhof, P. J. Mulders, and F. Pijlman. Single spin asymmetries in hadron-hadron collisions. *Phys. Rev.*, D72:034030, 2005.

[49] A. Bacchetta, U. D'Alesio, M. Diehl, and C. A. Miller. Single-spin asymmetries: The Trento conventions. *Phys. Rev.*, D70:117504, 2004.

[50] B. B. Back et al. The PHOBOS detector at RHIC. *Nucl. Instrum. Meth.*, A499:603–623, 2003.

[51] B. B. Back et al. The PHOBOS perspective on discoveries at RHIC. *Nucl. Phys.*, A757:28–101, 2005.

[52] M. Bai, L. Ahrens, and T. Roser. Overcoming intrinsic and coupling spin resonances in the AGS. *AIP Conf. Proc.*, 667:15–29, 2003.

[53] M. Bai, A. U. Luccio, W. W. MacKay, T. Roser, and V. Ranjbar. RHIC spin flipper commissioning. *AIP Conf. Proc.*, 675:771–775, 2003.

[54] B. L. G. Bakker, E. Leader, and T. L. Trueman. A critique of the angular momentum sum rules and a new angular momentum sum rule. *Phys. Rev.*, D70:114001, 2004.

[55] A. Baldit et al. Study of the isospin symmetry breaking the in the light quark sea of the nucleon from the Drell-Yan process. *Phys. Lett.*, B332:244–250, 1994.

[56] I. I. Balitsky and L. N. Lipatov. The Pomeranchuk singularity in Quantum Chromodynamics. *Sov. J. Nucl. Phys.*, 28:822–829, 1978.

[57] V. Bargmann, L. Michel, and V. L. Telegdi. Precession of the polarization of particles moving in a homogeneous electromagnetic field. *Phys. Rev. Lett.*, 2:435, 1959.

[58] R. Barlow. Systematic errors: Facts and fictions. In *Proceedings of the Conference on Advanced Statistical Techniques in Particle Physics, Durham, England, 18-22 Mar 2002*, pages 134–144, 2002. hep-ex/0207026.

[59] S. D. Bass. The spin structure of the proton. 2004. hep-ph/0411005. To appear in *Rev. Mod. Phys.*

[60] A. Bazilevsky et al. Measurement of single transverse-spin asymmetry in forward production of photons and neutrons in $p+p$ collisions at $\sqrt{s} = 200$ GeV. *AIP Conf. Proc.*, 675:584–588, 2003.

[61] J. D. Bjorken. Asymptotic sum rules at infinite momentum. *Phys. Rev.*, 179:1547–1553, 1969.

[62] E. D. Bloom et al. High-energy inelastic ep scattering at 6 degrees and 10 degrees. *Phys. Rev. Lett.*, 23:930–934, 1969.

[63] J. Blümlein and H. Böttcher. QCD analysis of polarized deep inelastic scattering data and parton distributions. *Nucl. Phys.*, B636:225–263, 2002.

[64] A. Bodek et al. Experimental studies of the neutron and proton electromagnetic structure functions. *Phys. Rev.*, D20:1471–1552, 1979.

[65] G. T. Bodwin. Factorization of the Drell-Yan cross-section in perturbation theory. *Phys. Rev.*, D31:2616, 1985. Erratum-ibid.D34:3932,1986.

[66] D. Boer. Sudakov suppression in azimuthal spin asymmetries. *Nucl. Phys.*, B603:195–217, 2001.

[67] D. Boer, P. J. Mulders, and F. Pijlman. Universality of T-odd effects in single spin and azimuthal asymmetries. *Nucl. Phys.*, B667:201–241, 2003.

[68] D. Boer and W. Vogelsang. Asymmetric jet correlations in $pp^{\uparrow}$ scattering. *Phys. Rev.*, D69:094025, 2004.

[69] C. J. Bomhof, P. J. Mulders, and F. Pijlman. Gauge link structure in quark quark correlators in hard processes. *Phys. Lett.*, B596:277–286, 2004.

[70] C. Bourrely and J. Soffer. On the size of the Coulomb - nuclear interference polarization in hadronic reactions at high-energy and large momentum transfer. *Nuovo Cim. Lett.*, 19:569, 1977.

[71] C. Bourrely and J. Soffer. Do we understand the single-spin asymmetry for π^0 inclusive production in $p+p$ collisions? *Eur. Phys. J.*, C36:371–374, 2004.

[72] A. Bravar. Transverse spin asymmetries in $p^{\uparrow}p \to \pi^{\pm}+X$ and $lp^{\uparrow} \to l'+\pi^{\pm}+X$. *Nucl. Phys.*, A666:314–317, 2000.

[73] M. Breidenbach et al. Observed behavior of highly inelastic electron - proton scattering. *Phys. Rev. Lett.*, 23:935–939, 1969.

[74] S. J. Brodsky, D. S. Hwang, and I. Schmidt. Final-state interactions and single-spin asymmetries in semi-inclusive deep inelastic scattering. *Phys. Lett.*, B530:99–107, 2002.

[75] M. Burkardt. Chromodynamic lensing and transverse single spin asymmetries. *Nucl. Phys.*, A735:185–199, 2004.

[76] M. Burkardt and D. S. Hwang. Sivers asymmetry and generalized parton distributions in impact parameter space. *Phys. Rev.*, D69:074032, 2004.

[77] C. G. Callan Jr. and D. J. Gross. High-energy electroproduction and the constitution of the electric current. *Phys. Rev. Lett.*, 22:156–159, 1969.

[78] J. C. Collins. Fragmentation of transversely polarized quarks probed in transverse momentum distributions. *Nucl. Phys.*, B396:161–182, 1993.

[79] J. C. Collins. Hard scattering in QCD with polarized beams. *Nucl. Phys.*, B394:169–199, 1993.

[80] J. C. Collins. Leading-twist single-transverse-spin asymmetries: Drell-Yan and deep-inelastic scattering. *Phys. Lett.*, B536:43–48, 2002.

[81] J. C. Collins, S. F. Heppelmann, and G. A. Ladinsky. Measuring transversity densities in singly polarized hadron - hadron and lepton - hadron collisions. *Nucl. Phys.*, B420:565–582, 1994.

[82] J. C. Collins and A. Metz. Universality of soft and collinear factors in hard-scattering factorization. *Phys. Rev. Lett.*, 93:252001, 2004.

[83] J. C. Collins and D. E. Soper. Back-to-back jets in QCD. *Nucl. Phys.*, B193:381, 1981. Erratum-ibid.B213:545,1983.

[84] J. C. Collins and D. E. Soper. Back-to-back jets: Fourier transform from b to k_T. *Nucl. Phys.*, B197:446, 1982.

[85] J. C. Collins and D. E. Soper. Parton distribution and decay functions. *Nucl. Phys.*, B194:445, 1982.

[86] J. C. Collins, D. E. Soper, and G. Sterman. Factorization for short distance hadron - hadron scattering. *Nucl. Phys.*, B261:104, 1985.

[87] J. C. Collins, D. E. Soper, and G. Sterman. Transverse momentum distribution in Drell-Yan pair and W and Z boson production. *Nucl. Phys.*, B250:199, 1985.

[88] J. C. Collins, D. E. Soper, and G. Sterman. Soft gluons and factorization. *Nucl. Phys.*, B308:833, 1988.

[89] A. M. Cooper-Sarkar, R. C. E. Devenish, and A. De Roeck. Structure functions of the nucleon and their interpretation. *Int. J. Mod. Phys.*, A13:3385–3586, 1998.

[90] G. Curci, W. Furmanski, and R. Petronzio. Evolution of parton densities beyond leading order: The nonsinglet case. *Nucl. Phys.*, B175:27, 1980.

[91] U. D'Alesio, September 2005. Private communication.

[92] Ya. S. Derbenev et al. Radiative polarization: Obtaining, control, using. *Part. Accel.*, 8:115–126, 1978.

[93] Yu. L. Dokshitzer. Calculation of the structure functions for deep inelastic scattering and e^+e^- annihilation by perturbation theory in Quantum Chromodynamics. (in Russian). *Sov. Phys. JETP*, 46:641–653, 1977.

[94] W. H. Dragoset et al. Asymmetries in inclusive proton - nucleon scattering at 11.75 GeV/c. *Phys. Rev.*, D18:3939–3954, 1978.

[95] R. K. Ellis, H. Georgi, M. Machacek, H. D. Politzer, and G. G. Ross. Factorization and the parton model in QCD. *Phys. Lett.*, B78:281, 1978.

[96] R. K. Ellis, H. Georgi, M. Machacek, H. D. Politzer, and G. G. Ross. Perturbation theory and the parton model in QCD. *Nucl. Phys.*, B152:285, 1979.

[97] R. Fatemi. Constraining the Sivers functions using transverse spin asymmetries at STAR. In D. Bruncko, J. Ferencei, and P Stríženec, editors, *Proceedings of the XII International Workshop on Deep Inelastic Scattering (DIS 2004), Štrbské Pleso, Slovakia, 14-18 Apr 2004*, pages 1086–1090, 2004.

[98] R. P. Feynman. Very high-energy collisions of hadrons. *Phys. Rev. Lett.*, 23:1415–1417, 1969.

[99] M. Gell-Mann and Y. Ne'eman. *The Eightfold Way.* WA Benjamin, New York, 1964.

[100] M. Glück, E. Reya, M. Stratmann, and W. Vogelsang. Models for the polarized parton distributions of the nucleon. *Phys. Rev.*, D63:094005, 2001.

[101] V. N. Gribov and L. N. Lipatov. Deep inelastic ep scattering in perturbation theory. *Yad. Fiz.*, 15:781–807, 1972.

[102] E. A. Hawker et al. Measurement of the light antiquark flavor asymmetry in the nucleon sea. *Phys. Rev. Lett.*, 80:3715–3718, 1998.

[103] A. A. Henneman, D. Boer, and P. J. Mulders. Evolution of transverse momentum dependent distribution and fragmentation functions. *Nucl. Phys.*, B620:331–350, 2002.

[104] M. Hirai, S. Kumano, and N. Saito. Determination of polarized parton distribution functions and their uncertainties. *Phys. Rev.*, D69:054021, 2004.

[105] A. Idilbi, X-D.. Ji, J.-P. Ma, and Feng Yuan. Collins-Soper equation for the energy evolution of transverse-momentum and spin dependent parton distributions. *Phys. Rev.*, D70:074021, 2004.

[106] R. L. Jaffe and X.-D. Ji. Chiral odd parton distributions and polarized Drell-Yan. *Phys. Rev. Lett.*, 67:552–555, 1991.

[107] B. Jäger, A. Schäfer, M. Stratmann, and W. Vogelsang. Next-to-leading order QCD corrections to high-p_T pion production in longitudinally polarized pp collisions. *Phys. Rev.*, D67:054005, 2003.

[108] X.-D. Ji, J.-P. Ma, and F. Yuan. QCD factorization for spin-dependent cross sections in DIS and Drell-Yan processes at low transverse momentum. *Phys. Lett.*, B597:299–308, 2004.

[109] X.-D. Ji, J.-P. Ma, and F. Yuan. QCD factorization for semi-inclusive deep-inelastic scattering at low transverse momentum. *Phys. Rev.*, D71:034005, 2005.

[110] O. Jinnouchi et al. RHIC pC CNI polarimeter: Status and performance from the first collider run. *AIP Conf. Proc.*, 675:817–825, 2003.

[111] Y. Kanazawa and Y. Koike. Chiral-odd contribution to single-transverse spin asymmetry in hadronic pion production. *Phys. Lett.*, B478:121–126, 2000.

[112] G. L. Kane, J. Pumplin, and W. Repko. Transverse quark polarization in large p_T reactions, e^+e^- jets, and leptoproduction: A test of QCD. *Phys. Rev. Lett.*, 41:1689, 1978.

[113] B. A. Kniehl, G. Kramer, and B. Pötter. Testing the universality of fragmentation functions. *Nucl. Phys.*, B597:337–369, 2001.

[114] S. Kretzer. Fragmentation functions from flavour-inclusive and flavour- tagged e^+e^- annihilations. *Phys. Rev.*, D62:054001, 2000.

[115] R. Kundu and A. Metz. Higher twist and transverse momentum dependent parton distributions: A light-front Hamiltonian approach. *Phys. Rev.*, D65:014009, 2002.

[116] E. A. Kuraev, L. N. Lipatov, and V. S. Fadin. Multi-Reggeon processes in the Yang-Mills theory. *Sov. Phys. JETP*, 44:443–450, 1976.

[117] E. A. Kuraev, L. N. Lipatov, and V. S. Fadin. The Pomeranchuk singularity in nonabelian gauge theories. *Sov. Phys. JETP*, 45:199–204, 1977.

[118] S. B. Libby and G. Sterman. Jet and lepton pair production in high-energy lepton - hadron and hadron - hadron scattering. *Phys. Rev.*, D18:3252, 1978.

[119] L. N. Lipatov. The parton model and perturbation theory. *Sov. J. Nucl. Phys.*, 20:94–102, 1975.

[120] B.-Q. Ma, I. Schmidt, and J.-J. Yang. Collins effect in single spin asymmetries of the $p^\uparrow p \to \pi X$ process. *Eur. Phys. J.*, C40:63–67, 2005.

[121] W. W. MacKay et al. Commissioning spin rotators in RHIC. page 1697. IEEE, 2003. Proc. of the 2003 Part. Acc. Conf.

[122] A. Metz. Gluon-exchange in spin-dependent fragmentation. *Phys. Lett.*, B549:139–145, 2002.

[123] D. A. Morozov. Spin effects in forward π^0 production in polarized proton-proton collisions at STAR. 2005. To appear in the proceedings of the 40th Rencontres de Moriond on QCD and High Energy Hadronic Interactions, La Thuile, Aosta Valley, Italy, 12-19 Mar 2005, hep-ex/0505024.

[124] A. H. Mueller, editor. *Perturbative Quantum Chromodynamics*. World Scientific Publ., Singapore, 1989.

[125] P. J. Mulders and R. D. Tangerman. The complete tree-level result up to order 1/Q for polarized deep-inelastic leptoproduction. *Nucl. Phys.*, B461:197–237, 1996. Erratum-ibid.B484:538-540,1997.

[126] A. Ogawa. Spin effects in large rapidity neutral pion production at STAR. In *Proceedings of the 16th International Spin Physics Symposium (SPIN 2004), Trieste, Italy, 10-16 Oct 2004*, pages 337–340. Trieste/Mainz, 2005. hep-ex/0412035.

[127] H. Okada et al. Measurement of the analyzing power in $p+p$ elastic scattering in the peak CNI region at RHIC. 2005. nucl-ex/0502022.

[128] K. Orginos, T. Blum, and S. Ohta. Nucleon structure functions with domain wall fermions. 2005. hep-lat/0505024.

[129] C. F. Perdrisat and V. Punjabi. The JLab polarization transfer measurements of proton elastic form factor. *Pramana*, 61:827–835, 2003. Prepared for QCD 2002, Kanpur, India, 18-22 Nov 2002.

[130] H. D. Politzer. Asymptotic freedom: An approach to strong interactions. *Phys. Rept.*, 14:129–180, 1974.

[131] J. Pumplin et al. New generation of parton distributions with uncertainties from global QCD analysis. *JHEP*, 0207:012, 2002.

[132] J.-W. Qiu and G. Sterman. Single transverse-spin asymmetries in hadronic pion production. *Phys. Rev.*, D59:014004, 1999.

[133] J. P. Ralston and D. E. Soper. Production of dimuons from high-energy polarized proton proton collisions. *Nucl. Phys.*, B152:109, 1979.

[134] T. Roser. Properties of partially excited Siberian Snakes. *AIP Conf. Proc.*, 187:1442, 1989. Proc. of the 8th International Symposium on High-Energy Spin Physics.

[135] T. Roser. Acceleration of polarized beams using multiple strong partial snakes. In *Proceedings of the 16th International Spin Physics Symposium (SPIN 2004)*, page 687, Singapore, 2005. World Scientific.

[136] S. Saroff et al. Single spin asymmetry in inclusive reactions polarized-p p goes to π^+, π^-, and p at high p_T at 13.3 GeV/c and 18.5 GeV/c. *Phys. Rev. Lett.*, 64:995, 1990.

[137] I. Schmidt. Talk presented at the Transversity 2005 Workshop in Como, Italy, 7-10 Sep 2005.

[138] I. Schmidt and J. Soffer. Transverse single-spin asymmetries in gauge boson production. *Phys. Lett.*, B563:179–182, 2003.

[139] I. Schmidt, J. Soffer, and J.-J. Yang. Transverse single spin asymmetries in photon production. *Phys. Lett.*, B612:258–262, 2005.

[140] D. W. Sivers. Single spin production asymmetries from the hard scattering of point - like constituents. *Phys. Rev.*, D41:83, 1990.

[141] D. W. Sivers. Hard scattering scaling laws for single spin production asymmetries. *Phys. Rev.*, D43:261–263, 1991.

[142] J. Soffer. Positivity constraints for spin dependent parton distributions. *Phys. Rev. Lett.*, 74:1292–1294, 1995.

[143] H. Spinka. Note on RHIC polarimetry. 1999. ANL-HEP-TR-99-113.

[144] L. H. Thomas. *Philos. Mag.*, 3:1, 1927.

[145] R. S. Towell et al. Improved measurement of the anti-d/anti-u asymmetry in the nucleon sea. *Phys. Rev.*, D64:052002, 2001.

[146] F. Videbaek. Single spin asymmetries in the BRAHMS experiment. 2005. To appear in the proceedings of 13th International Workshop on Deep Inelastic Scattering (DIS 05), Madison, Wisconsin, 27 Apr - 1 May 2005, nucl-ex/0508015.

[147] W. Vogelsang and F. Yuan. Single-transverse spin asymmetries: From DIS to hadronic collisions. *Phys. Rev.*, D72:054028, 2005.

[148] A. Zelenski et al. Optically-pumped polarized H^- ion source for RHIC spin physics. *Rev. Sci. Instrum.*, 73:888–891, 2002.

[149] A. Zelenski et al. Absolute polarized H^- jet polarimeter development, for RHIC. *Nucl. Instrum. Meth.*, A536:248–254, 2005.

Appendix A

Relative luminosity considerations

In a collider environment, different considerations must be made in determining the relative luminosity of crossings with different spin configurations in the case of double- or single-spin asymmetry measurements, and for transverse or longitudinal spin in the case of single-spin asymmetry measurements. Care must be taken in designing a MB trigger that has no spin-dependent bias and can make an accurate measurement of the relative luminosity. To make double-spin asymmetry measurements, the principal concern is that there may be a non-zero double-spin asymmetry in the production of particles that fire the MB trigger. For PHENIX, the MB trigger fires when at least one charged particle produces a hit in each BBC ($3.0 < \eta < 3.9$). A physics asymmetry in the production of such charged particles in the kinematic range to fire the BBC's would thus lead to a spin-dependent bias in the "minimum-bias" trigger. While it is extremely difficult to *prove* that there is no such bias, checks can be performed against alternative "minimum-bias" triggers, sensitive to different physics processes. The relative luminosity measured by the different processes can be compared. This technique has been used in the measurement of the double-longitudinal asymmetry in neutral pion production at PHENIX [17].

A MB detector used simultaneously as a relative luminosity detector will bias the measurement if there is a double-longitudinal asymmetry in the particles to which it is sensitive. If the detector is capable of measuring the multiplicity of the produced particles, it may be possible to understand this bias. This will not be the case if it

has only a simple binary hit/no-hit response.

The physics asymmetry in the MB/relative luminosity detector could also potentially be measured by looking for dependence of the relative luminosity on beam polarization. If for example the same-helicity cross section is higher than the opposite-helicity cross section in the case of double-longitudinal observables, then the measured relative luminosity should be enhanced when a higher fraction of the beam is polarized.

An additional idea to measure the physics asymmetry in the MB/relative luminosity detector would be to examine the MB rate change upon changing the spin combinations in a single fill. Start for example with all bunches in both beams having positive helicity (designated by "+"), creating only ++ collisions, and measure the MB event rate. Use the spin flipper described in Section 4.2.6 to flip all spins in a single beam in order to achieve +− collisions, and measure the MB event rate again. Assuming the spin flipper does not affect other beam conditions, a different MB rate implies a different physics cross section for ++ and +− helicity combinations. This procedure could be repeated several times throughout a fill. In order to check for other beam effects, it would be possible to compare ++ event rates after zero and two beam flips, or to compare the original ++ event rates to − − rates, with both beams flipped, which should be same as ++ rates if parity is conserved.

If the luminosity is high enough such that there is a non-negligible probability of multiple collisions per bunch crossing occurring, it may present a problem for both double- and single-spin asymmetry measurements. If the occurrence of multiple collisions per crossing is not spin-dependent, the relative luminosity measurement is not affected. If the probability of multiple collisions per crossing is spin-dependent due to spin-dependent beam conditions, it can likely be studied using the spin flipper. If it is spin-dependent due to a physics asymmetry, the problem is similar to the one discussed above in the case of no more than a single interaction per crossing.

It should be noted that the analogous formula to Eq. 5.1 for longitudinal double-

spin asymmetries is Eq. A.1,

$$A_{LL} = \frac{1}{P_1 P_2} \frac{N^{++} - \mathcal{R} N^{+-}}{N^{++} + \mathcal{R} N^{+-}} \tag{A.1}$$

where P_1 and P_2 are the polarizations of the two beams, N^{++} represents the particle yield from same-helicity crossings ($++$ and $--$), N^{+-} represents the particle yield from opposite-helicity crossings ($+-$ and $-+$), and $\mathcal{R}$ is the relative luminosity between same- and opposite-helicity crossings. For longitudinal double-spin asymmetries, because there is no formula analogous to Eq. 5.8, in which luminosity differences cancel to several orders, it is essential to determine the relative luminosity accurately.

The transverse double-spin asymmetry, A_{TT}, is expected to have the form $A + B\cos 2\varphi$, where A and B are constants. Therefore there is a potentially non-zero constant term as well as an azimuthal dependence. The same techniques for understanding the relative luminosity as in the double-longitudinal case should be applicable.

In the case of a transverse single-spin asymmetry, A_N, as in the present analysis, the form is expected to be purely azimuthal, expressible as $A\cos\varphi$. In this case there is no concern regarding physics asymmetries present in the detectors used as the MB trigger and to measure the relative luminosity, as long as the detectors cover the full 2π in azimuth. A new concern arises, however. An azimuthal dependence of the detector efficiency could produce bias in the "minimum-bias" trigger and the relative luminosity measurement. Comparing the asymmetry results obtained using Eq. 5.8, which is largely insensitive to the relative luminosity, provides a handle on this issue. In addition, many of the cross checks and systematic studies discussed above for the double-spin asymmetries would also be relevant.